EUROPEAN SCHOOL OF MOLECULAR MEDICINE, NAPLES SITE

UNIVERSITA' DEGLI STUDI DI NAPOLI "FEDERICO II"

Ph.D. in Molecular Medicine – XXI Cycle

Molecular Oncology

"UNRAVELLING THE MECHANISMS OF RESISTANCE TO IMATINIB MESYLATE IN CHRONIC MYELOID LEUKEMIA: A PROTEOMIC APPROACH"

Tutor:

Prof. Francesco Salvatore

Internal Supervisor:

Prof. Fabrizio Pane

External Supervisor:

Prof. Junia Vania Melo

Coordinator:

Prof. Francesco Salvatore

Ph.D. student:

Dr. Irene Colavita

Academic Year: 2008-2009

To Roberto

TABLE OF CONTENT

LIST OF ABBREVIATIONS

2DE	Bidimensional Electrophoresis
ALL	Acute lymphoblastic leukemia
AP	Accelerated phase
BC	Blast phase
CHAPS	3-[(3-Cholamidopropyl)Dimethylammonio]-1-Propanesulfonate Hydrate
CID	Collision-induced dissociation
CML	Chronic myeloid leukemia
CP	Chronic phase
DIGE	Differential Gel Electrophoresis
DMSO	Dimethylsulfoxide
DTT	Ditiotreitolo
ECL	Enhanced Chemio-Luminescence
EDTA	Ethylenediamine-Tetraacetic Acid
ESI	Electrospray Ionization
FBS	Fetal Bovine Serum
HPLC	High Performance Liquid Chromatography
IAA	Iodoacetamide
IEF	Isoelectrofocusing
IPG	Immobyline Polyacrilamide Gel
LC	Liquid Chromatography
MALDI	Matrix Assisted Laser Desorption Ionisation
MS	Mass Spectrometry
NCBI	National Center For Biotechnology Information
PAGE	Polyacrilamide Gel Electrophoresis
PBS	Phosphate Buffered Saline
Ph	Philadelphia chromosome
pI	Isoelectric point
PMSF	Phenylmethanesulfonyl Fluoride
Q	Quadrupole
SDS	Sodio Dodecil Solfato
TOF	Time Of Flight

FIGURES INDEX

TABLES INDEX

ABSTRACT

Imatinib mesylate is a potent inhibitor of the Bcr-Abl tyrosine kinase, an oncoprotein that plays a key role in the development of chronic myeloid leukemia. Consequently, imatinib is used as front-line therapy for this disease. A major concern in imatinib treatment is the emergence of resistance to the drug. The aim of this study was to obtain further insights into the Bcr-Abl activity-independent mechanisms underlying imatinib resistance, in chronic myeloid leukemia. The imatinib-resistant KCL22R and sensitive KCL22S cells were used as experimental model. None of the already described resistance mechanisms has been detected so far in KCL22R cells; therefore additional mechanisms independent of Bcr-Abl kinase activity could be envisaged. Moreover, KCL22S cells exhibited typical features of the quiescent hematopoietic Ph+ stem cells, thereby representing a good experimental model to investigate imatinib resistance. To this aim differentially expressed proteins between KCL22S and KCL22R cells were characterized using a proteomic approach: two-dimensional differential gel electrophoresis (2D-DIGE) coupled with Tandem Mass Spectrometry. 51 proteins were identified: 27 over-expressed and 24 under-expressed in KCL22R cells versus KCL22S cells. Bioinformatic analysis with GeneSpring and Ingenuity Pathway Analysis (IPA) softwares showed that several of these proteins were involved in the modulation of redox balance and activation of anti-apoptotic pathways mediated by NF-kB and Ras-MAPK signaling. Since the Erk pathway has been shown to influence chemotherapeutic drug resistance of hematopoietic cells, the level of activation of Erk in KCL22R and KCL22S cells was investigated. This analysis demonstrated that continuous activation of Erk occurred in KCL22R cells as compared to sensitive cells. Interestingly, examination of the most statistically significant protein network showed that several differentially expressed

proteins, between KCL22R and KCL22S cells, were directly or indirectly connected with Erk. In particular, among them, this study focused on two SH2-containing, non-receptor protein tyrosine phosphatases: Shp1 (PTPN6) and Shp2 (PTPN11). It has been shown that Shp2 positively regulates the Ras-Erk pathway and is activated by phosphorylation. This study demonstrated that the level of phosphorylation and hence of activation of Shp2 in KCL22R cells was higher than in KCL22S cells. In addition the knock-down of Shp2 expression, in combination with imatinib treatment, significantly reduced the activation of Erk 1/2 in KCL22R cells and produced a reversion of the KCL22R phenotype, suggesting that Shp2 plays a role in the Bcr-Abl activity-independent mechanisms of imatinib resistance. Interestingly this study also demonstrated that Shp1, that was found down-regulated in KCL22R cells, interacted with Shp2 and that Shp1 played a negative role in the Shp2 activation in KCL22S cells. Moreover Annexin A1 and Hsp70, belonging to the same protein network, were found down-regulated in KCL22R cells. They could also play a role in imatinib resistance by the direct or indirect interaction with Shp2.

Taken together these results suggest that a reduced Shp1 expression in KCL22R cells could contribute to a continuous Shp2 activation, sustaining a Bcr-Abl activity-independent pathway of proliferation and survival to imatinib treatment. These two proteins could be used as putative biomarkers to evaluate the efficacy of imatinib treatment and to develop new combinatorial therapeutic approaches.

Chapter 1

INTRODUCTION

1.1 Bcr-Abl and its oncogenic activity in chronic myeloid leukemia

Chronic myeloid leukemia (CML) results from the neoplastic transformation of hematopoietic stem cells (Figure 1). CML is characterized by three distinct clinical phases namely chronic phase (CP), accelerated phase (AP) and blast phase (BC) [1]. The initial chronic phase is characterized by a massive expansion of the granulocyte cells. The median duration of the chronic phase is 3-4 years. As the disease progresses, after the acquisition of additional genetic and/or epigenetic abnormalities, patients enter an accelerated phase followed by blast crisis. This is the most aggressive phase and is characterized by a block of cell differentiation that results in the presence of 30% or more myeloid or lymphoid blast cells in peripheral blood or bone marrow [2]. The molecular hallmark of chronic myeloid leukemia (CML) is the Philadelphia chromosome (Ph), which results from a reciprocal translocation between the long arms of chromosomes 9 and 22 [t(9;22) (q11;q34)]. The Philadelphia chromosome contains a BCR-ABL hybrid gene that encodes an oncogenic fusion protein. The Bcr-Abl protein has deregulated tyrosine kinase activity that promotes cell growth through phosphorylation of signaling proteins [3-7].

Depending on the precise breakpoints in the translocation and RNA splicing, different forms of Bcr-Abl protein with different molecular weights (p185 Bcr-Abl, p210 Bcr-Abl and p230 Bcr-Abl) can be generated in patients [4].

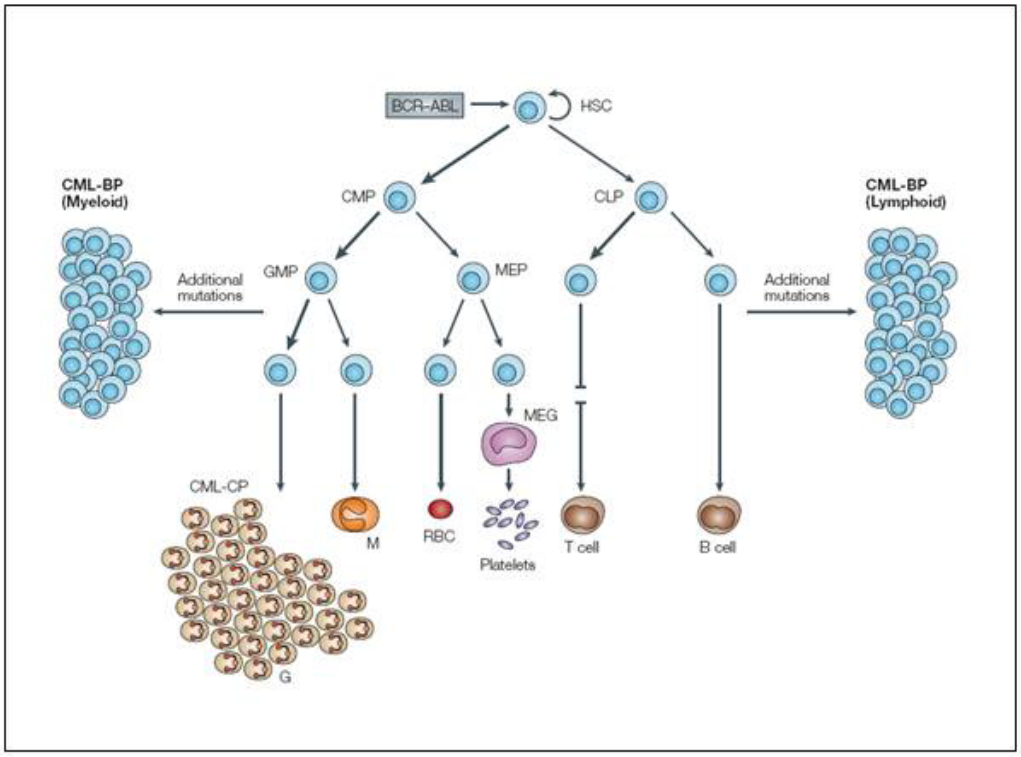

Figure 1. Chronic myeloid leukemia (CML) is a disease initiated by expression of the BCR–ABL fusion gene product in self-renewing hematopoietic stem cells (HSCs). HSCs can differentiate into common myeloid progenitors (CMPs), which then differentiate into granulocyte/macrophage progenitors (GMPs; progenitors of granulocytes (G) and macrophages (M)) and megakaryocyte/erythrocyte progenitors (MEPs; progenitors of red blood cells (RBCs) and megakaryocytes (MEGs), which produce platelets). HSCs can also differentiate into common lymphoid progenitors (CLPs), which are the progenitors of lymphocytes such as T cells and B cells. The initial chronic phase of CML (CML-CP) is characterized by a massive expansion of the granulocytic-cell series. Acquisition of additional genetic mutations beyond expression of BCR–ABL causes the progression of CML from chronic phase to blast phase (CML-BP).

1.2 Molecular mechanisms of BCR-ABL translocation

The breakpoints within the BCR gene on chromosome 22 are found within three defined regions [4]. In the 95% of patients with CML and approximately one third of patients with ALL, the BCR gene is truncated within a 5.8-kb region known as the major breakpoint cluster region (M-bcr) (Figure 2). This region contains five exons, originally named b1 to b5, but now referred to as e12 to e16, according to their true positions in the gene [8]. Breakpoints within the ABL gene can occur anywhere within a 5′ segment that extends for over 300 kilobases (kb) [9]. Typically, breakpoints form within intronic sequences, most frequently between the two alternative first exons of ABL. Thus, BCR-ABL fusion genes may contain both exons 1b and 1a, exon 1a alone, or neither of the alternative first exons. BCR-ABL mRNA lacks exon 1, regardless of the structure of the fusion gene, with the transcript consisting of BCR exons fused directly to ABL exon a2 (Figure 2). Because processing of BCR-ABL mRNA results in the joining of BCR exons to ABL exon a2, hybrid transcripts are produced that have an e13a2 (b2a2) or an e14a2 (b3a2) junction. In both cases, the mRNA consists of an 8.5-kb sequence that encodes a 210-kDa fusion protein, p210 Bcr-Abl (Figure 2). In two-thirds of patients with Ph-positive ALL and in rare cases of CML and acute myelogenous leukemia, the breakpoint in BCR occurs in a region upstream of the major breakpoint cluster region known as the minor breakpoint cluster region (m-bcr) (Figure 2). The hybrid mRNA consists of sequences that are approximately 7 kb in length in which exon e1 from BCR is joined to exon a2 of ABL. The translated product is a 190-kDa fusion protein, p190Bcr-Abl (also referred as p185Bcr-Abl) [10]. The third defined breakpoint cluster region within the BCR gene was named “micro” breakpoint cluster region (μ-bcr), (Figure 2) [11]. In this case, the breaks occur within a 3 ′ segment of the BCR gene between exons e19 and e20

(known as c3 and c4 in the original nomenclature). Transcription of the hybrid gene yields an e19a2 BCR-ABL fusion transcript that encodes a 230-kDa protein, p230 Bcr-Abl.

1.3 Pathways downstream of Bcr-Abl

The cytoplasmic location of Bcr-Abl oncoprotein allows access to many cellular substrates leading to the activation of proliferation and survival pathways. Same of them are here described (Figure 3). Many signaling proteins have been shown to interact with Bcr-Abl through various functional domains/motifs (for example, Grb2, Crkl, Shc, 3Bp2, Abl-interacting protein 1 and 2, and Crk-associated substrate (Cas)), and/or to become phosphorylated in Bcr-Abl-expressing cells (for example, Crkl, Shc, Docking protein 1, Gab2, Cbl, Cas, Signal transducer and activator of transcription 5 (Stat5), the p85 subunit of pi3k, phospholipase cγ, Synaptophysin, Vav1, Ras GTPase-activating protein, Focal adhesion kinase, Fes, Paxillin and Talin [4,12]. These proteins in turn control a range of signaling pathways that activate proteins such as Ras, pi3k, Akt, Jnk, Src family kinases, protein and lipid phosphatases, and their respective downstream targets, as well as transcription factors such as the Stats, Nuclear factor-kb and Myc [4]. Bcr-Abl expression also seems to be correlated to the expression of Src kinases family such as Lyn. At this regard is interesting that down-regulation of Lyn expression by small interfering RNA induces apoptosis of human blast-phase CML cells [13]. Bcr-Abl also recruits the scaffold adapter Gab2 through Grb2. The major Grb2-binding site at Y177 of Bcr-Abl was shown to regulate the tyrosine phosphorylation of Gab2 [14] (Figure 3). In this way Gab2 mediates the ability of Bcr-Abl to confer cytokine-independent growth of primary myeloid cells. Gab2 also contains binding sites for the SH2 domains of the p85 subunit of pi3k and for Shp2 [14]. The pi3k and Shp2 signaling pathways could

be required for Bcr-Abl leukemogenesis. In particular Shp2 is required for normal activation of the Ras-Erk (extracellular signal-regulated kinase) pathway (Figure 3). The mechanism of the activation of Ras-Erk pathway by Shp2 is not completely known. In addition to Shp2, Ras can be activated directly by Bcr-Abl through the Grb2-Sos complex [15] (Figure 3).

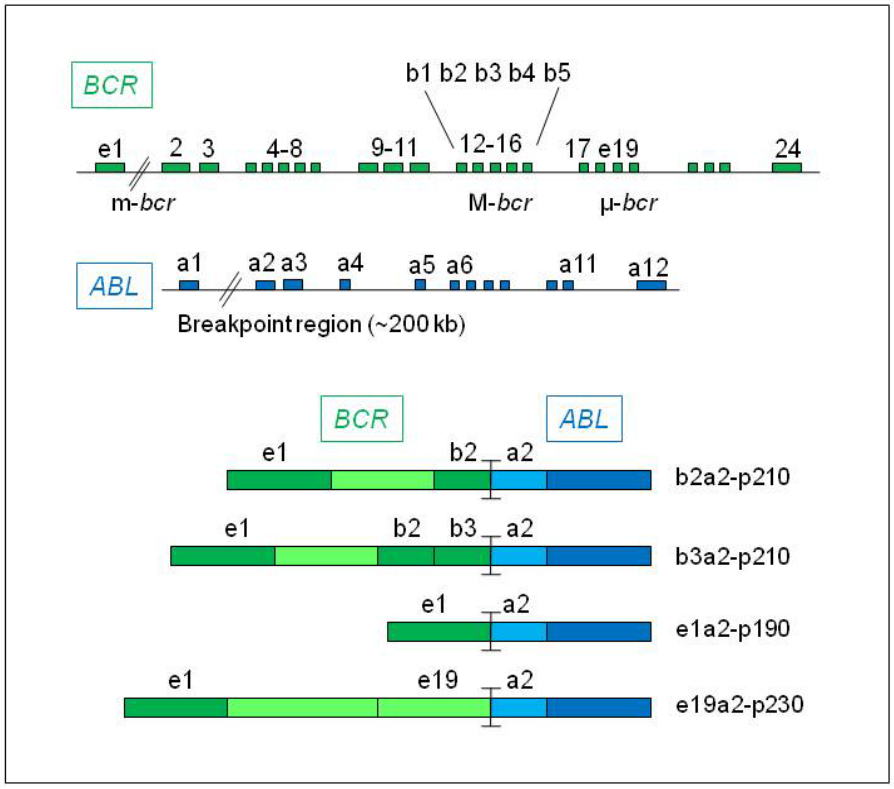

Figure 2. The t(9;22) translocation and its products with breakpoint locations at the *BCR* and *ABL* loci.

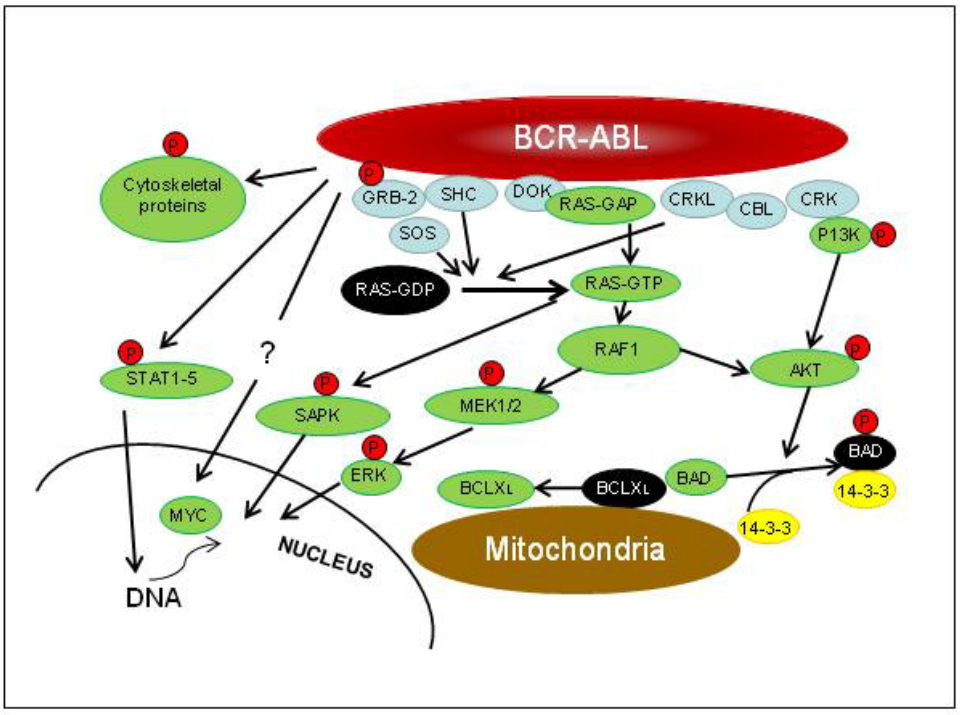

Figure 3. A simplified diagram of the associations between Bcr-Abl and signaling proteins.

1.4 Imatinib in CML therapy

Allogenic stem-cell transplantation is the only known curative therapy for CML. However, most patients are not eligible for this therapy, because of advanced age (making them unable to tolerate the serious side effects of the treatment) or lack of a suitable stem-cell donor [16]. Because Bcr-Abl plays a key role in the pathogenesis of CML and because the tyrosine-kinase activity of Abl is essential for Bcr-Abl-mediated neoplastic transformation, Abl kinase has became a potential target for therapeutic intervention. In 1998, imatinib mesylate (STI571®, Gleevec) (Figure 4), a tyrosine kinase inhibitor belonging to the 2-phenylaminopyrimidine group of pharmacological compounds, was introduced as first line therapy of CML [17]. Imatinib has a high affinity for the ATP-binding site of Abl, in addition to other kinases such as Pdgfr, Kit and Arg. Imatinib is a potent inhibitor of the Abl tyrosine kinase and has been shown to selectively induce apoptosis of Bcr-Abl positive cells [17,18]. Imatinib locks the Bcr-Abl protein in an inactive conformation (Figure 5), thus preventing phosphorylation of target proteins and blocking the proliferation in CML cells [19]. There are two major obstacles to imatinib-based therapies for patients with CML. One is the persistence of Bcr-Abl-positive cells. This is known as ‘residual disease’, and is detected by a sensitive nested reverse-transcriptase PCR assay [20,21]. The second is related to the emergence of resistance to imatinib during disease progression, namely ‘acquired resistance’, in addition to ‘primary resistance’. Most of the mechanisms implicated in resistance to imatinib involve mutations in the Bcr-Abl kinase domain that impair the drug binding or protein kinase over-expression [22, 23], but they do not account for all the resistance mechanisms.

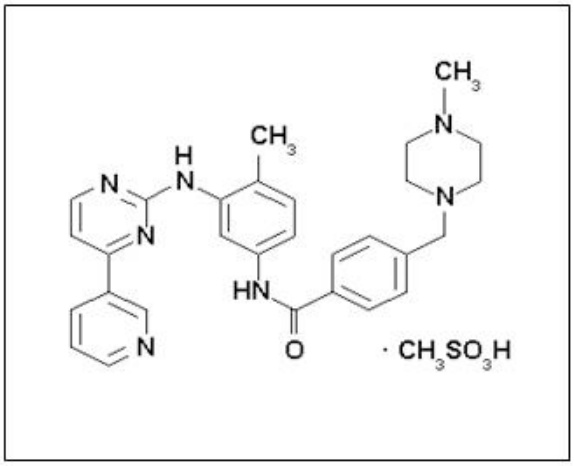

Figure 4. Imatinib chemical structure.

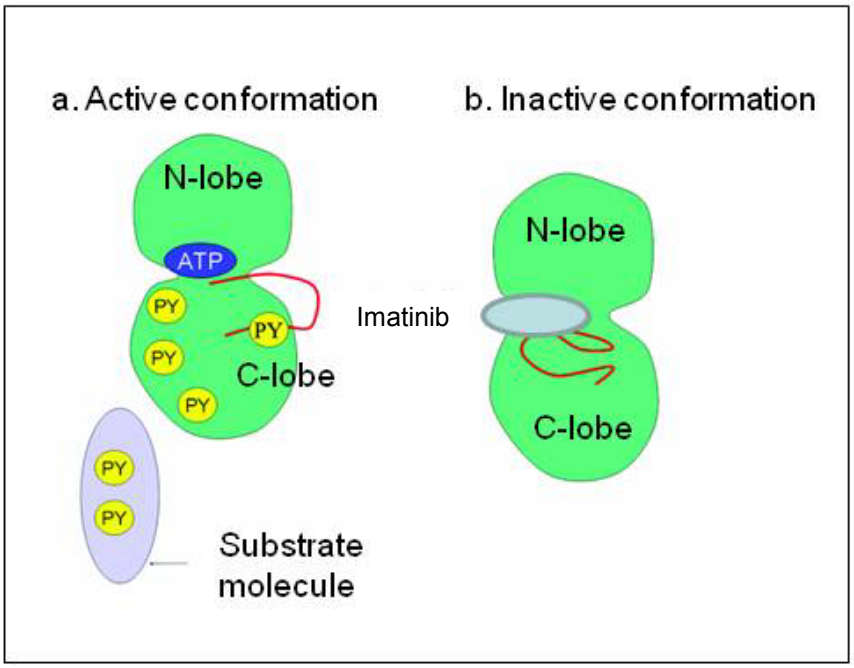

Figure 5. (a) Bcr-Abl activation and phosphorylation of downstream substrates. (b) Imatinib works by binding to the ATP binding site of Bcr-Abl kinase thus preventing its activation and inhibiting the enzyme activity. Inhibition of Bcr-Abl activity blocks deregulated signaling as altered cellular adhesion, abnormal proliferation and apoptosis inhibition.

1.5 Imatinib resistance

Studies of resistance to imatinib mesylate were long hampered by the lack of cells resistant to the drug. However, in the year 2000, the group led by Junia V. Melo produced resistant sub-lines from various Ph-positive cells [24]. They demonstrated that human Bcr-Abl-positive cells can evade the inhibitory effect of imatinib by different mechanisms. The two most common affect the BCR-ABL gene itself such as mutations in its tyrosine kinase domain and over-expression of the Bcr-Abl protein due to amplification of the BCR-ABL gene [24-27]. Resistance may also be related to Bcr-Abl-independent mechanisms. These include the up-regulation of the drug efflux pumps [28-30], the down-regulation of drug influx transporters [31,32], the drug sequestration mediated by alpha-1-acid lipoprotein (AGP) [33], and other Bcr-Abl-independent mechanisms such as the over-expression of Src family kinases, Lyn and Hck [34] and the activation of pathways downstream of Bcr-Abl, independent of its kinase activity, that confer resistance to imatinib [35].

1.5.1 Mutations in the Abl kinase domain

The emergence and selection of clones exhibiting point mutations in the Abl kinase domain is the most frequently identified mechanism of resistance in patients treated with imatinib [36, 37]. These mutations are not induced by imatinib, but rather, just like antibiotic resistance in bacteria, arise through a process whereby the drug itself selects for rare pre-existing mutant clones, which gradually outgrow drug-sensitive cells [38]. Mutations can be categorised into 4 groups: (i) those which directly impair imatinib binding; (ii) those within the ATP binding site; (iii) those within the activation loop, preventing the kinase from achieving the conformation required for imatinib binding; and (iv) those within the catalytic domain (Figure 6). The substitution of the

amino acid threonine with isoleucine at position 315 of the Abl protein was the first mutation to be detected in resistant patients [39]. At least 73 different point mutations leading to substitution of 50 amino acids in the Abl kinase domain have been isolated from CML patients resistant to imatinib so far, and this number is likely to increase with more sensitive methods of detection (Figure 6).

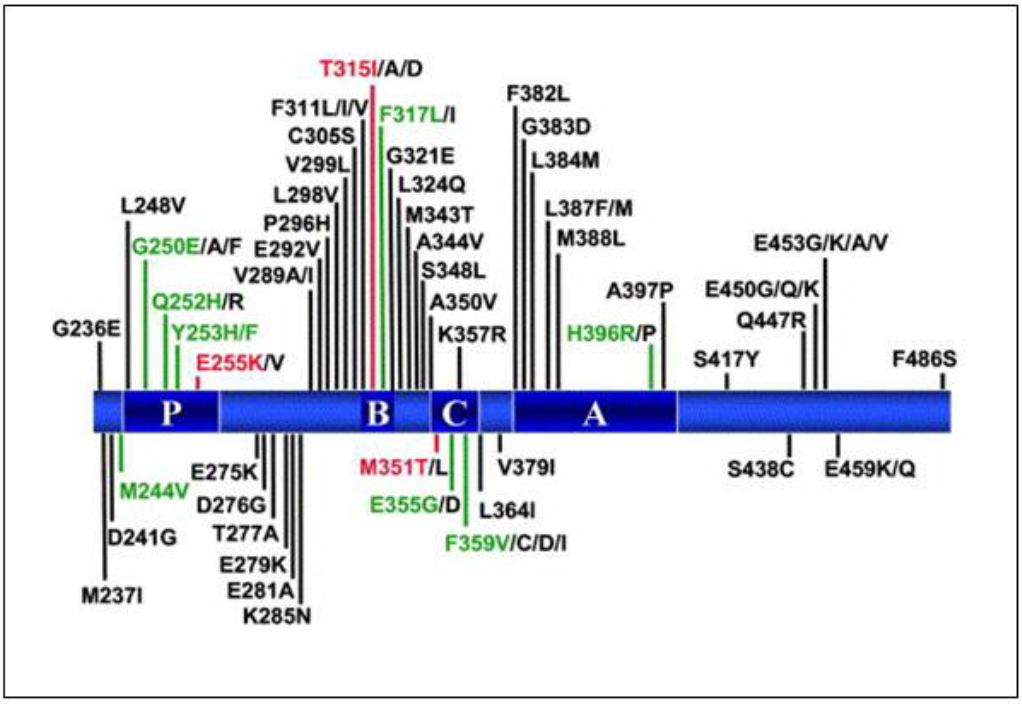

Figure 6. Map of Bcr-Abl kinase domain mutations associated with clinical resistance to imatinib. Abbreviations: P, P-loop; B, imatinib binding site; C, catalytic domain; A, activation loop. Amino-acid substitutions in green indicate mutations detected in 2–10% and in red in >10% of patients with mutations.

1.5.2 Bcr-Abl over-expression

Over-expression of the Bcr-Abl protein due to amplification of the BCR-ABL gene was first observed in vitro when resistant CML cell lines were generated by exposure to gradually increasing doses of imatinib [24,40]. Over-expression of Bcr-Abl leads to resistance by increasing the amount of target protein needed to be inhibited by the therapeutic dose of the drug. It is also possible that a transient over-expression of Bcr-Abl may be an early phenomenon in the establishment of imatinib resistance, preceding the emergence of a dominant clone with a mutant kinase domain, as suggested by kinetic studies in cell lines [40].

1.5.3 Drug efflux and influx transporters

Multidrug resistance (MDR) is mediated by an increased expression at the cell surface of the MDR1 gene product, Pgp, an energy dependent efflux pump, which reduces intracellular drug concentrations and leads to ineffective levels of the drug reaching its target [28,41]. Imatinib and other tyrosine kinase inhibitors are substrates of Pgp, and the intracellular levels of imatinib were shown to be significantly lower in Pgp-expressing cells [31,42]. An imatinib-resistant CML cell line generated by gradual exposure to increasing doses of the drug was shown to exhibit Pgp over-expression, and MDR1 over-expression in CML cell lines also confers resistance to imatinib [24]. Recently, two other drug transporters, breast cancer resistance protein (BCRP)/ABCG2 and human organic cation transporter 1 (hOCT1), have been implicated as possible mechanisms for promoting imatinib resistance. Imatinib has been variably reported to be a substrate and/or an inhibitor for the BCRP/ABCG2 drug efflux pump which is over-expressed in many human tumours and also found to be functionally expressed in CML stem cells [29,30]. The drug transporter, hOCT1

mediates the active transport of imatinib into cells, and inhibition of hOCT1 decreases the intracellular concentration of imatinib [31,32].

1.5.4 Other Bcr-Abl activity-independent mechanisms of imatinib resistance

The Src family kinases, Lyn and Hck, are activated in Bcr-Abl-expressing cell lines. Very recently, over-expression of Lyn and Hck kinases has been reported in some imatinib-resistant patients [43]. Lyn and Hck belong to the SRC family of kinases that are expressed in CML cells and activated by Bcr-Abl kinase [44]. However, kinase activation is also controlled by other mechanisms that could cause imatinib resistance. In fact, Lyn over-expression, irrespective of Brc-Abl, occurs in the K562 CML cell line [34] and in some CML patients [44]. Microarray analysis have shown that transcripts from genes with anti-apoptotic or malignant transformation properties and with involvement in signal transduction/transcriptional regulation are over-expressed in CML cells innately resistant to imatinib. This would suggest that pathways downstream of Bcr-Abl and independent of its kinase activity may be important factors which confer resistance to imatinib [35].

1.6 The proteomic approach

Proteomics, defined in the 1995 as "the total protein complements of a genome", has burst onto the scientific scene with stunning rapidity over the past few years, perhaps befitting a discipline that can enjoy the virtually instantaneous conversion of a genome sequence to a set of predicted proteins. In fact, for almost two decades, major efforts have been directed at the polynucleotide level and, particularly, at the gene sequencing of a variety of different organisms. Complete genome sequencing has been achieved for a wide variety of organisms, and efforts to sequence the

complete human genome have resulted in completion of a first draft. While it is often conceptualized that one gene produces one protein, it is known that the expressed products of a single gene in reality represent a protein population that can contain large amounts of microheterogeneity [45-46]. More than 100 modification types are recorded and additional ones are yet to be discovered [47]. All modified forms from one protein can vary in abundance, activity or location inside a cell. Indeed, cellular proteins are not invariant products of genes, but are subject to a high degree of interdependent processing at the protein level that is a critical component of cellular function and regulation. In addition, protein expression is dynamically regulated in response to external and internal perturbations under developmental, physiological, pathological, pharmacological and aging conditions. In fact, in contrast to the static genome, where all information could in principle be obtained from the DNA of a single cell, the proteome is dynamic and highly dependent not only on the type of cell, but also on the state of the cell [48].

Proteome analysis presents specialized analytical problems in three major areas: **expression proteomics** [49], which aims to measure up- and down-regulation of protein levels, **functional proteomics**, which aims at the characterisation of cellular compartments, multi-protein complexes and signaling pathways [50] and **chemical proteomics** [51] that comes in two different fields: (i) activity based probe profiling (ABPP), which focuses on the enzymatic activity of a particular protein family, and (ii) a compound-centric approach, which focuses on characterizing the molecular mechanism of action of an individual bioactive small molecule.

1.6.1 Expression proteomics: qualitative and quantitative proteome analysis

Classical proteomic approaches have relied upon separating whole cell lysates by 2D Gel Electrophoresis (2DE). Historically, 2DE has been the tool of choice to resolve complex protein mixtures and to detect differences in protein expression patterns between normal and diseased tissue. High-resolution gel electrophoresis, of which 2DE is currently the most powerful protein separation method, was already used as an analytical tool in the late 70s [52]. The 2DE consists in the separation of proteins by isoelectric point in one dimension and molecular weight in the second dimension (Figure 7). Proteins carry a negative, positive or zero net charge depending on their amino acid composition and covalent modification (such as phosphorylation, nitrosylation, sulphation and glycosylation), and the pH of the environment. The pI of a protein is the pH at which the protein carries no net charge. If the proteins are electrophoresed in a pH-gradient they will migrate until they reach a position in the pH-gradient where their overall net charge is zero i.e. the pH is equal to the pI of the protein (Figure 7).

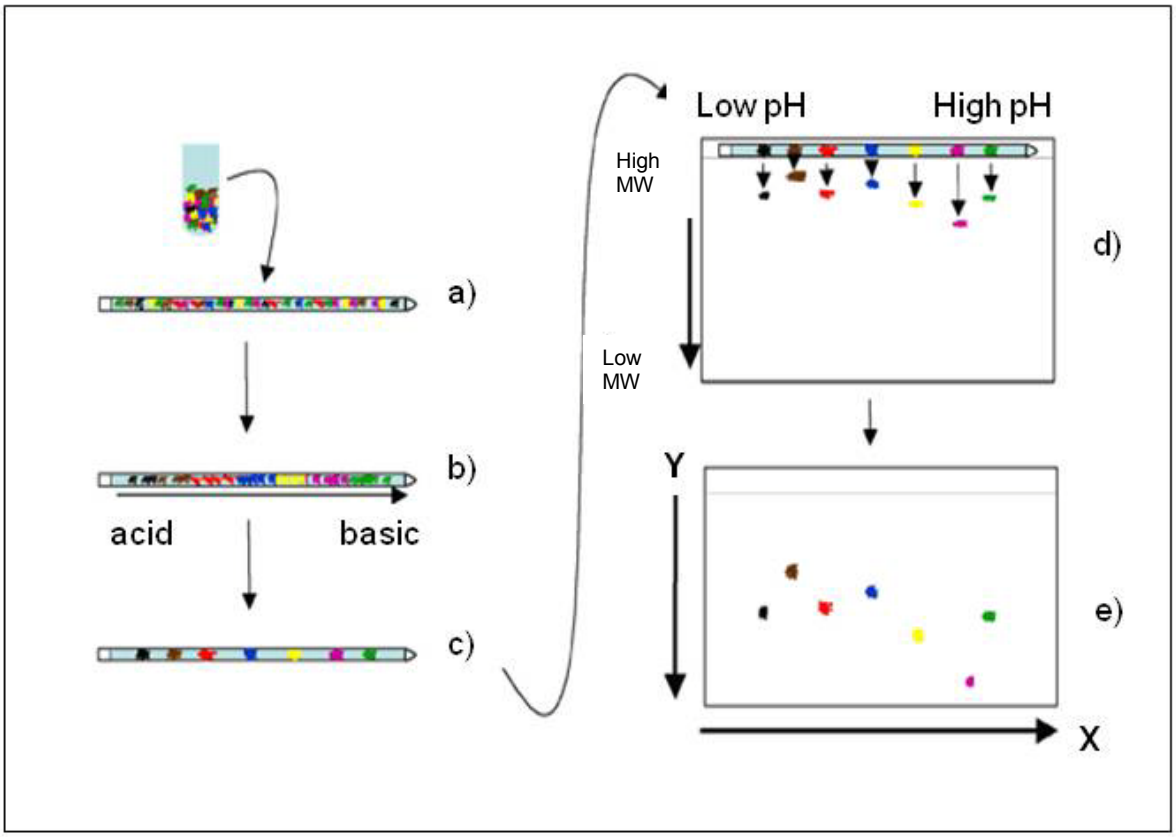

Figure 7. Schematic representation of a 2D-PAGE**.** a), b), c) The first step in the 2D-PAGE is the separation of the proteins according to their isoelectric points (pI). At this point the protein becomes 'focused' at its isoelectric point (pI). A protein with a net negative charge will migrate towards the anode and proteins with a positive charge will migrate to the cathode. A protein will stop migrating when the pH is equal to its pI. d), e) The second step in the 2D-PAGE is the separation of the proteins according to their molecular weight.

Isoelectric focusing (IEF) allows the separation of proteins in a mixture according to very small differences in their isoelectric points. The original 2DE method, described by O'Farrell (1975) [52], used carrier ampholytes in tube gels to create and maintain a pH-gradient. Carrier ampholytes are small amphoteric molecules with high buffering capacity near their isoelectric points and are usually employed as mixtures covering a set pH range. When an electric field is applied across a mixture of carrier ampholytes the most negatively charged move towards the anode and the most positive towards the cathode. In this way it is possible to form a continuous pH-gradient within a gel, which is suitable for the focusing of larger amphoteric molecules such as proteins. However, the cylindrical tube gels and carrier ampholytes used to create the pH-gradient had limitations in resolving power and other technical difficulties. The pH-gradients formed by carrier ampholytes are unstable and have a tendency to drift during longer focusing periods. In 1982 Bjellqvist [53] introduced important modifications which involved the carrier ampholytes being co-polymerised into the gel matrix itself as it was being cast. The creation of this ampholyte pH-gradient decreased markedly the drift observed using the tube gel system of isoelectric focusing. Further developments included the gel being cast onto a plastic support strip making the system much more robust and easier to handle. These innovations significantly improved reproducibility and performance of the first dimension focusing step (IEF) in 2D-PAGE. The second dimension utilises the traditional SDS-PAGE technique with the low percentage of acrylamide IEF strip replacing the stacking gel. Despite being a well-established technique for protein analysis, traditional 2D gel electrophoresis is time-consuming and labor-intensive. In addition, the lack of reproducibility between gels leads to significant system variability making it difficult to distinguish between system variation and induced biological change, which means

that real differences between protein abundance attributed, for example, to a disease state can rarely be predicted with confidence. The group of Unlu [54] first described a method, 2D difference gel electrophoresis (2D-DIGE) that enabled more than one sample to be separated in a single 2D polyacrylamide gel. 2D-DIGE differs from 2D-PAGE in that each sample is pre-labeled with a fluorescent dye (called Cy2, Cy3 and Cy5, Figure 8), prior to isoelectric focusing. The labeled samples can be run at any one time and on the same gel (Figure 9). The ability to pre-label each sample with different dyes and run them together on the same gel makes 2D-DIGE a much more powerful technique than running single samples on individual 2D-PAGE gels. Analysing 3 samples on one 2D-DIGE rather than three individual 2D-PAGE gels reduces experimental gel-to-gel variation. Traditionally 2D-PAGE gels are stained using coomassie blue or the more sensitive silver staining procedures. Gels are then compared using computer software for changes in protein expression. However, the degree of linearity of both silver and coomassie blue stains are limited compared to the 5 orders of magnitude possible using CyDye technology. The CyDye technique is a much quicker and sensitive method for the detection of proteins (low nanogram) than silver and coomassie blue. With silver and coomassie staining, gels require being fixed and stained/destained using time-consuming techniques. However with DIGE, immediately after completion of electrophoresis each gel is scanned three times, at three different wavelengths (red, blue and green) and the analyses is complete. The three samples can then be compared and analysed using sophisticated computer software and subtle changes in protein expression detected very accurately [55].

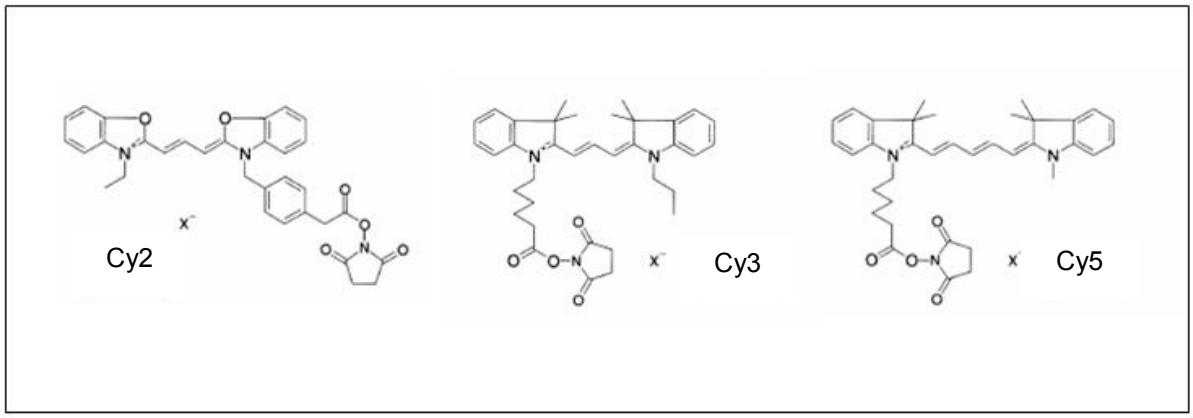

Figure 8. Cy2, Cy3 and Cy5 chemical structures.

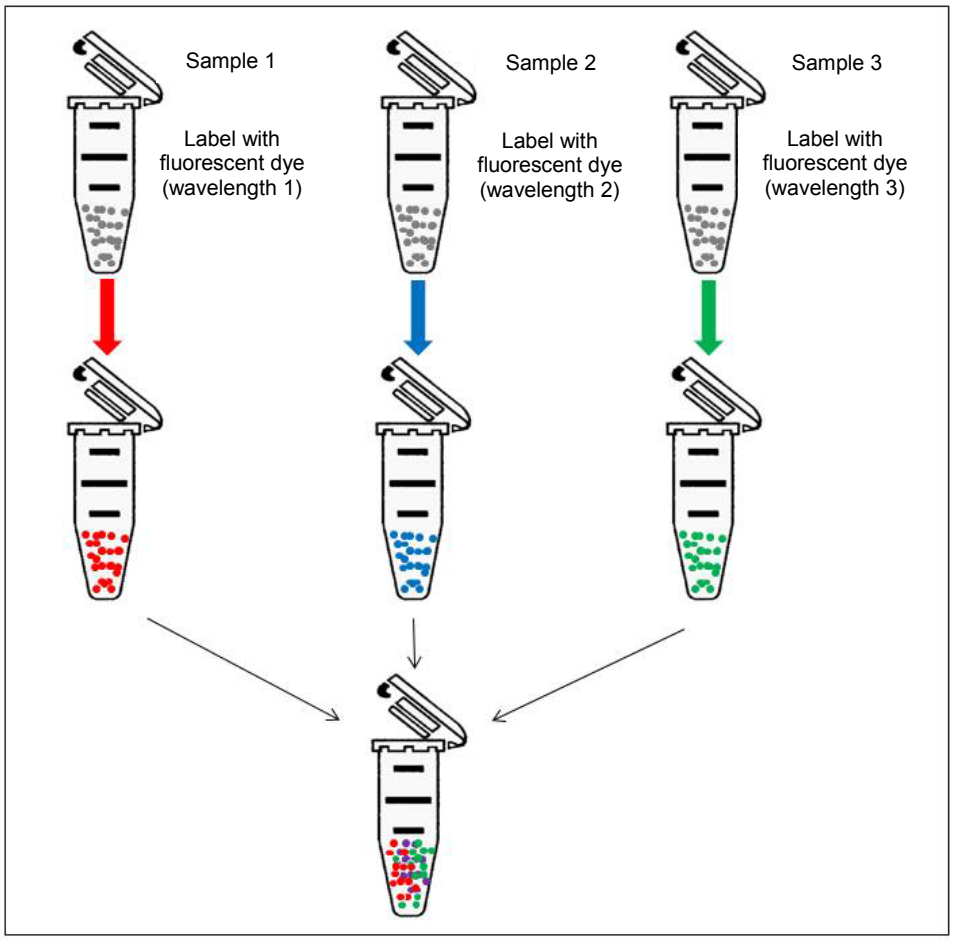

Figure 9. Three samples, differentially labeled with CyDyes, are mixed and analysed together.

In addition the introduction in the analysis of an internal standard increases the accuracy of the analysis. The internal standard, obtained by pooling equal amounts of protein from each biological sample in the experiment, is labeled with one of the CyDye DIGE fluor dyes, which is usually Cy2 for “minimal labeling”. The last results in the labeling of 3-5% of total proteins in the sample. This means that every protein from all samples will be represented in the internal standard. The internal standard is then run on every single gel along with each individual sample labeled. Linking every sample in-gel to a common internal standard has several advantages. It means that each sample within a gel can be normalized to the internal standard present on that gel. In addition, the abundance of each protein spot in a biological sample can be measured as a ratio to its corresponding spot present in the internal standard. This enables accurate quantization and accurate spot statistics between gels and, most importantly, separation of experimental variation from inherent biological variation. This has not been possible with conventional 2D gel electrophoresis, because of the high level of variation associated with running all samples on individual gels.

In summary the greater quantitative accuracy of 2D-DIGE is enabled by two main factors:

- the ability to run multiple samples on the same gel
- an internal standard (reference) sample which can be run on all gels

The image analysis allows to compare the samples in the experiment. To this aim fluorescence-labeled proteins in the 2D gels are scanned at different wavelengths using an imager to generate an image specific for each CyDye. To compare protein expression across a range of experimental samples and gels, two distinct steps are required (Figure 10):

- Intra-gel co-detection of sample and internal standard protein spots

- Inter-gel matching of internal standard samples across all gels within the experiment

In the first step three scans are made of each gel, Cy2, Cy3 and Cy5 scans. Scanned images of each sample and the internal standard are overlaid by a software. The algorithms within the software co-detect the spots present in each scan-image, effectively identifying the position of each spot within the gel (Figure 10a). In this way every protein in the sample is intrinsically linked to the corresponding protein spot in the internal standard sample. In the second step, the inter-gel comparisons of spot abundance are carried out. Following co-detection, each image has a spot map species. The internal standard image with the most detected spots is assigned as the 'Master'. The spot map species for the internal standard assigned as the Master, is used as a template to which all remaining spot map species for the other internal standards (intrinsically linked to their co-detected sample images) are matched (Figure 10b). Once the protein spots have been matched, the ratio of protein abundance between samples can be determined. Spot volume (*i.e.* the sum of the pixel values within a spot minus background) for each experimental sample is compared directly to the internal standard by the software. Spot ratios are calculated indicating the change in spot volume between the two images. The protein abundance for each spot in each sample is then expressed as a (normalized) ratio relative to the internal standard. Statistical tests such as the Student's T-test can then be applied to the data-software. The statistical tests verify that any change between the groups is significant and give the user a level of confidence by taking into account the inherent biological variation within a group compared to the induced difference between groups. It assigns a confidence rating as to whether this change is above the biological variation.

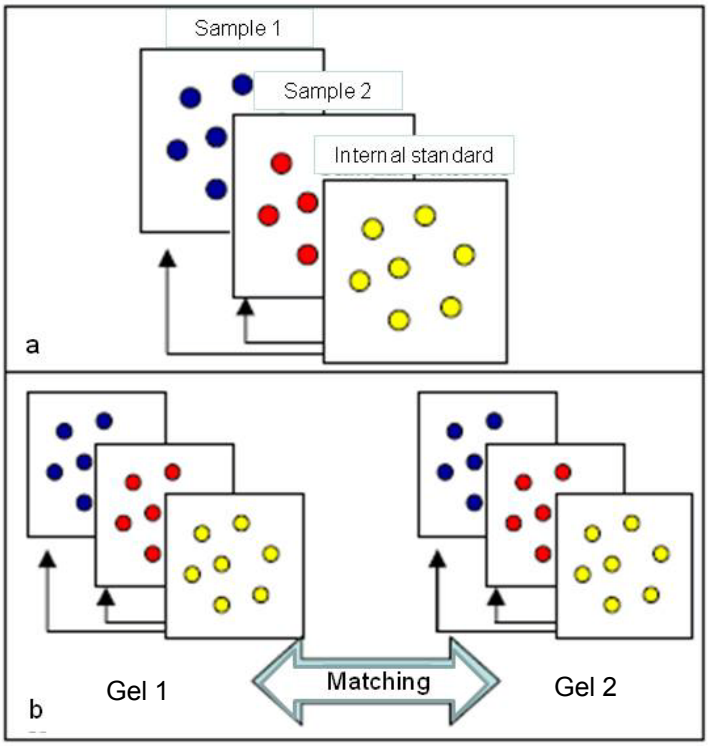

Figure 10. 2D-DIGE image analysis: a) intra-gel co-detection of sample and internal standard protein spots; b) inter-gel matching of internal standard samples across all gels within the experiment.

1.6.2 Protein Identification by mass spectrometry

To measure the mass of molecules, the sample must be charged (hence ionized) and desolvated (dry). The two most successful mechanisms for ionization of peptides and proteins are matrix-assisted laser desorption ionization (MALDI) and electrospray ionization (ESI) [56-58]. In MALDI the analyte of interest is embedded in a matrix that is dried and then volatilized in a vacuum under ultraviolet laser irradiation. Typically, the mass analyzer coupled with MALDI is a time-of-flight (TOF) mass analyzer that simply measures the elapsed time from acceleration of the charged (ionized) molecules through a field-free drift region. The other common ionization source is ESI, in which the analyte is sprayed from a fine needle at high voltage toward the inlet of the mass spectrometer at a lower voltage [59]. The spray is typically either from a

reversed phase HPLC (RP-HPLC) column or a nanospray device that is similar to a microinjection needle. During this process, the droplets containing analyte are dried and gain charge (ionize). The ions formed during this process are directed into the mass analyzer, which could be either a single or a triple quadrupole, an ion trap, a Fourier-transform ion cyclotron resonance (FT-ICR), or a hybrid quadrupole TOF (Qq-TOF) type [60-62]. A mass spectrometric method for rapid identification of proteins uses the characteristic distribution of peptide masses obtained by chemical or enzymatic fragmentation of proteins [61]. A number of computer programs are available for using the observed peptide masses to search gene sequence databases for proteins that fit the mass fingerprint [63-64]. Searching of gene sequence databases is again used to identify the protein at the gene level. Indeed, the typical proteomics experiment consists of five steps. In step 1, the proteins to be analyzed are isolated from cell lysate or tissues by biochemical fractionation, 2D-GE separation or affinity selection. Proteins are then degraded enzymatically to peptides in step 2, usually by trypsin, leading to peptides with N-terminally protonated amino acids, providing an advantage in subsequent MS masses (obtained generally by MALDI-MS) with the calculated list of all peptide masses of each entry in a database. Mass fingerprint method works well for isolated proteins, but the resulting protein identifications are not sufficiently specific for protein mixtures (e.g. for co-migrating proteins). The addition of sequencing capability to the MALDI method should make protein identifications more specific than those obtained by simple peptide-mass mapping. In step 3, the peptide mixtures are separated by one or more steps of high-pressure liquid chromatography. In step 4, a mass spectrum of the peptides eluting at this time point is taken (MS spectrum). The program generates a list of these peptides for fragmentation and a series of tandem mass spectrometric experiments (step 5).

MS-MS data consist in the isolation of a given peptide ion, fragmentation by energetic collision with gas, recording of the tandem or MS-MS spectrum and storing for matching against protein sequence databases. The outcome of the experiment is the identity of the peptides and therefore the proteins making up the purified protein population. Often MS-MS instruments are classified in one of two categories: tandem in space or tandem in time. Tandem in space instruments require a distinct analyser for each stage (isolation and fragmentation) of MS-MS. Today, almost all tandem in space MS-MS instruments are either triple quadrupole (QqQ) or hybrid instruments quadrupole/time-of-flight (Q/TOF). Trapping instruments are typically tandem in time. The various stages of MS-MS are performed in the same analyzer but separated in time. In MS-MS experiments the isolated ions (termed parent ions) are induced to undergo a reaction that increases the internal energy of the ions, leading to dissociation. The ions resulting from the various reactions (product ions) are analyzed in the second stage of MS-MS. The scheme of a tandem MS experiment can be summarized in the following reaction:

$$M_p^+ \rightarrow M_d^+ + M_n$$

M_p^+ is the parent ion

M_d^+ is the product or fragment ion

M_n is the neutral fragment or another product ion if the parent ion is multiply charged

The dissociation method almost universally used is collision-induced dissociation (CID) [65]. In CID, the parent ion collides with a neutral target (collision) gas and some of the kinetic energy of the parent ion can be converted to internal energy. The CID spectra of peptides obtained by a collision energy shows abundant fragment ions generated by the cleavage of the peptide bonds. In mass spectrometric sequencing, the information that describes the amino acid sequence of a peptide is contained in a product ion spectrum. This product ion spectrum is obtained in a tandem mass spectrometry experiment by using collision induced dissociation of a protonated or multiply protonated peptide ion. Understanding the structure of protonated peptides and their fragmentation pathways plays key roles in one's ability to interpret ion spectra. Peptide sequence identification by mass spectrometry involves fragmentation of a peptide to produce smaller m/z fragments; ideally, measured m/z values of these pieces can be assembled to produce the original peptide sequence. Cleavage of the backbone typically occurs at the peptide bond to produce **b** ions, if the amino terminal fragment retains the charge, or **y** ions, if the carboxy-terminal fragment retains the charge (Figure 11). In the case of multiply charged ions, a charge separation can occur to produce complementary ion pairs. Both partners of the complementary pair are not always detected in equal abundance, because they are not equally stable against further fragmentation or because instrument discrimination may enhance or diminish one partner of the pair. Although **b** and **y** ions are considered to be the most useful sequence ion types, because they correspond to cleavage of the amide bond, other ion types are observed and used in spectral interpretation as reported in Figure 11.

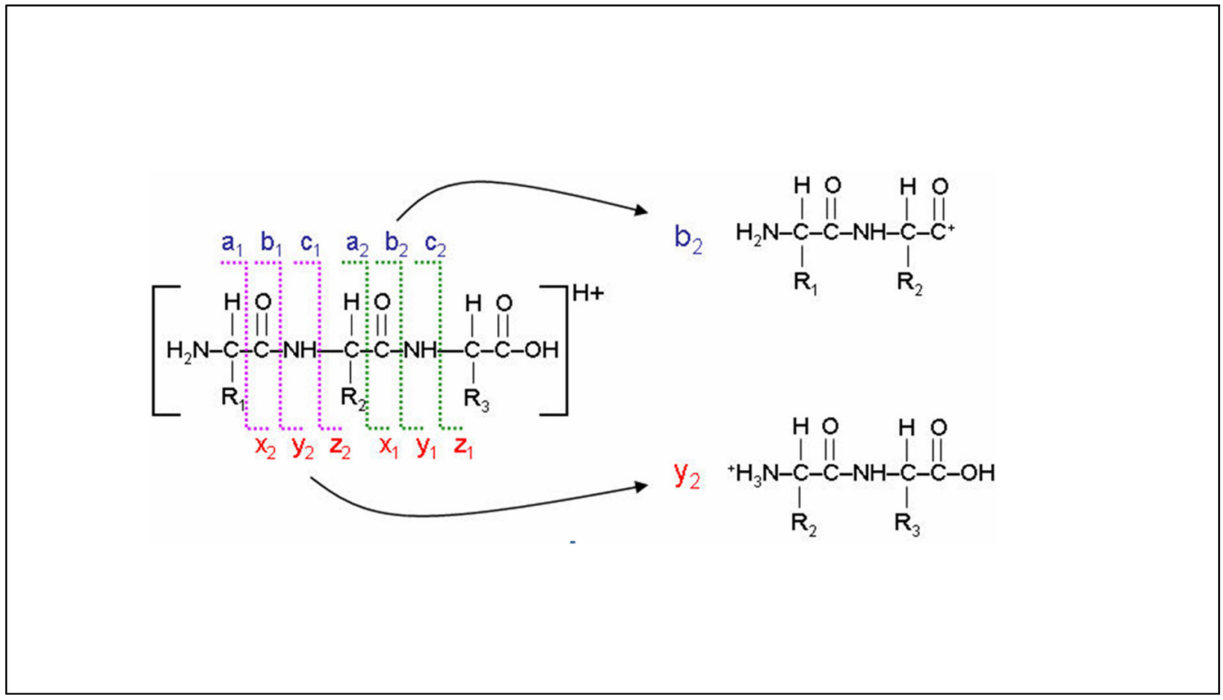

Figure 11. Although **b** and **y** ions are considered to be the most useful sequence ion types, because they correspond to cleavage of the amide bond, other ion types are observed and used in spectral interpretation. These include **a** ions which correspond formally to loss of CO from **b** ion; a Δm= 28 Da between two peaks suggests an **a-b** ion pair and is useful in identifying the ion series to which the peaks belong. The **y** series is sometimes accompanied by satellite peaks formally corresponding to NH3 loss from the **y** ions, allowing designation of **y** ion series. Ions that correspond to immonium ions, or fragments of immonium ions, of individual amino acid residues in a peptide are often detected, even for residues from the internal portion of the sequence.

1.7 Aim of the thesis

The aim of this study was to obtain insights into mechanisms of imatinib resistance independent from the Bcr-Abl activity. The imatinib-resistant KCL22R and sensitive KCL22S cells were used as experimental model. The KCL22R cells and its sensitive counterpart KCL22S were established by Junia Melo and co-workers [24], to analyse imatinib resistance *in vitro.* Because none of the known resistance mechanisms has been detected in these cell lines [24], novel mechanisms could be envisaged. Imatinib resistance has been studied in four imatinib-resistant cell lines: AR230, LAMA84, K562 and KCL22 [24,66]. AR230 cells are characterized by up-regulation of the Bcr-Abl protein associated with amplification of the BCR-ABL gene. In addition to this mechanism, LAMA84 cells over-express the multidrug resistance P-glycoprotein, thereby indicating that imatinib resistance occurs via at least two mechanisms in these cells. Bcr-Abl is not over-expressed in K562 cells, but the imatinib IC50 for the inhibition of Bcr-Abl autophosphorylation was increased in resistant clones [24]. None of the afore-reported mechanisms of resistance was detected in KCL22R cells. Imatinib caused an elevated growth rate and resistance to apoptosis in KCL22R cells [67]. Autophosphorylation of Bcr-Abl in KCL22R cells was suppressed by imatinib, as occurs in KCL22S cells [68], which suggests that KCL22R cells have evolved an alternative means for survival that bypasses dependence on the primary oncoprotein activity. KCL22R cells did not require higher imatinib threshold for tyrosine kinase inhibition. Moreover, KCL22S cells exhibited typical features of the quiescent hematopoietic Ph+ stem cells [69]. It has been in fact shown that imatinib, in combination with a farnesyltransferase inhibitor, induced KCL22S growth arrest but the apoptosis was less evident in KCL22S than in other CML cells [70]. KCL22 cells are then a good model to be used to gain insights into

the mechanisms of imatinib resistance. This PhD project was a part of a multi-topic project that combines microarray, proteomic and clinical studies. Here the author illustrates the results obtained during the four year PhD course.

Chapter 2

MATERIALS AND METHODS

2.1 Drug

STI571 was kindly provided by Novartis Pharma (Basel, Switzerland). A 10 mM stock solution was prepared by dissolving the compound in sterile phosphate-buffered saline (PBS) or dimethylsulfoxide (DMSO).

2.2 Cell Culture

KCL22S, KCL22R and K562 cells were grown in RPMI 1640 medium (Gibco, Paisley, UK) supplemented with 10% fetal bovine serum (FBS) and 1 mM L-glutamine, 100 U/ml penicillin, and 50 µg/ml streptomycin at 37 °C in a water saturated atmosphere of 5% CO_2 in air. KCL22R cells were supplemented with 1µM imatinib mesylate. This cell line has been supplied from Professor Junia V. Melo of the Division of Haematology, Institute of Medical & Veterinary Science, Adelaide SA, Australia.

2.3 Cell viability assay

Cells were plated at a density of 5×10^5 cells/ml in RP-10 with or without 1µM and 5 µM imatinib. Cells were stained with 0.5% Trypan Blue solution and vital cells were counted after 5 min at 37°C. Aliquots were taken out at 24-hour intervals for assessment of cell viability by Trypan Blue exclusion for 4 days. K562 cells, sensitive to imatinib treatment, served as internal control.

2.4 Sample preparation for 2D-DIGE

To obtain total protein extracts, cells were washed twice with cold PBS, centrifugated at 1000 rpm for 5 min and resuspended with a lysis buffer containing 7M urea, 2M

thiourea, 30 mM Tris-HCl pH 8.5, 4% CHAPS (w/v), 1x Complete® EDTA free, containing a cocktail of protease inhibitors (Roche Applied Science, Indianapolis, IN, USA). Protein extracts were incubated at 4°C for 5 min and than sonicated to disrupt the cells and to shear the DNA and RNA in the cell. Protein samples were cleared from cell debris by centrifugation at 14000 rpm at 4°C for 20 min and then purified using the 2-D Clean-up Kit (GE Healthcare, Piscataway, NJ, USA) following supplier's instructions. Protein samples were then resuspended in lysis buffer. In order to perform the reaction between the N-hydroxysuccinimidyl ester reactive group of the CyDye fluorochrome and the epsilon amino group of lysine residues of proteins, protein solution pH was adjusted to the value of 8.5. Protein quantification was performed with the 2-D Quant Kit (GE Healthcare) by reading protein absorbance at 480 nm. To perform a successful CyDyes labeling using the Ettan DIGE Manual, protein concentrations was adjusted between 5 and 10 mg/ml of lysis buffer.

2.5 Labeling efficiency and same same same tests

The labeling efficiency of the samples with the CyDye DIGE Fluors was tested, before DIGE experiment, by performing the following reactions:

- 50 µg of total KCL22 protein extract was labeled with 400 pmol of Cydye Cy5.
- 50 µg of total *E. coli* protein extract, used as control, was labeled with 400 pmol of Cydye Cy5. *E. coli* protein extract has already been labeled successfully.

Labeling reactions were carried out in the dark on ice for 30 min before quenching with 1 µl of a 10 mM L-Lysine solution for 10 min. Serial dilutions of 25 µg, 12.5 µg and 6.25 µg of KCL22 and *E.coli* protein lysates were made. Proteins were then resolved on two one-dimensional SDS gel with a concentration of 12.5%

polyacrylamide. The gels were than acquired at the Cy5 wavelength using the Typhoon 9400 imager (GE Healthcare) and processed and analyzed with Image Quant Analysis software (GE Healthcare) to verify that the labeling efficiency of the protein sample is comparable to the control.

The “same same same” test was performed to verify that none of the three Cydyes labels the same test sample preferentially. 50 µg of total KCL22 protein extract was labeled with 400 pmol of each Cydye. Proteins were resolved on a two-dimensional SDS 12.5% polyacrylamide gel (26x20 cm) by using an Ettan DaltTwelve system (GE Healthcare). After electrophoretic separation, gels were scanned using the Typhoon 9400 imager (GE Healthcare). Fluorescence-labeled proteins were visualized at the appropriate wavelength for Cy3, for Cy5 and for Cy2. Images were acquired with Image Quant Analysis software (GE Healthcare). The images were processed and analyzed by DeCyder v5.02 software (GE Healthcare). The comparison of the volume of fluorescence for all spots allowed us to define a threshold. All variations under this threshold were not considerate.

2.6 Protein labeling with CyDye DIGE Fluor dyes

Protein extracts were labeled with Cy2, Cy3 and Cy5, according to the Ettan DIGE User Manual (18-1173-17 Edition AA, GE Healthcare). Labeling reactions were carried out in the dark on ice for 30 min before quenching with 1 µl of a 10 mM L-Lysine solution for 10 min. 50 µg of each protein sample from KCL22R and KCL22S cells, labeled with 400 pmol of Cy3 or Cy5, were loaded in each analytical gel. 4 different biological replicates for KCL22S and 4 replicates for KCL22R were loaded on 4 gels as reported in Table 1. To avoid technical interferences and fluorochromes bias the experiments were performed swapping the dyes as reported in Table 1. In

each gel the pool standard was constituted by 50 µg of protein derived from a mixture of all biological replicates, labeled with Cy2. This standard enables accurate inter-gel statistical analysis.

Table 1. 2D-DIGE experimental design

Gel	Cy3[a] (50 µg)	Cy5[a] (50 µg)	Cy2[a] (50 µg)
1	KCL22S replicate 1	KCL22R replicate 2	Pool standard[b]
2	KCL22S replicate 2	KCL22R replicate 1	Pool standard[b]
3	KCL22R replicate 3	KCL22S replicate 4	Pool standard[b]
4	KCL22R replicate 4	KCL22S replicate 3	Pool standard[b]

[a]Fluorochrome compounds used for protein labeling

[b]Constituted by 25µg of protein from each of the eight samples

2.7 2D separation of KCL22R and KCL22S protein samples

Protein samples, mixed as described in Table 1, were separated on 18-cm-long IPG-strips with a 3-11 non linear pH range (GE Healthcare). Strips were rehydrated before use, without protein samples, with 350 µl of rehydration buffer containing 7M urea, 2M thiourea, 4% CHAPS (w/v), DTT 2% (w/v), 2% Pharmalyte range PH3-10 (v/v), overnight at room temperature. The samples were mixed to an equal volume of sample buffer containing 7M urea, 2M thiourea, 4% CHAPS, 2% DTT (w/v) and 1% Pharmalyte, range PH3-10 (v/v), (GE Healthcare). The samples were loaded on the pH 3-11NL IPG strips by the anodic cup-loading method. The first dimension (IEF) was carried out on the Ettan IPGphor system (GE Healthcare) for 18 h for a total of 60 kV/h at 20°C using the following protocol:

- Step 1 300 V for 4h
- Step 2 from 300 V to 1000 V for 6 h
- Step 3 from 1000 V to 8000 V for 3 h
- Step 4 8000 V for 5 h

After IEF, the proteins were reduced by incubating strips in 100 mM Tris pH 8.0, 7M urea, 30% glycerol (v/v), 2% SDS (w/v) containing 0.5% DTT for 15 min. Proteins were then alkylated for 15 min using the same buffer containing 4.5% IAA (w/v) instead of DTT. The second dimension (SDS-PAGE) was carried out on 11% polyacrylamide gels (18x20 cm) by using an Ettan DaltTwelve system (GE Healthcare) at 2W/gel until the bromophenol blue reached the bottom of the gel.

Two independent two-dimensional preparative gels were run with the same condition applied for the analytical gels, using for each gel, 0.5 mg of protein extract from KCL22R and KCL22S cells, respectively. Preparative gels were washed with a fixing solution of 40% methanol, 10% acetic acid, 50% water for 3 h before overnight staining in SYPRO Ruby (Molecular Probes, USA) with gently agitation, in the dark.

2.8 Image analysis with DeCyder software

After electrophoretic separation, gels were scanned using the Typhoon 9400 imager (GE Healthcare) at a resolution of 100 μm. Fluorescence-labeled proteins were visualized at the appropriate excitation/emission wavelengths: 532/580 nm for Cy3, 633/670 nm for Cy5 and 488/520 nm for Cy2. Preparative gel images were acquired using the Typhoon imager at excitation/emission wavelengths of 457/610 nm. All gels were scanned by using the same parameters, selected to prevent pixel saturation.

Images were acquired with Image Quant Analysis software (GE Healthcare). The images were processed and analyzed with the Differential In-gel Analysis (DIA) and

Biological Variation Analysis (BVA) modules contained in the DeCyder v5.02 software package (GE Healthcare). Protein spots were detected and quantified with the DIA module. The maximum number of estimated spots was fixed at 5000. The Cy2, Cy3 and Cy5 images derived from all single gels were merged using DIA. In addition, DIA was used to detect spot boundaries and calculate spot volumes, normalized versus the volume of the corresponding spot present in the pool standard of the same gel. Protein spots that matched between gels were obtained using the biological variation analysis module (BVA). The Cy2 image that contained the highest number of spots was assigned as "Master image". The spot boundary maps of the master image were used as template. Matching of protein spots across gels was performed automatically. A standard abundance for each spot was thus calculated thereby allowing inter-gel variations. Each spot intensity was then expressed as mean of 4 standard abundances calculated for the four gels described in Table 1. Spot intensities were then compared in the two conditions used: KCL22R and KCL22S cells. Statistical significance of differences in spot intensity was determined by Student's t-test. Only protein spots with at least 1.25-fold changes in volume ($p \leq 0.01$) after normalization were considered significantly altered. The accuracy of spot matching was verified by manual inspection of gels.

2.9 In *situ* idrolysis of protein spots

Protein spots on preparative gels were chosen for excision on comparison with the analytical gel. Spots of interest were picked using an Ettan Spot Picker (GE Healthcare). Gel pieces were washed in 100% ACN for 15 min and subsequently rehydrated in a modified trypsin (Sigma) solution (10 ng/µl) in 50 mM ammonium bicarbonate pH 8.5, at 4°C for 1 h. The enzymatic solution was then removed. A new

aliquot of buffer solution was added to the gel particles and incubated at 37°C overnight. The supernatant was collected whereas gel pieces were subjected to another extraction in ACN at 37°C for 15 min. The supernatant fraction and samples obtained from extraction steps were pooled and dried in a vacuum centrifuge.

2.10 Protein identification by mass spectrometry and bioinformatics

Peptides obtained by protein digestion with trypsin were resuspended in 0.2% formic acid before injection using the LC/MSD Trap XCT Ultra (Agilent Technologies, Palo Alto, CA, USA) equipped with a 1100 HPLC system and a chip cube (Agilent Technologies). After loading, the peptide mixture (7 µl in 0,2% HCOOH) was first concentrated and washed at 4 µl/min in 40 nl enrichment column (Agilent Technologies chip), with 0.1% formic acid as the eluent. The sample was then fractionated on a C18 reverse phase capillary column (75 µm x 43 mm) at a flow rate of 200 nl/min with a linear gradient of eluent B (2% formic acid in acetonitryl) in eluent A (2% formic acid) from 5 to 60% in 50 min. Elution was monitored on the mass spectrometer without a splitting device. Peptides were analyzed using data-dependent acquisition of one MS scan (mass range from 400 to 2000 m/z) followed by MS/MS scans of the three most abundant ions. Dynamic exclusion was used to acquire a more complete survey of the peptides by automatic recognition and temporary exclusion (2 min) of ions from which definitive mass spectral data had previously been acquired. Moreover a permanent exclusion list of the most frequent peptide contaminants (keratins and trypsin doubly and triply charged peptides, 403,20; 517,00; 519,32; 525,00; 532,90; 559,32; 577,30; 587,86; 616,85; 618,23; 721,75; 745,90; 747,32; 758,43; 854,30; 858,43; 896,30; 1082,06) was used in the acquisition method in order to focus the analyses on significant data.

Data analysis was performed using Mascot software (http://www.matrixscience.com) against the NCBI database (www.ncbi.nlm.nih.gov). The protein search was based on the following parameters: specificity of the proteolytic enzyme used for hydrolysis (trypsin); no protein molecular weight was considered; up to 1 missed cleavage; cysteines as S-carbamidomethylcysteines; unmodified N- and C-terminal ends; methionines both unmodified and oxidized; putative pyroGlu formation by Gln; precursor peptide maximum mass tolerance of 400 ppm and a maximum fragment mass tolerance of 0.6 Da. According to the probability-based Mowse score, the ion score is -10xLog(P), where P is the probability that the observed match is a random event. Individual scores >41 indicate identity or extensive homology ($p \leq 0.05$). All the MS/MS spectra displaying a Mascot score higher than 41 had a good signal/noise ratio leading to an unambiguous interpretation of the data. Individual MS/MS spectra for peptides with a Mascot score equal to 41 were inspected manually and included in the statistics only if a series of at least four continuous y or b ions were observed.

2.11 Western blot analysis

KCL22R and KCL22S protein extracts (25 µg) were resolved on a 10% SDS-PAGE gel and then transferred onto nitrocellulose membranes (GE Healthcare) by Mini Tans-Blot electrophoretic transfer (Biorad). The membranes were blocked in 5% non-fat milk in PBS pH 7.5 for 2 h and incubated over night at 4°C with 1% milk/PBS pH 7.5 and 0.05% TWEEN containing specific mouse anti-Annexin A1 (1:5000) (BD Biosciences, Erembodegem, Belgium), anti-Heat shock protein 70 (1:200), anti-Rho GDP dissociation inhibitor (2.5 µg/ml) (Abnova Corporation, Taipei, Taiwan), anti-Grp78 (1:500) (Santa Cruz Biotechnology, Heidelberg, Germany), anti-Heat shock protein 60 (1:1000) (Stressgen, Victoria, BC Canada) and anti-Nqo2 (1:1000)

(Abnova Corporation, Taipei, Taiwan) or rabbit anti-Heat Shock Protein 27 (1:1000), anti-human transcription factor 1 (1:5000) (Stressgen, Victoria, BC Canada), anti-Hck (1:1000), anti-p-Hck (1:1000), anti-Lyn (1:2000), anti-pLyn (1:1000), anti-Crkl (1:1000), anti-Erk 1/2 (1:1000) and anti-pErk (1:500) (Santa Cruz Biotechnology), anti-pCrkl (Cell Signaling Technology, Danvers, MA, USA), anti-Carbonic anhydrase II (2 µg/ml) (Rockland Gilbertsville, PA, USA), anti-Malic enzyme (0,5 µg/ml) and anti-Idh1 (1 µg/ml) (Sigma Prestige Antibodies, Saint Louis, USA), anti-Eef1d (1:1000), anti-Shp1 (1:500) and anti-Shp2 (1:1000) (Santa Cruz Biotechnology, Heidelberg, Germany), anti-Shp2-pTyr 542 (1:1000) (Cell Signaling Technology, Danvers, MA, USA), and goat anti-Peroxiredoxin I (1:200) and anti-Fuse Binding Protein 1 (1:200) (Santa Cruz Biotechnology). A mouse anti-Gapdh (Sigma-Aldrich, Saint Louis, MO, USA) antibody was used as loading control, at a dilution of 1:5000 at 4°C overnight. Immunoblot detections were carried out using HRP-conjugated anti-mouse (1:5000), anti-rabbit (1:10000), or anti-goat (1:40000) secondary antibodies (Ge Healthcare) with 1% milk/PBS pH 7.5 and 0.05% TWEEN for 45 min. Immunoblots were detected using the ECL-Advance Western Blotting Detection kit (GE Healthcare) by chemioluminescence. The resulting western blot images were scanned by PDquest 7.1 software (Biorad). The protein band images on X-ray films were acquired with the Chemidoc XRS system (Bio-Rad). Band volumes were normalized by using Gapdh as control, visualized on the same film. Densitometric measurements were made using the Quantity One 4.5 tool (Bio-Rad).

2.12 Real-time quantitative PCR assay

Total RNA was extracted using the RNeasy kit (Qiagen, Hilden, Germany) and treated with RNase-free DNase (Qiagen), according to the manufacturer direction. One microgram of total RNA was pre-warmed for 10 min at 70°C and incubated for 10 min at 25°C; the RNA solution was then incubated for 45 min at 42°C and 3 min at 99°C in a 20-μL reaction mixture containing 10 mM Tris–HCl (pH 8.3), 50 mM KCl, 5.5 mM $MgCl_2$, 1 mM of each deoxyribonucleotide, 20 U of RNAsin (Pharmacia, Uppsala, Sweden), 25 mM random examers (Pharmacia), 10 mM of DTT (Pharmacia), and 100 U of MoMLV reverse transcriptase (BRL, Bethesda, MD, USA). Real-time reverse transcription-PCR (RT-PCR) for ANXA1, BCR-ABL (p210) and the housekeeping gene ABL was performed with an ABI PRISM 7900 HT Sequence Detector (Applied Biosystems, Milan, Italy) using TaqMan inventoried gene expression assays (Applied Biosystems), according to the manufacturer's protocol. Linearity of PCR amplification and equal efficiency for primer/probe systems was demonstrated for BCR-ABL, ANXA1 and ABL. The ($2^{-\Delta\Delta Ct}$) algorithm was used to determine the expression of BCR-ABL and ANXA1 mRNA. The experiments were carried out from quadruplicate independent cultures.

2.13 In *silico* characterization of identified proteins: data mining

Proteins were grouped with regard to their Gene Ontology molecular functions and cellular localization annotations (www.geneontology.org) using GeneSpring GX software version 7.3, setting p-value equal to or smaller than 0.05. In addition, data were analyzed through the use of Ingenuity Pathway Analysis software 7.0 (IPA) (Ingenuity Systems, Inc. www.ingenuity.com). Drawing on published, peer-reviewed literature, IPA constructs networks of direct and indirect interactions between

orthologous mammalian genes, proteins and endogenous chemicals. These relationships include those that occur due to disease and/or environmental input. This system can generate a set of networks with a maximum size of 35 genes/gene products. Each network is characterized by a score computed according to the fit of the user's set of focus genes/gene products with all the genes/gene products stored in the knowledge base. The score is derived from a p-value (equal to or smaller than 0.05, Fischer's exact test) and indicates the likelihood of the focus genes/gene products in a network being found together due to random chance. Biological functions were then assigned to each network.

2.14 NADPH assay

NADP and NADPH levels were determined using commercial colorimetric system (Biovision, Mountain View, CA). Briefly, $1x10^6$ KCL22R and KCL22S cells were lysed. Half of the lysate was used to measure total NADP/NADPH (NADPt) and the other half to measure NADPH only. In the latter case, NADP was decomposed by heating at 60 °C for 30 min, while NADPH was still intact. The corresponding OD 450 nm measurements were read in a NADPH standard curve to obtain concentrations. The NADP/NADPH ratio was calculated as (NADPt-NADPH)/NADPH. All the above assays were done in triplicates in three independent experiments.

2.15 GSH assay

$1x10^6$ KCL22R and KCL22S cells were washed twice in PBS, harvested and centrifuged at 1700xg for 10 min at 4°C. The pellets were lysed by adding 100 µl of perchloric acid (3%) for 15 s and centrifuged at 20,000g for 10min at 4°C. The supernatant was neutralized with NaH_2PO_4 0.1 M, EDTA 5mM. GSH content was

measured by adding 600 mM DTNB 5,5'-dithio-bis(2-nitrobenzoic acid) and read at 412 nm. After lysis, pellets from perchloric acid were resuspended in NaOH 1M and protein amount was measured by the Bradford assay. GSH content was normalized as the ratio between O.D./mg protein.

2.16 Shp1 knock-in and Shp2 Knock-down in KCL22R cells

Human full-length SHP1 sequence (NCBI NM_002831.4) was cloned in retroviral p-IRES2-EGFP (p-IRES-SHP1-neo) expression vector (Clontech, Montain View, CA, USA) by polymerase chain reaction (PCR) using primers pIRES-SHP1. KCL22R cell line was transfected by Lipofectamine 2000 (Invitrogen Life Technologies, Carlsbad, CA) in 6-well plates with 4 μg/ml of p-IRES-SHP1 or mock vector (p-Control-neo) according to the protocol provided by the company.

Knock-down of SHP2 was obtained by shRNA technology using pShag Magic retroviral vector (pSM2) purchased from Open Biosystem (Huntville, AL, USA, clone ID V2HS_170946). KCL22R cell line was transfected with 4 μg/ml of pSM2-shRNASHP-2-puro or pSM2 carrying a scramble shRNA sequence (pSM2-Control-puro) by Lipofectamine 2000 (Invitrogen) in 6-well plates following the manufacturer's instructions. After transfection, cells were grown in RPMI complete media containing 1μg/mL puromycin (Sigma, St. Louis, MO) or 0.8 mg/ml neomycin to select clones with a stable expression.

2.17 Immunoprecipitation assay

2×10^7 KCL22R and KCL22S cells were washed with cold phosphate-buffered saline three times and centrifugated at 1000 rpm for 10 min. The pellet was incubated with 1,5 ml of cold lysis buffer containing Tris-HCl 50 mM pH 7.5, 150 mM NaCl, 1mM

NaF, 1 mM PMSF, 1% Nonidet P-40, 1mM EDTA, 1mM sodium orthovandate, protease inhibitor cocktail (Complete mini EDTA-free Roche Applied Science) for 30 min in ice and then cleared by centrifugation at 15,000xg for 20 min at 4°C. 500 µg of protein lysates were pre-clearing with 2 µg of the appropriate control, normal rabbit IgG (Santa Cruz Biotechnology, Santa Cruz, CA, USA), corresponding to the host species of the primary antibody used for the immunoprecipitation, for 2h at 4°C on a rocker platform. The solution was then incubated with 50 µl of slurry Protein A/G-PLUS-Agarose beads (Santa Cruz Biothecnology Santa Cruz, CA, USA) for 1h at 4°C on a rocker platform. Lysate pre-clearing allows to reduce non-specific binding of proteins to agarose beads and to remove proteins that bind immunoglobulins non-specifically. Beads were then centrifugated at 8000xg for 5 min at 4°C. The supernatant was incubated with primary polyclonal antibodies (20 ug) of anti-Shp1, anti-Shp2 or anti-Annexin A1 (Santa Cruz Biotechnology, Santa Cruz, CA, USA), to perform the relative immunoprecipitation assay, overnight at 4°C on a rocker platform and then incubated with 50 µl of fresh Protein A/G-PLUS-Agarose beads for 5h at 4°C. Beads were then centrifugated at 8000xg for 5 min at 4°C. After extensive washing of the pellet beads with IP buffer, containing Tris-HCl 50 mM pH 7.5, NaCl 150 mM, NaF 1mM, PMSF 1 mM, Nonidet P-40 1%, 1mM EDTA, 1mM sodium orthovandate, Protease inhibitor cocktail, (Complete mini EDTA-free Roche Applied Science), the resulting immune complexes were eluted from the beads with 2X electrophoresis sample buffer at 90°C for 10 min. Supernatants were then separated by electrophoresis in 10% SDS/polyacrylammide gels and then transferred to nitrocellulose paper for immunoblot analysis, performed as described above.

2.18 Primary cells from CML patients

Before imatinib treatment, bone marrow samples from nine patients with CML in chronic phase at diagnosis were analysed. Written informed consent to the use of their cells in this study was obtained in all cases, according to the requirements of the local research ethic committee. None of the patients carried a mutated Bcr-Abl, as shown by sequencing of the tyrosine kinase or BCR-ABL gene amplification (the analysis was performed at the sequencing facility of Ceinge, in Naples). Mononuclear cells were isolated by density-gradient separation from bone marrow of CML patients. Cells were cryopreserved at 10^7/ml in liquid nitrogen. To prepare protein samples, the cells were rapidly thawed, washed three times in PBS, and 10^7 cells were resuspended in lysis buffer constituted by 10 mM NaH_2PO_4 (pH 7.4), 150 mM NaCl, 5mM EDTA, 1% TritonX-100, supplemented with 2 mM Na_3VO_4, 2 mM PMSF, 10 mM NaF and 1x Complete® EDTA free containing a cocktail of protease inhibitors (Roche Applied Science, Indianapolis, IN, USA).

Chapter 3

RESULTS

3.1 Evaluation of the known imatinib resistance mechanisms in KCL22R cells

To determine if already known mechanisms of imatinib resistance [23] operate in KCL22R cells, the level of proteins already involved in such mechanisms was measured. Therefore the expression of pHck, Hck, pLyn, Lyn, pCrkl and Crkl was analysed by Western blot. As shown in Figure 12, the expression of these proteins and their pattern of phosphorylation were similar in the KCL22R and KCL22S cell lines.

In addition BCR-ABL mRNA expression, evaluated by quantitative RT-PCR, was similar in KCL22S and KCL22R cells (Figure 13).

Furthermore there were no mutations in the Bcr-Abl kinase domain (the analysis was performed at the sequencing facility of Ceinge, in Naples).

A previous study showed similar levels of P-gp in KCL22S and KCL22R cells [68]. Cell viability was next examined in KCL22S and KCL22R cells with K562 cells as control. Cell viability was reduced in KCL22S and K562 treated with 1μM or 5μM imatinib (Figure 14A and B). In contrast, the viability of KCL22R cells (Figure 14C) was not affected by 1μM and 5μM imatinib. Moreover in KCL22 cells, significant differences in growth inhibition between sensitive and resistant clones were observed only after 4 days of 1μM imatinib, in contrast to K562 (Figure 14A and B) and other sensitive cell lines [24] in which the same effect was achieved in less time. KCL22S cells were intrinsecally less sensitive than other CML cell lines to imatinib. Taken together, these observations indicate that resistance may occur in KCL22R cells by mechanisms other than those already known.

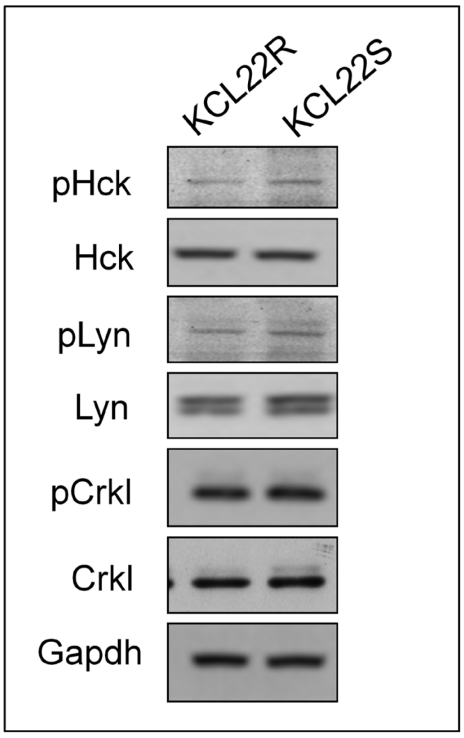

Figure 12. Western blot analysis of total protein lysates of KCL22R and KCL22S cells. Proteins were separated on 10% SDS-PAGE and immunoblotted with antibodies against pHck, Hck, pLyn, Lyn, pCrkl and Crkl. Gapdh served as control.

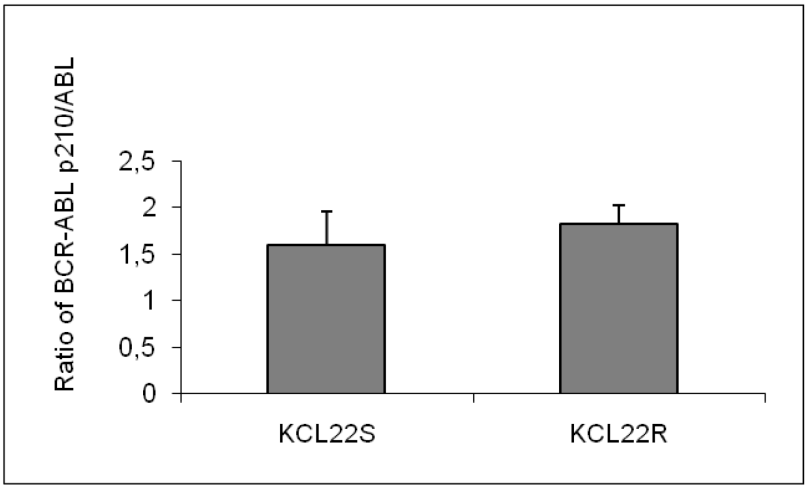

Figure 13. Quantitative RT-PCR analysis. Expression level of BCR-ABL mRNA in KCL22S and KCL22R cell lines. The results, obtained from quadruplicate independent cultures, are shown as means±SD.

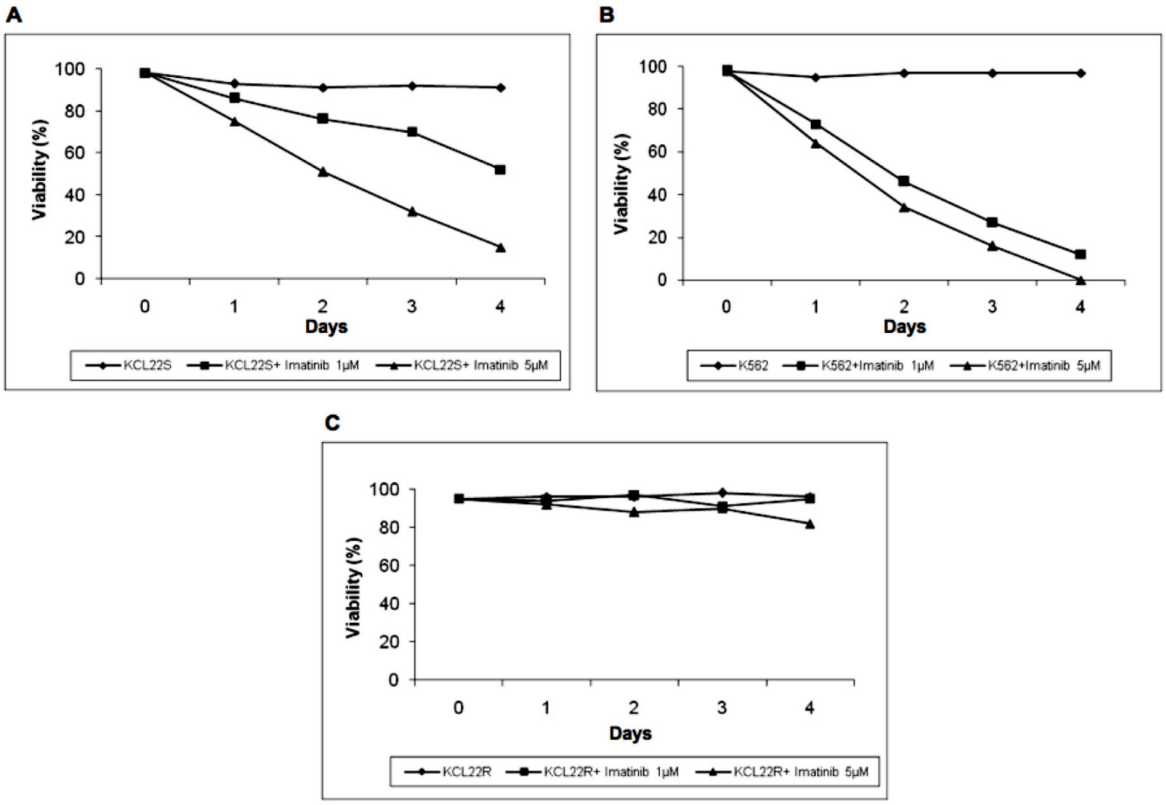

Figure 14. Cell viability assessed by Trypan Blue exclusion of KCL22S (A), K562 (B) and KCL22R (C) cell lines cultured without or with 1 µM and 5 µM imatinib. Results represent the mean ± SD of viable cells taken from independent quadruplicate cultures.

3.2 2-DIGE analysis: labeling efficiency and same same same tests

Before DIGE experiment the labeling efficiency of the samples with the Cy5 dye was tested. To this aim, the labeling efficiency of KCL22 protein extract was compared with that of a control that has already been labeled successfully. The control was constituted by *E. coli* total protein extract. As shown in Figure 15 proteins were resolved on two one-dimensional SDS-PAGE gels, as described in the “Materials and methods” section. The gels were acquired at the Cy5 wavelength using the Typhoon imager and the relative images were processed and analyzed with the Image Quant Analysis software. The volume of fluorescence, measured for each lane, the relative average values and the labeling efficiency values are listed in Table 2. The labeling efficiency was calculated as ratio between the average volumes of fluorescence of the sample with that of the control.

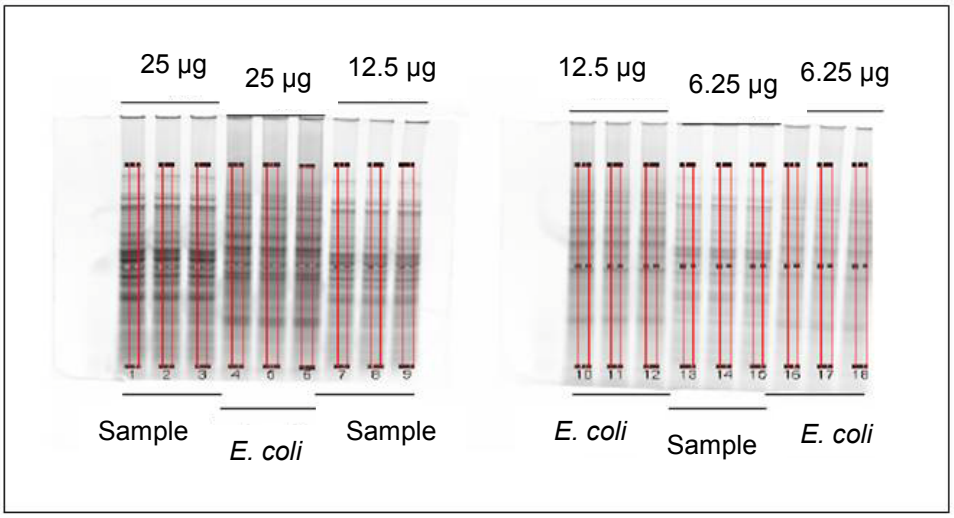

Figure 15. Cy5-gel images of KCL22 (Sample) and *E.coli* protein lysates. Cy5-labeled proteins were loaded and resolved on two one-dimensional 12.5% SDS-PAGE gels using a serial dilution of 25 µg, 12.5 µg and 6.25 µg. The gels were acquired using the Typhoon 9400 imager.

Table 2. Labeling efficiency analysis

Lanes	Volume of fluorescence	Average	Labeling efficiency %
RECT-1	217716363.4	197585916.8	104
RECT-2	186203112.5		
RECT-3	188838274.6		
RECT-4	201880089.1	190129064	
RECT-5	172124090.4		
RECT-6	196383012.5		
RECT-7	102913614.9	92375399.96	112
RECT-8	85961155.73		
RECT-9	88251429.29		
RECT-10	93054671.39	82385220.24	
RECT-11	80334319.81		
RECT-12	73766669.51		
RECT-13	43882175.05	40577700.86	102
RECT-14	37347132.77		
RECT-15	40503794.76		
RECT-16	38429891.99	39635754.45	
RECT-17	37217010.96		
RECT-18	43260360.41		

In addition, to verify that none of the three CyDyes labels the same test sample preferentially, the “same same same” test was performed. By DeCyder software, the volumes of fluorescence for all spots of the sample labeled with Cy2 were compared with those labeled with Cy3 and Cy5, obtaining a similarity of labeling of 98% (Figure 16). The threshold was then set to 1.25 fold-change. All variations under this threshold were not considerate (Figure 17).

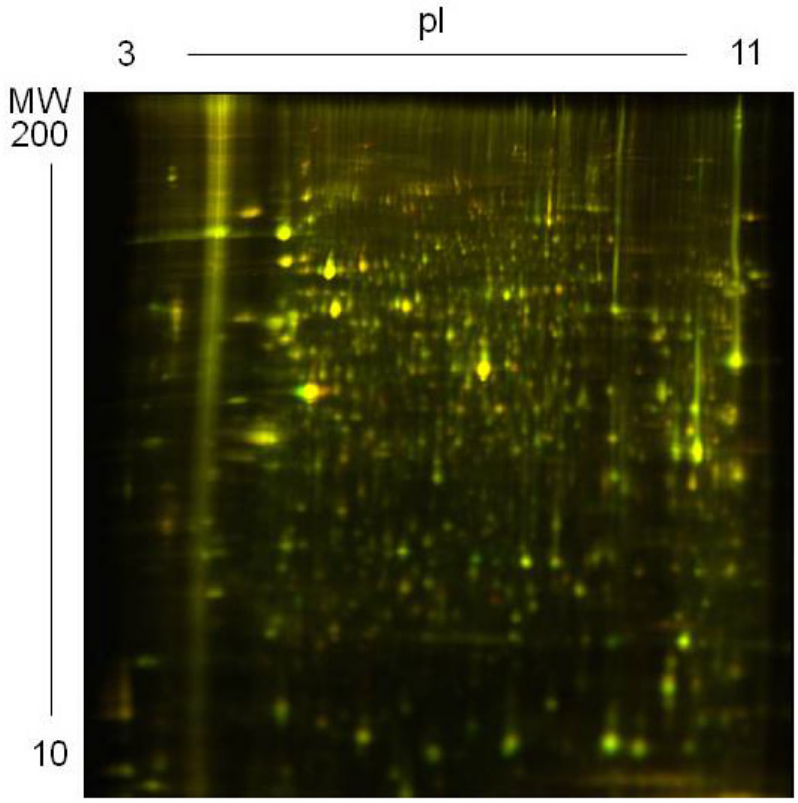

Figure 16. 2D-DIGE image of the same same same gel. Overlapped image of Cy2, Cy3, Cy5 gel images. Isoelectrical focusing was performed using non linear pH 3-11 in the first dimension and 12,5% SDS-PAGE in the second dimension.

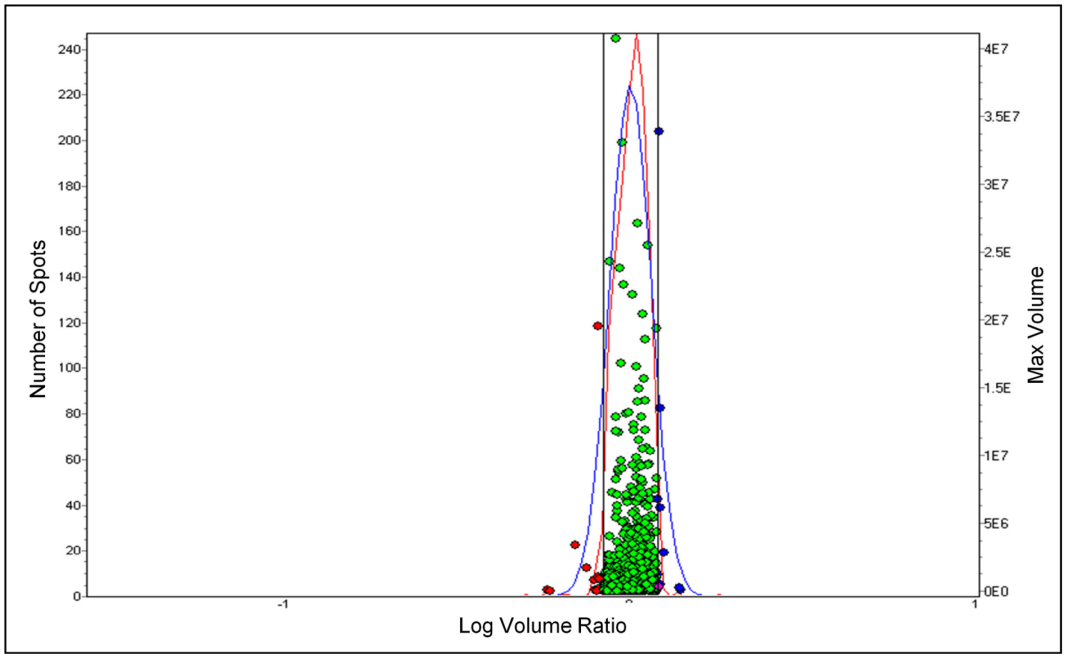

Figure 17. Statistical representation of the overall protein distribution in individual samples, in the same same same test. The red line indicates the number of spots with a specific abundance ratio (log scale). The blue line represents the calculated Gaussian distribution. Red dots represent decreased and blue increased protein content in individual spots detected in both samples (considered from Cy3 → Cy5). Green dots represent equal protein content between the samples. The threshold was set to 1.25 fold-change.

3.3 Identification of differentially expressed proteins by DIGE

To identify proteins differentially expressed between KCL22R and KCL22S cells, protein extracts were first compared between the analytical gels, using two-dimensional DIGE analysis (see "Materials and methods" section and Table 1). Fluorescence-labeled proteins in the 2D analytical gels were acquired at different wavelengths using an imager to generate an image specific for each CyDye. In this way three scans were made of each gel, Cy2, Cy3 and Cy5 scans. In the co-detection step scanned images of each sample were overlaid with the internal standard by the DIA module of the DeCyder software (Figure 18A). By this way every protein in the sample was linked to the corresponding protein spot in the internal standard sample. Following co-detection step, the matching of protein spots across the gels was performed using the BVA module of the DeCyder software. The spot map for the internal standard, with the most detected spots, was used as a template to which all remaining spot maps, for the other internal standards (intrinsically linked to their co-detected sample images), were matched. The spot volume (*i.e.* the sum of the pixel values within a spot minus background) for each experimental sample was directly compared, by the software, to the internal standard. By this way changes in the expression level of individual protein spots, expressed as ratio of protein abundance between KCL22R and KCL22S cells, normalized to the internal standard, were identified. Each spot intensity was then expressed as mean of 4 standard abundances calculated for the four gels described in the Table 1. Statistical significance of differences in spot intensity was determined by Student's t-test. Only protein spots with at least 1.25 fold-changes in volume ($p \leq 0.01$), after normalization, were considered significantly altered. DeCyder software displayed in a graphic the relative abundance of each protein spot in the two conditions used, KCL22R and

KCL22S cells, and defined a fold change expression of each protein, above a biological variation. An example of the DeCyder analysis is reported in Figure 19. After this analysis sixty-eight differentially expressed spots were visualized (Figure 18 B). Differentially expressed protein spots were then matched between the analytical and the SYPRO Ruby stained preparative gels for KCL22R and KCL22S protein extracts. Of the sixty-eight differentially expressed spots, obtained by DIGE analysis, forty-nine spots were matched on the preparative gels. 27 spots were excised from KCL22R (Figure 20A) and 22 from KCL22S (Figure 20B) preparative gels.

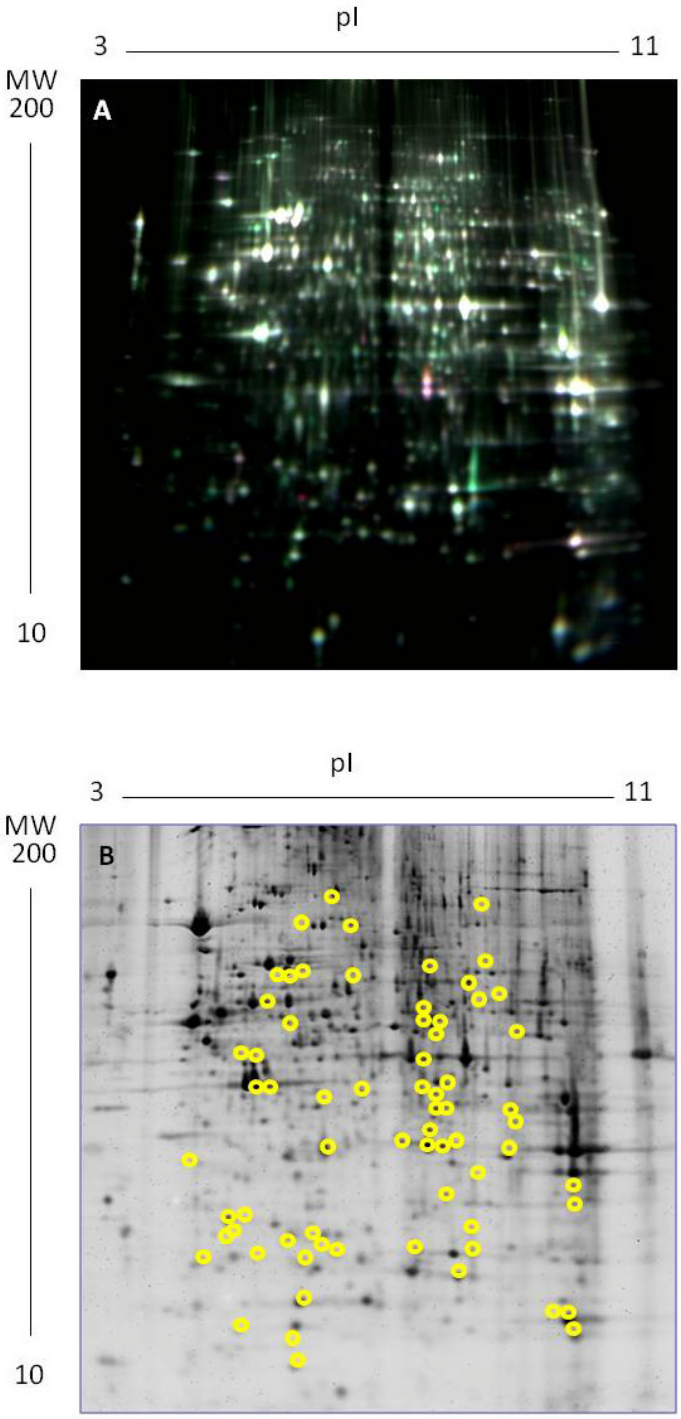

Figure 18. Representative 2D-DIGE analytical (A) and preparative (B) gel images. A: overlapped image of the Cy2, Cy3, Cy5 images of the analytical gel number 1 reported in Table 1. B: Differentially expressed protein spots between KCL22R and KCL22S cells are highlighted in yellow. Isoelectrical focusing was performed using non linear pH 3-11 in the first dimension and 11% SDS PAGE in the second dimension.

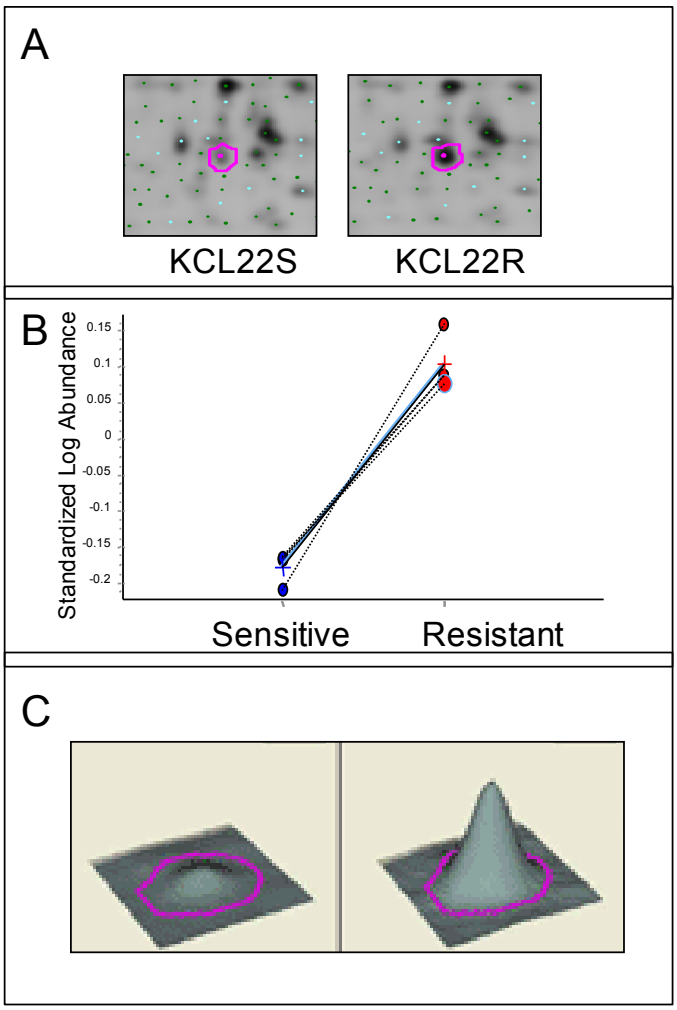

Figure 19. DeCyder software analysis of Me2 protein spot expression in KCL22S and KCL22R cells. A: enlargement of 2D gel region of the spot number 1570 corresponding to the Me2 protein. B: DeCyder graphic displays the relative abundance of Me2 protein spot in the two conditions used: KCL22S and KCL22R cells. C: three-dimensional representation of the relative abundance of Me2 protein spot.

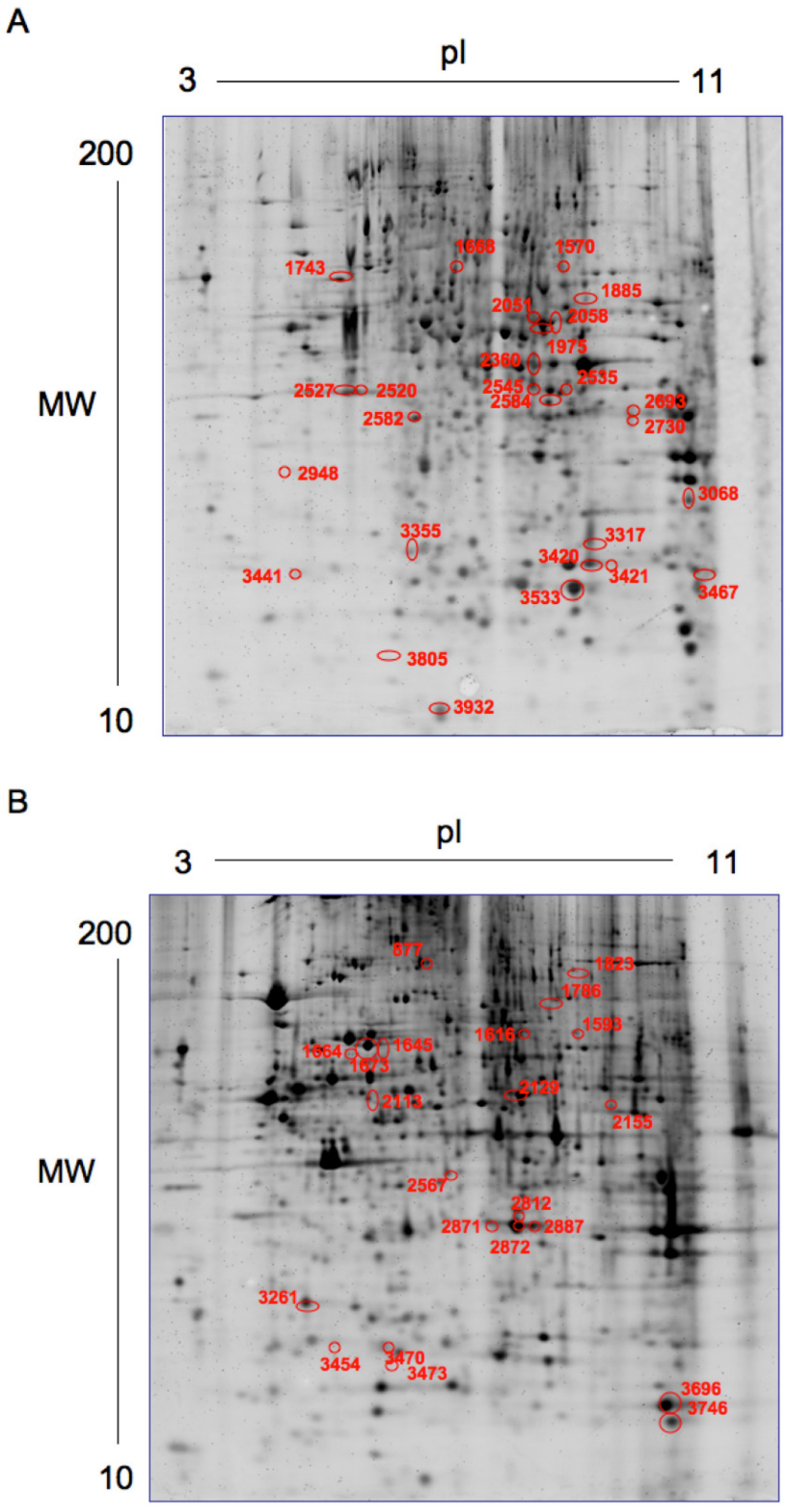

Figure 20. SYPRO Ruby stained preparative 2D gel of KCL22R (A) and KCL22S (B) protein extracts. Gels were carried out with non linear pH 3-11 in the first dimension and 11% SDS PAGE in the second dimension. Red circles indicate spots that were differentially expressed and were picked for mass spectrometry protein identification.

The excised protein spots were subjected to tryptic digestion and the resulting peptides were analysed by mass spectrometry. The proteins over-expressed or under-expressed in KCL22R versus KCL22S cells are listed in Tables 3 and 4, respectively. Proteins over-expressed and under-expressed in KCL22R cells were picked from the gels as shown in Figure 20A and 20B, respectively. 42/49 excised spots were unequivocally identified as a single protein. The 7 spots containing more than one protein were reported on the bottom of Tables 3 and 4. Carbonic anhydrase II, Beta actin, Phosphoserine aminotransferase 1, Phosphoglycerate dehydrogenase, Heat shock 27-kDa protein 1, Annexin A1 and Heat shock 70-kDa protein 1A were detected in more than one spot. This can happen because of post-translational modifications or splice variant status.

TABLE 3. Over-expressed proteins in KCL22R *versus* KCL22S cells

Spot[a]	Fold increase[b]	Gene symbol	Protein name	Gene ID	p-value
1570	2.83	ME2	Malic enzyme 2, NAD(+)-dependent, mitochondrial	4505145	6.7 E-04
3420	2.35	CA2	Carbonic Anhydrase II	179780	5.1 E-06
3317	2.3	CA2	Carbonic Anhydrase II	179780	2.0 E-06
3421	2.24	CA2	Carbonic Anhydrase II	179780	2.5 E-03
3805	1.88	APRT	Adenine phosphorybosyltransferase	76827869	1.6 E-05
3467	1.84	MACROD1	MACRO domain containing 1	13112029	3.2 E-03
1743	1.77	LCP1	L-plastin	62898171	1.1 E-04
3932	1.63	FTL	Ferritin light subunit	182516	1.5 E-04
2582	1.61	LDHB	Lactate dehydrogenase B	4557032	2.2 E-03
1668	1.5	LTA4H	Leukotriene A4 hydrolase	4505029	7.8 E-03
2527	1.41	ACTB	Beta actin	4501885	5.3 E-04
2948	1.48	EEF1D	Human elongation factor-1-delta	38522	6.0 E-03
3441	1.47	ARHGDIA	Rho GDP dissociation inhibitor	36038	1.9 E-03
2584	1.43	FAHD1	Fumarylacetoacetate hydrolase	4557587	2.3 E-04
1975	1.42	TCP1	Chaperonin containing TCP1	4502643	3.7 E-05
2520	1.38	ACTB	Beta actin	4501885	4.3 E-03
2693	1.36	PSAT1	Phosphoserine aminotransferase 1	16741698	2.4 E-06
1885	1.36	CAP1	Adenyl cyclase-associated protein 1	15530330	1.3 E-03
2535	1.36	IDH1	NADP-dependent isocitrate dehydrogenase	3641398	5.7 E-03
3355	1.35	PSME1	Proteasome activator complex subunit 1	2780871	1.7 E-04
2730	1.3	PSAT1	Phosphoserine aminotransferase 1	16741698	2.4 E-04
3533	1.29	TPI1	Triosephosphate Isomerase	4507645	1.8 E-04
3068	1.26	VDAC1	Porin 31HM	238427	2.5 E-03
2058	1.33	PHGDH	Phosphoglycerate dehydrogenase	23308577	5.1 E-03
		IMPDH2	Inosine-5'-monophosphate dehydrogenase	307066	
2545	1.29	ACTR2	Actin-related protein 2 isoform b	5031571	8.3 E-03
		PCBP2	Poly(rC)-binding protein 2 isoform b	14141166	
2360	1.28	EEF1G	Eukaryotic translation elongation factor-1-gamma	496902	9.4 E-04
		SSB	Autoantigen La	10835067	
		SNX5	Sorting nexin 5	55957200	
2051	1.28	DARS2	Aspartyl-tRNA synthetase	45439306	6.0 E-03
		PHGDH	Phosphoglycerate dehydrogenase	23308577	

[a] Spot numbers correspond to those included in the 2D gel image (Figure 20A).
[b] Average ratio between KCL22R and KCL22S cells, expressed as mean of 4 standard protein abundances calculated for the four gels described in Table 1. Only statistically significant ratios between KCL22R and KCL22S (Student's t-test, $p \leq 0.01$) are reported. The four spots containing more than one protein are the last ones in the table.

TABLE 4. Under-expressed proteins in KCL22R *versus* KCL22S cells

Spot [a]	Fold decrease [b]	Gene symbol	Protein name	Gene ID	p-value
3470	-3.51	HSPB1	Heat Shock 27 KDa protein1	450517	7.80 E-06
3454	-3.28	HSPB1	Heat Shock 27 KDa protein1	450517	5.2 E-03
1823	-2.87	MTHFD1	Methylenetetrahydrofolate dehydrogenase	115206	2.70 E-05
2872	-2.71	ANXA1	Annexin A1	54696696	1.70 E-06
3473	-2.29	ERP29	Endoplasmic reticulum protein 29	75517652	2.1 E-03
2567	-2.02	SERPINB1	Serine proteinase inhibitor	14290494	2.0 E-03
3696	-1.71	PRDX1	Peroxiredoxin 1	55586231	1.2 E-06
2871	-1.67	ANXA1	Annexin A1	54696696	5.2 E-03
1593	-1.64	FUBP1	Fuse binding protein 1	16878077	6.6 E-03
877	-1.63	HSPA4L	Heat Shock 70 KDa protein 4L	31077164	2.1 E-03
1673	-1.60	HSPA1A	Heat shock 70kDa protein 1A	4529892	1.5 E-03
3261	-1.58	CLIC1	Stress induced phosphoprotein 1	895845	8.9 E-07
1664	-1.43	HSPA1A	Heat Shock 70 kDa protein 1 A	4529892	2.3 E-03
1616	-1.37	XRCC5	ATP-dependent DNA helicase II	4503841	9.0 E-03
1645	-1.28	HSPA1A	Heat shock 70kDa protein 1A	4529892	6.2 E-03
2113	-1.27	NAPRT1	Nicotinate phosphoribosyltransferase domain containing 1	37787307	5.0 E-03
2155	-1.26	ATP5A1	ATP synthase	15030240	3.3 E-04
1786	-1.26	HNRPL	Heterogeneous nuclear ribonucleoprotein L	133274	8.7 E-03
3746	-1.25	TAGLN2	Transgelin 2	12803567	5.6 E-04
2812	-2.64	ANXA1	Annexin A1	54696696	5.9 E-06
		HNRPH3	Heterogeneous nuclear ribonucleoprotein H3	62898443	
2887	-1.38	ANXA1	Annexin A1	54696696	2.9 E-03
		LASP1	LIM and SH3 protein 1	5453710	
2129	-1.27	LAP3	Leucine aminopeptidase 3	4335941	9.4 E-03
		SEPT6	Septin 6	14424536	

[a] Spot numbers correspond to those included in the 2D gel image (Figure 20B).
[b] Average ratio between KCL22R and KCL22S cells, expressed as mean of 4 standard protein abundances calculated for the four gels described in Table 1. Only statistically significant ratios between KCL22R and KCL22S (Student's t-test, $p \leq 0.01$) are reported. The three spots containing more than one protein are the last ones in the table.

Protein species identified by a single peptide were analyzed further. The peptide sequence stretch was manually reconstructed, and the peptide sequence and peptide precursor ion mass were analyzed using the in-house MASCOT in the sequence query mode. All searches were performed against the NCBI database. The peptide sequence was searched for using the BLAST program (http://ncbi.nlm.nih.gov/blast). Peptides with ambiguously identification were removed from the tables, i.e., the candidate protein was removed from the list when it matched other proteins. Figure 21 shows the MS full scan and the MS/MS scan properly annotated (with masses and fragment assignments) of proteins identified by a single peptide.

a) Proteasome activator complex subunit 1 (PSME1)

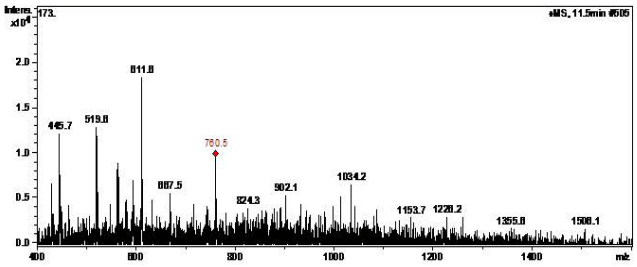

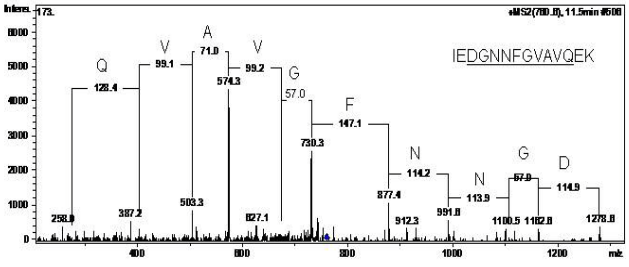

AVNCNEKIVVLLQRLKPEIKDVIEQLNLVTT
WLQLQIPRIEDGNNFGVAVQEKVFELMTSL
HTKLEGFHTQISKYFSERGDAVTKAAKQPH
VGDYRQLVHELDEAEYRDIRLMVMEIRNAY
AVLYDIILKNFEKLKKPRG

b) Adenine phosphoribosyltransferase (APRT)

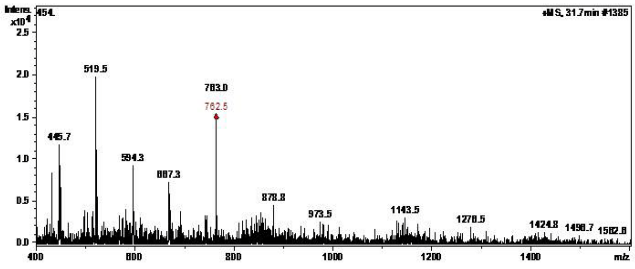

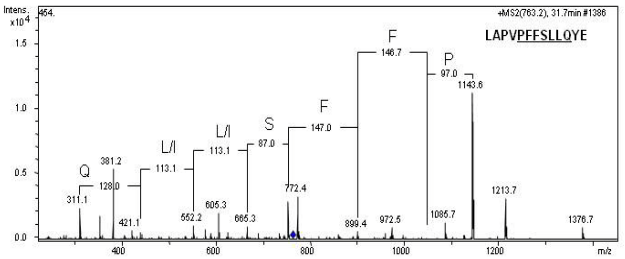

MADSELQLVEQRIRSFPDFPTPGVVFRDISP
VLKDPASFRAAIGLLARHLKATHGGRIDYIA
GLDSRGFLFGPSLAQELGLGCVLIRKRGKLP
GPTLWASYSLEYGKAELEIQKDALEPGQRV
VVVDDLLATGGTMNAACELLGRLQAEVLEC
VSLVELTSLKGREKLAPVPFFSLLQYE

c) Macro domain containing 1 (MACROD1)

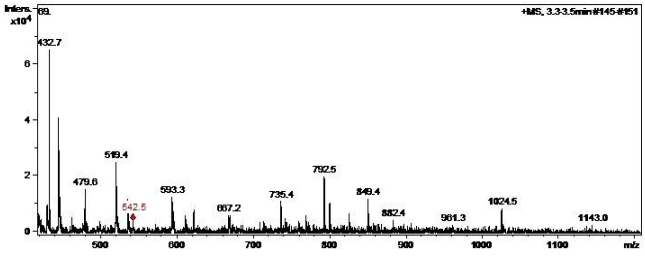

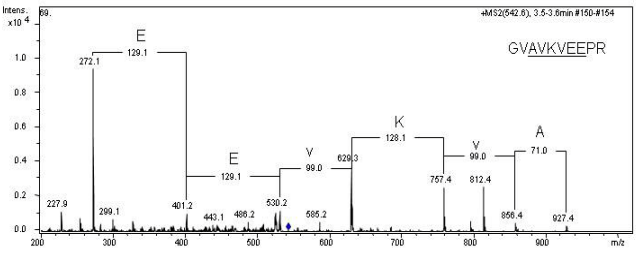

MSLQSRLSGRLAQLRAAGQLLVPPRPRPGHLAG
ATRTRSSTCGPPAFLGVFGRRARTSAGVGAWGA
AAVGRTAGVRTWAPLAMAAKVDLSTSTDWKEAK
SFLKGLSDKQREEHYFCKDFVRLKKIPTWKEMAK
GVAVKVEEPRYKKDKQLNEKISLLRSDITKLEVDAI
VNAANSSLLGGGGVDGCIHRAAGPLLTDECRTLQ
SCKTGKAKITGGYRLPAKCESPTRPQLWGADRA
PVCHWDIRGAAPTGVLGNSSGGPS

d) Endoplasmic reticulum protein 29 (ERP29)

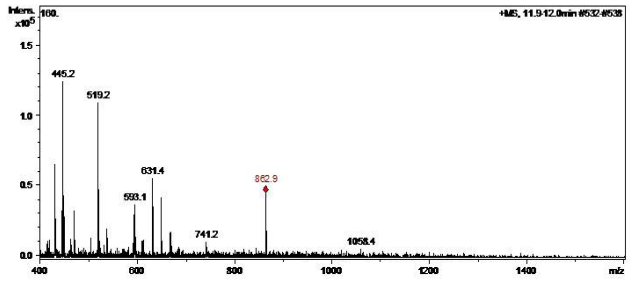

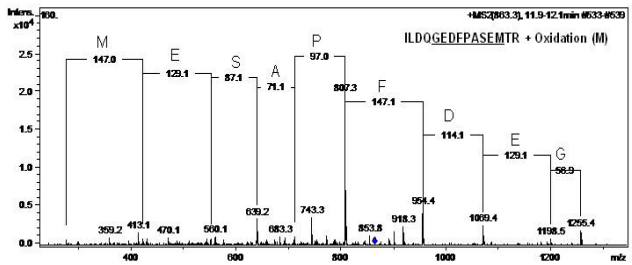

MAAAVPRAAFLSPLLPLLLGFLLLSAPHGGSGLH
TKGALPLDTVTFYKVIPKSKFVLVKFDTQYPYGEK
QDEFKRLAENSASSDDLLVAEVGISDYGDKLNME
LSEKYKLDKESYPVFYLFRDGDFENPVPYTGAVK
VGAIQRWLKGQGVYLGMPGCLPVYDALAGEFIR
ASGVEARQALLKQGQDNLSSVKETQKKWAEQY
LKIMGKILDQGEDFPASEMTRIARLIEKNKMSDGK
KEELQKSLNILTAFQKKGAEKEEL

e) Ferritin light subunit (FTL)

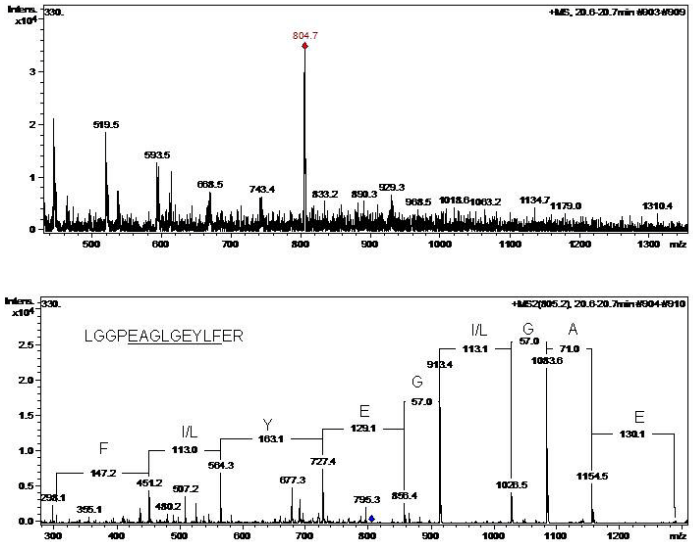

Figure 21. The survey scan (MS), MS/MS scan and amino acid sequence of a) PSME1, b) APRT, c) MACROD1, d) ERP29 and e) FTL proteins identified by a single peptide. The mass spectrums show the reconstructed peptide sequence and the tryptic peptide used for the identification by Mascot. In the protein sequences, the identified peptide is underlined. ♦ indicates the m/z signal of the parent ion. Single charged ions in the same survey spectrum are not fragmented.

Definitively, 19 over-expressed and 15 under-expressed proteins in KCL22R cells, that were present as a single protein species in single spots, were identified. Eight over-expressed and four under-expressed proteins were mixed with others in several spots, thus making it difficult to assign a defined value of fold change for each protein. Details of the mass spectrometry characterization of the over-expressed and under-expressed proteins are provided in Tables 5 and 6, respectively.

TABLE 5. Details of the mass spectrometry characterization of over-expressed proteins in KCL22R *versus* KCL22S cells

n. SPOT	Protein name	Precursor Mass (m/z)	Charge State (z)	Mass Errors (ppm)	Identified Peptide Sequence	Single peptide MASCOT score	Sequence Coverage
1570	Malic enzyme 2, NAD(+)-dependent, mitochondrial	504.35	2+	139	GLFISISDR	44	7.8%
		651.35	2+	30,7	YIYIMGIQER	42	
		658.82	2+	38	HISDSVFLEAAK	60	
		816.5	2+	104.24	ALTSQLTDEELAQGR	80	
		834.97	2+	23.9	AVQQPDGLAVLGIFLK	80	
3317	Carbonic Anhydrase II	492.89	2+	193.1	VGSAKPGLQK	41	11%
		494.37	2+	162.1	VVDVLDSIK	41	
		585.32	2+	94.1	SADFTNFDPR	49	
3421	Carbonic Anhydrase II	468.27	2+	74.9	GGPLDGTYR	43	29%
		494.39	2+	202.7	VVDVLDSIK	42	
		585.28	2+	25.6	SADFTNFDPR	52	
		647.81	2+	7.7	QSPVDIDTHTAK	54	
		835.03	2+	47.9	AVQQPDGLAVLGIFLK	81	
		713.92	3+	163.6	YDPSLKPLSVSYDQATSLR	47	
3805	Adenine phosphoribosyltransferase	762.53	2+	157.6	LAPVPFFSLLQYE	56	7%
3467	MACRO domain containing 1	542.51	2+	369.4	GVAVKVEEPR	51	4%
1743	L-plastin	663.05	2+	317.2	GSVSDEEMMELR	43	6%
		708.01	2+	304.1	IGNFSTDIKDSK	49	
		793.74	2+	397.5	VYALPEDLVEVNPK	69	
3932	Ferritin light subunit	804.66	2+	317.4	LGGPEAGLGEYLFER	66	10%
2582	Lactate dehydrogenase B	457.35	2+	120.5	IVVVTAGVR	56	9.8%
		480.38	2+	208.6	GLTSVINQK	47	
		755.98	2+	119.2	IVADKDYSVTANSK	46	
1668	Leukotriene A4 hydrolase	559.84	2+	44.7	ELVALMSAIR	52	19%
		604.35	2+	33.1	LTYTAEVSVPK	82	
		481.54	3+	20.8	DGETPDPEDPSRK	47	
		729.94	2+	61.7	GSPMEISLPIALSK	63	
		769.37	2+	39	SAYEFSETESMLK	71	
		959.56	2+	67.8	TLTGTAALTVQSQEDNLR	62	
		979.46	2+	5.11	MQEVYNFNAINNSEIR	117	
		1169.56	2+	25.6	LVVDLTDIDPDVAYSSVPYEK	68	
2527	Beta actin	566.72	2+	79.5	GYSFTTTAER	56	59%
		589.25	2+	101.9	EITALAPSTMK	45	
		599.73	2+	58.4	DSYVGDEAQSK	51	
		599.85	2+	8.3	AVFPSIVGRPR	41	
		750.34	2+	0	QEYDESGPSIVHR	47	
		543.24	2+	43	QEYDESGPSIVHRK	43	
		895.95	2+	0	SYELPDGQVITIGNER	43	
		977.55	2+	15.3	VAPEEHPVLLTEAPLNPK	42	
		116.08	2+	40.3	DLYANTVLSGGTTMYPGIADR	55	
		787.18	3+	156.9	KDLYANTVLSGGTTMYPGIADR	41	
		856.09	3+	35	LCYVALDFEQEMATAASSSSLEK	50	
2948	Human elongation factor-1-delta	729.06	3+	54.9	SLAGSSGPGASSGTSGDHGELVVR	67	9%
		712.16	2+	267	ATAPQTQHVSPMR	41	
3441	Rho GDP dissociation inhibitor	959.67	2+	203.4	SIQEIQELDKDDESLR	51	8%
		475.31	2+	73.8	YKEALLGR	60	
2584	Fumarylacetoacetate hydrolase	477.33	2+	94.4	LGEPIPISK	45	5%
		586.85	2+	25.6	ASSVVVSGTPIR	50	
1975	Chaperonin containing TCP1, subunit 6A isoform a	469.26	2+	21.3	GLVLDHGAR	50	3%
		511.25	2+	19.5	SEDTSLIR		
2520	Beta actin	566.73	2+	61.8	GYSFTTTAER	56	13%
		589.29	2+	33.9	EITALAPSTMK	41	
		750.33	2+	13.3	QEYDESGPSIVHR	48	

		896.06	2+	122.9	SYELPDGQVITIGNER	44	
2693	Phosphoserine aminotransferase 1	563.36	2+	62.2	FGTINIVHPK	42	9%
		593.34	2+	8.4	IINNTENLVR	41	
		775.5	2+	6.4	ASLYNAVTIEDVQK	74	
1885	Adenyl cyclase-associated protein 1	502.32	2+	69.8	LVTTVTEIAG	51	5%
		713.96	2+	70.1	LSDLLAPISEQIK	41	
2535	NADP-dependent isocitrate dehydrogenase	544.31	2+	27.6	ATDFVVPGPGK	46	17.8%
		633.79	2+	23.7	LIDDMVAQAMK	66	
		671.37	2+	44.7	TVEAEAAHGTVTR	51	
		719.87	2+	20.8	VEITYTPSDGTQK	45	
		763.39	2+	78.7	SDYLNTFEFMDK	62	
3355	Proteasome activator complex subunit 1	760.51	2+	177.7	IEDGNNFGVAVQEK	44	10%
2730	Phosphoserine aminotransferase 1	574.35	2+	43.6	ALELNMLSLK	63	10.3%
		775.94	2+	45.1	ASLYNAVTIEDVQK	71	
		550.99	3+	24.2	FLDKALELNMLSLK	42	
3533	Triosephosphate Isomerase	617.93	2+	202.59	SNVSDAVAQSTR	52	29%
		663.85	2+	15	IIYGGSVTGATCK	82	
		699.57	2+	264.8	QSLGELIGTLNAAK	64	
		729.88	2+	20.5	HVFGESDELIGQK	64	
		1096.59	2+	45.6	VPADTEVVCAPPTAYIDFAR	53	
3068	Porin 31HM	515.61	2+	388.5	LTLSALLDGK	48	10%
		980.55	2+	35.7	SENGLEFTSSGSANTETTK	77	
2058	Phosphoglycerate dehydrogenase	550.25	2+	91	GGIVDEGALLR	74	4%
		744.93	2+	100.8	AGTGVDNVDLEAATR	62	
	Inosine-5'-monophosphate dehydrogenase	482.14	2+	259.7	VRDVFEAK	52	4%
		550.68	2+	163.7	YFSEADKIK	45	
2545	Actin-related protein 2 isoform b	675.8	2+	22.2	DLMVGDEASELR	63	6.1%
		685.39	2+	21.9	ILLTEPPMNPTK	41	
	Poly(rC)-binding protein 2 isoform b	679.94	2+	17.27	IANPVEGSTDR	47	6%
		579.8	2+	51.55	IITLAGPTNAIFK	46	
2360	Autoantigen La	590.84	2+	110.2	AELMEISEDK	42	14.7%
		658.85	2+	15.2	IIEDQQESLNK	75	
		698.32	2+	21.5	SKAELMEISEDK	60	
		749.92	2+	33.4	GSIFVVFDSIESAK	48	
		775.49	2+	84	LTTDFNVIVEALSK	87	
	Sorting nexin 5	583.33	2+	3.43	SADEVLFTGVK	68	7.8%
		616.24	2+	105.6	YYMLNIEAAK	43	
	Eukaryotic translation elongation factor 1 gamma	674.39	2+	22.3	ALIAAQYSGAQVR	79	6%
		722.83	2+	55.4	LDPGSEETQTLVR	72	
2051	Aspartyl-tRNA synthetase	530.32	2+	85	GEEILSGAQR	41	14.3%
		580.89	2+	94.8	IYVISLAEPR	55	
		601.32	2+	8.3	ESIVDVEGVVR	52	
		604.33	2+	16.5	FQTEIQTVNK	53	
		755.42	2+	39.7	NNAYLAQSPQLYK	77	
		976.47	2+	66.6	EAGVEMGDEDDLSTPNEK	55	
		741.75	3+	67.5	LPLQLDDAVRPEAEGEEEGR	97	
	Phosphoglycerate dehydrogenase	550.33	2+	36.4	GGIVDEGALLR	75	13.5%
		565.79	2+	26.5	VTADVINAAEK	52	
		649.88	2+	15.4	ILQDGGLQVVEK	84	
		673.43	2+	59.5	GTIQVITQGTSLK	91	
		744.92	2+	67.2	AGTGVDNVDLEAATR	75	

TABLE 6. Details of the mass spectrometry characterization of under-expressed proteins in KCL22R *versus* KCL22S cells

n. SPOT	Protein name	Precursor Mass (m/z)	Charge State (z)	Mass Errors (ppm)	Identified Peptide Sequence	Single peptide MASCOT score	Sequence Coverage
3470	Heat Shock 27 KDa protein1	582.31	2+	0	LFDQAFGLPR	41	21%
		822.4	2+	18.2	AQLGGPEAAKSDETAAK	54	
		1081.6	3+	15.7	LATQSNEITIPVTFESR	51	
3454	Heat Shock 27 KDa protein1	582.32	2+	17.2	LFDQAFGLPR	54	20%
		1081.85	3+	274.4	KYTLPPGVDPTQVSSSLSPEGTLTVEAPMPK	41	
1823	Methylenetetrahydrofolate dehydrogenase	529.37	2+	141.9	ITIGQAPTEK	63	15%
		549.48	2+	282.5	GALALAQAVQR	60	
		572.01	2+	376	QPSQGPTFGIK	69	
		689.98	2+	210.5	TDTESELDLISR	68	
		724.97	2+	117.4	AYIQENLELVEK	58	
		752.86	2+	0	TDPTTLTDEEINR	74	
		816.07	2+	141.1	YVVVTGITPTPLGEGK	57	
		570.87	3+	374.4	APAEILNGKEISAQIR	66	
		905.1	2+	55.3	EIGLLSEEVELYGETK	79	
		706.58	3+	288.2	KGEPVSAEDLGVSGALTVLMK	64	
2872	Annexin A1	607.27	2+	0	DITSDTSGDFR	63	37%
		631.83	2+	47.5	TPAQFDADELR	60	
		686.37	2+	29.1	VLDLELKGDIEK	41	
		694.4	2+	21.6	GVDEATIIDILTK	71	
		772.47	2+	45.3	GVDEATIIDILTKR	59	
		775.95	2+	51.6	GTDVNVFNTILTTR	71	
		547.58	3+	30.4	DLAKDITSDTSGDFR	58	
		839.97	2+	17.8	KGTDVNVFNTILTTR	66	
		851.96	2+	17.6	GLGTDEDTLIEILASR	107	
		870.39	2+	23	SEDFGVNEDLADSDAR	89	
		689.9	3+	96.7	GDRSEDFGVNEDLADSDAR	86	
		786.36	3+	386.3	GGPGSAVSPYPTFNPSSDVAALHK	54	
3473	Endoplasmic reticulum protein 29	862.88	2+	17.4	ILDQGEDFPASEMTR	58	37%
2567	Serine proteinase inhibitor	604.35	2+	49.7	LGVQDLFNSSK	66	13%
		644.34	2+	0	HNSSGSILFLGR	51	
		653.32	2+	45.9	FQSLNADINKR	67	
		825.91	2+	6	IPELLASGMVDNMTK	50	
3696	Peroxiredoxin 1	410.26	2+	109.9	SVDETLR	44	28%
		598.96	2+	234.1	LVQAFQFTDK	58	
		606.48	2+	231.2	QITVNDLPVGR	50	
		680.48	2+	198.7	GLFIIDDKGILR	72	
		811.47	2+	67.8	QGGLGPMNIPLVSDPK	62	
2871	Annexin A1	607.41	2+	230.9	DITSDTSGDFR	59	18%
		821.03	2+	170.7	DLAKDITSDTSGDFR	61	
		840.06	2+	119.1	KGTDVNVFNTILTTR	63	
		870.42	2+	57.5	SEDFGVNEDLADSDAR	90	
		635.77	3+	136.5	AAYLQETGKPLDETLKK	49	
1593	Fuse binding protein 1	574.82	2+	52.2	GTPQQIDYAR	41	7%
		677.09	2+	340.3	IQIAPDSGGLPER	69	
		987.44	2+	5	IGGDAGTSLNSNDYGYGGQK	76	
877	Heat Shock 70 KDa protein 4L	525.39	2+	209.8	FITPEDLSK	41	14%
		646.07	2+	356.6	IGSFTIQNVFPQSDGDSSK	50	
		654.04	2+	344.6	SFDDPIVQTER	63	
		703.03	2+	292	NAVEEYVYDFR	72	
		756.37	2+	26.4	SGGIETIANEYSDR	59	
		877.55	2+	91.2	EFSITDLVPYSITLR	41	

		887.47	2+	11.2	LMNETTAVALAYGIYK	100	
		910.98	2+	27.4	QLGQDLLNSYIENEGK	57	
		1014.04	2+	49.3	QDLPPLDEKPR	50	
1673	Heat shock 70kDa protein 1A	474.28	2+	84.5	SAVEDEGLK	44	32%
		502.3	2+	49.8	LSKEEIER	49	
		599.39	2+	66.8	DAGVIAGLNVLR	66	
		602.92	2+	249.2	GGSGSGPTIEEVD	45	
		614.92	2+	162.9	VEIIANDQGNR	58	
		631.42	2+	142.7	SAVEDEGLK	44	
		652.48	2+	268.6	NALESYAFNMK	52	
		658.34	2+	53.2	SAVEDEGLK	44	
		733.47	2+	81.9	AQIHDLVLVGGSTR	71	
		744.5	2+	195	TTPSYVAFTDTER	77	
		711.94	2+	90.8	ARFEELCSDLFR	50	
		815.93	2+	30.6	AQIHDLVLVGGSTR	71	
		830.2	2+	325.7	NQVALNPQNTVFDAK	67	
		838.44	2+	83.5	ATAGDTHLGGEDFDNR	68	
		563.35	3+	77	IINEPTAAAIAYGLDR	53	
		1160.74	2+	137.9	SINPDEAVAYGAAVQAAILMGDK	83	
3261	Stress induced phosphoprotein 1	641.37	2+	46.8	GVTFNVTTVDTK	94	36%
		664.78	2+	67.7	NSNPALNDNLEK	68	
		719.35	2+	55.6	GVTFNVTTVDTKR	45	
		870.45	2+	23	NSNPALNDNLEKGLLK	67	
		923.14	2+	162.6	LAALNPESNTAGLDIFAK	78	
		998.48	3+	344.3	VLDNYLTSPLPEEVDETSAEDEGV SQR	51	
		1040.74	3+	89.7	VLDNYLTSPLPEEVDETSAEDEGV SQRK	63	
1616	ATP-dependent DNA helicase II	604.31	2+	33.14	DSLIFLVDASK	68	4.1%
		787.55	2+	171.6	NIYVLQELDNPGAK	74	
1664	Heat Shock 70 kDa protein 1 A	502.25	2+	49.8	LSKEEIER	43	22%
		509.3	2+	19.6	ITITNDKGR	50	
		599.41	2+	100.2	DAGVIAGLNVLR	59	
		602.75	2+	33.2	GGSGSGPTIEEVD	44	
		614.8	2+	32.5	VEIIANDQGNR	55	
		652.36	2+	84.4	NALESYAFNMK	54	
		744.38	2+	33.6	TTPSYVAFTDTER	77	
		815.88	2+	30.06	AFYPEEISSMVLTK	57	
		829.96	2+	36.1	NQVALNPQNTVFDAK	66	
		559.26	3+	17.9	ATAGDTHLGGEDFDNR	63	
		844.52	2+	77	IINEPTAAAIAYGLDR	82	
1645	Heat shock 70kDa protein 1A	599.41	2+	100.2	DAGVIAGLNVLR	64	16%
		602.8	2+	49.8	GGSGSGPTIEEVD	43	
		744.41	2+	73.9	TTPSYVAFTDTER	77	
		816	2+	116.5	AFYPEEISSMVLTK	60	
		830	2+	84.4	NQVALNPQNTVFDAK	65	
		844.53	2+	88.9	IINEPTAAAIAYGLDR	81	
		774.17	3+	150.9	SINPDEAVAYGAAVQAAILMGDK	51	
2113	Nicotinate phosphoribosyltransferase	479.81	2+	41.7	ALAQLSLSR	65	10.6%
		622.81	2+	16.08	DAAEFELFFR	60	
		648.91	2+	77.1	AAFVAYALAFPR	46	
		688.97	2+	159.9	SPAQYQVVLSER	85	

		793.48	2+	82	LDSGDLLQQAQEIR	75	
2155	ATP synthase	788.42	2+	31.7	ILGADTSVDLEETGR	101	6%
		812.93	2+	26.4	TGAIVDVPVGEELLGR	41	
1786	Heterogeneous nuclear ribonucleoprotein L	611.8	2+	0	SSSGLLEWESK	66	8%
		941.48	2+	42.5	NGVQAMVEFDSVQSAQR	85	
		633.98	3+	36.8	SKPGAAMVEMADGYAVDR	53	
3746	Transgelin 2	640.48	2+	281.5	NFSDNQLQEGK	52	13%
		840.25	2+	399.3	QMEQISQFLQAAER	48	
2812	Annexin A1	775.96	2+	64.52	GTDVNVFNTILTTR	60	8.6%
		851.98	2+	41.1	GLGTDEDTLIEILASR	74	
	Heterogeneous nuclear ribonucleoprotein H3	636.36	2+	70.8	STGEAFVQFASK	57	7.5%
		714.8	2+	7	DGMDNQGGYGSVGR	48	
2887	Annexin A1	607.26	2+	16.49	DITSDTSGDFR	52	28.6%
		631.81	2+	7.93	TPAQFDADELR	61	
		694.39	2+	0	GVDEATIIDILTK	64	
		775.94	2+	38.7	GTDVNVFNTILTTR	79	
		820.88	2+	12.2	DLAKDITSDTSGDFR	53	
		870.44	2+	80.5	SEDFGVNEDLADSDAR	107	
		690.01	3+	62.9	GDRSEDFGVNEDLADSDAR	80	
	LIM and SH3 protein 1	709.87	2+	7.05	GFSVVADTPELQR	50	15%
		481.98	3+	90.1	LKQQSELQSQVR	44	
		784.41	2+	51.06	TGDTGMLPANYVEAI	52	
2129	Leucine aminopeptidase 3	584.82	2+	17.13	ETLNISGPPLK	49	38%
		597.84	2+	33.5	GITFDSGGISIK	67	
		619.31	2+	8.08	LFEASIETGDR	54	
		659.82	2+	7.58	TIQVDNTDAEGR	72	
		480.04	2+	180.9	LRETLNISGPPLK	54	
		763.44	2+	45.9	GSPNANEPPLVFVGK	59	
		544.31	2+	61.35	GSDEPPVFLEIHYK	46	
		817.39	2+	30.62	QLMETPANEMTPTR	58	
		855.43	2+	17.5	ADMGGAATICSAIVSAAK	71	
	Septin 6	569.28	2+	8.79	SLDDEVNAFK	59	4.8%
		643.83	2+	15.55	STLMDTLFNTK	58	

3.4 Western blot analysis of differentially expressed proteins between KCL22R and KCL22S cells

To validate the 2D-DIGE results, the expression of the following proteins was analysed by Western blot: Hsp27, Hsp70, Peroxiredoxin 1 (Prdx1), Annexin A1 (Anxa1), Fuse binding protein1 (Fubp1), Rho GDP dissociation inhibitor (Arhgdia), Carbonic anhydrase II (Ca2) and Malic enzyme (Me2). As shown in Figure 22A, Hsp27, Hsp70, Prdx 1, Anxa1 and Fubp1 protein expression decreased in KCL22R samples, whereas Arhgdia, Ca2 and Me2 protein expression increased in KCL22R. The results of three Western blot experiments were examined by densitometry using Gapdh protein expression to normalize the data (Figure 22B), thus validating DIGE analysis.

Because Hsp27 and Hsp70 were under-expressed in KCL22R cells, the expression of other members of the heat shock protein family, namely Grp78 and Hsp60, which are differentially expressed in cancer cells, including leukemia, and are resistant to apoptosis [71], was measured. The expression of these two proteins, analysed by Western blot, was reduced in KCL22R cells (Figure 23A and B).

The down-regulation of Hsp70, Hsp27, Anxa1 proteins in KCL22R cells could occur at genetic level as demonstrated by a preliminary study of the gene expression profiles (performed at the facility of microarray at Ceinge, in Naples) across imatinib-resistant and sensitive KCL22 cells. These experiments are only briefly described because they were not carried out by the PhD student presenting this thesis. In addition, quantitative RT-PCR showed a significant decrease in the expression of the Annexin A1 gene in KCL22R cells (Figure 24).

Because Hsp70 expression is under the control of Hsf-1 transcription activation factor, the expression of Hsf-1 was measured by Western blot analysis. The

expression of Hsf-1 was reduced in KCL22R (Figure 23A) as confirmed by densitometric analysis (Figure 23B). These data suggest that down-regulation of Hsp70 may be mediated by an Hsf-1-dependent mechanism.

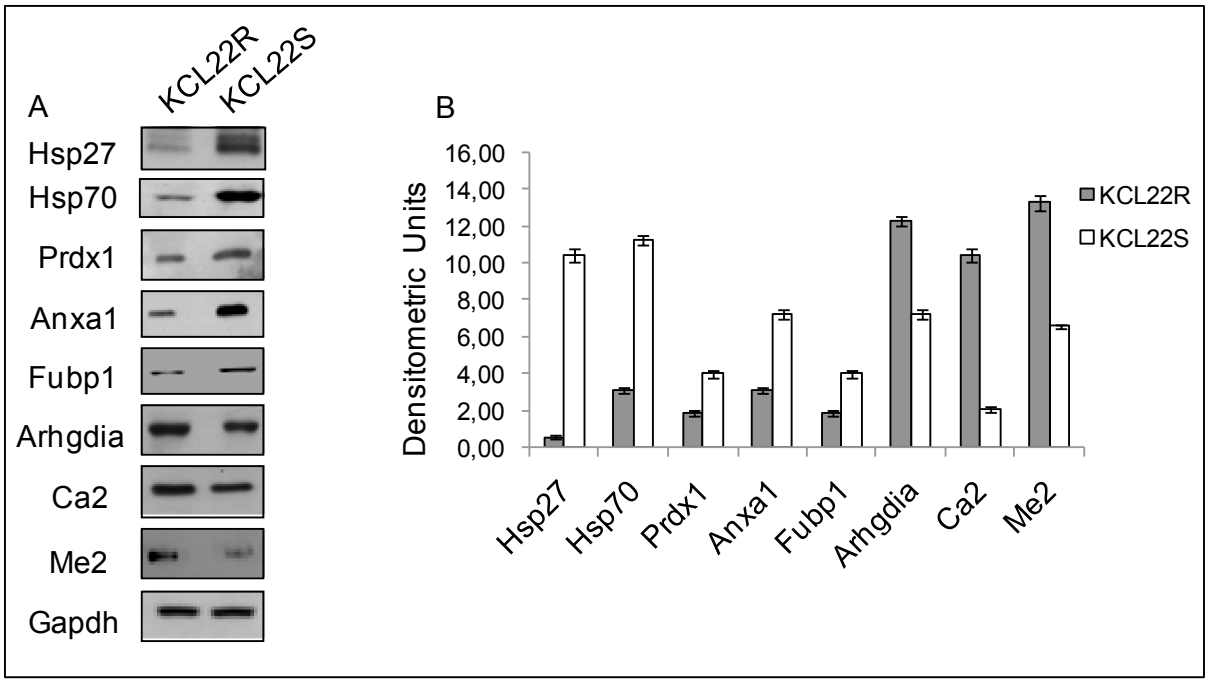

Figure 22. Western blot analysis of total protein lysates of KCL22R and KCL22S cells. Proteins were separated on 10% SDS-PAGE and immunoblotted with antibodies against Hsp27, Hsp70, Prdx1, Anxa1, Fubp1, Arhgdia, Ca2 and Me2 (A). Gapdh served as control. The densitometric analysis was performed on three samples; the results are shown as means±SD (B).

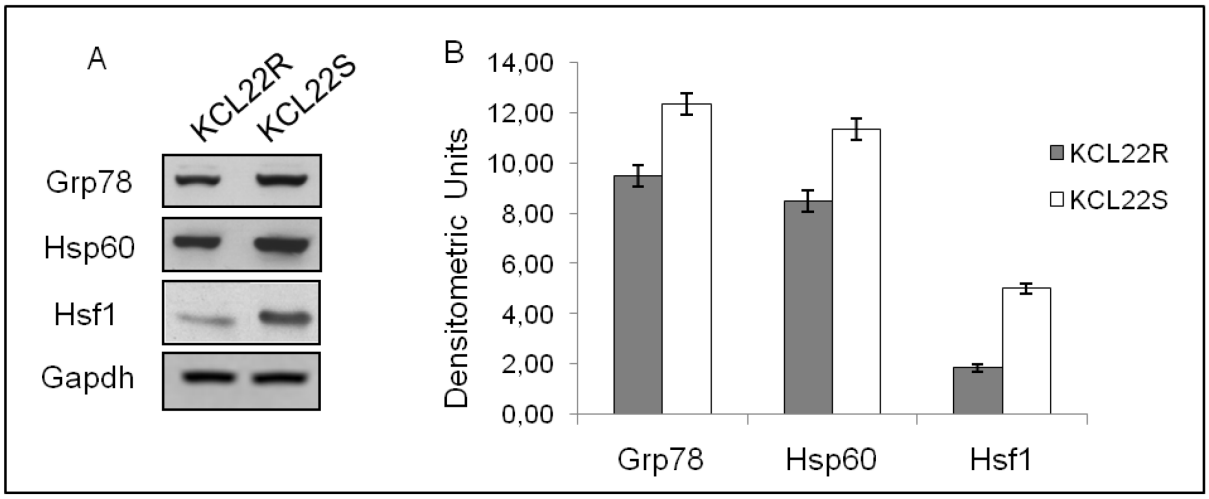

Figure 23. Western blot analysis of total protein lysates of KCL22R and KCL22S cells. Proteins were separated on 10% SDS-PAGE and immunoblotted with antibodies against Grp78, Hsp60 and Hsf1 (A). Gapdh served as control. The densitometric analysis was performed on three samples; the results are shown as means±SD (B).

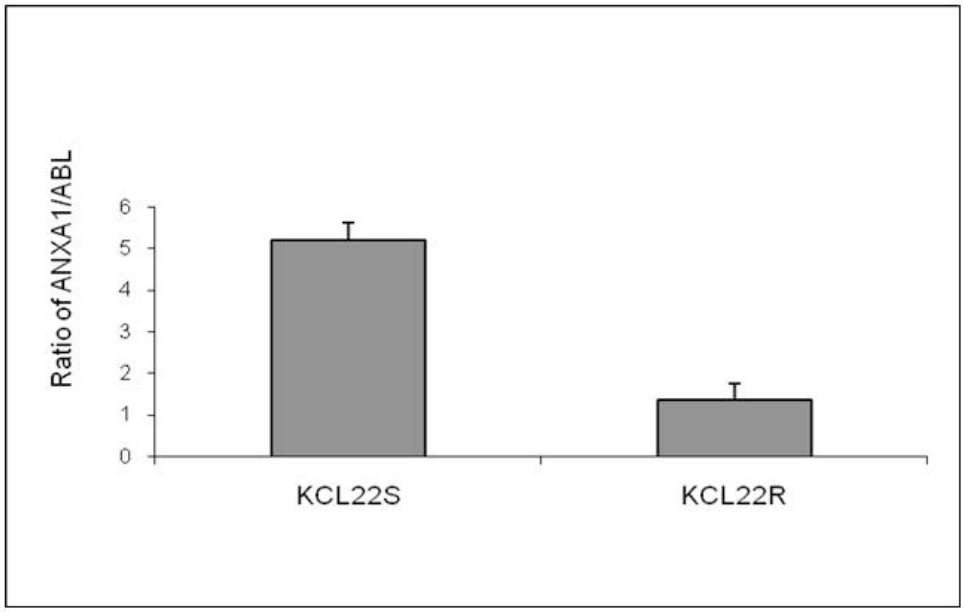

Figure 24. Quantitative RT-PCR analysis. Expression level of ANXA1 mRNA in KCL22S and KCL22R cell lines. The results, obtained from quadruplicate independent cultures, are shown as means±SD.

Moreover gene expression profile analysis (carried out at the facility of microarray at Ceinge, in Naples) showed that SHP1 expression was reduced in KCL22R cells while SHP2 was expressed at similar level. The level of Shp1 protein was measured in KCL22R and KCL22S cells. Western blot analysis showed that Shp1 was down-regulated in KCL22R cells (Figure 25). Since Shp1 could act as a negative regulator of cell proliferation essentially as antagonist of Shp2 [72], the expression level of Shp2 was measured in KCL22R and KCL22S cells. Western blot analysis showed that the level of Shp2 was similar in resistant and sensitive cells (Figure 25).

Recently, a chemical proteomic screen for imatinib interactors [73-75] identified a non-kinase target, the oxidoreductase Nqo2. Therefore, the expression of the oxidoreductase Nqo2 between KCL22R and KCL22S cells was analysed**.** Western blot analysis showed that Nqo2 was down-regulated in the resistant cells (Figure 25).

Interference of imatinib in the protein pattern expression of KCL22R cannot be fully ruled out. Therefore Western blot analysis was also performed on protein extracts from KCL22R cells imatinib-deprived for 3 days. The obtained results validated the changes observed above for all the proteins identified in presence of imatinib (Figure 26).

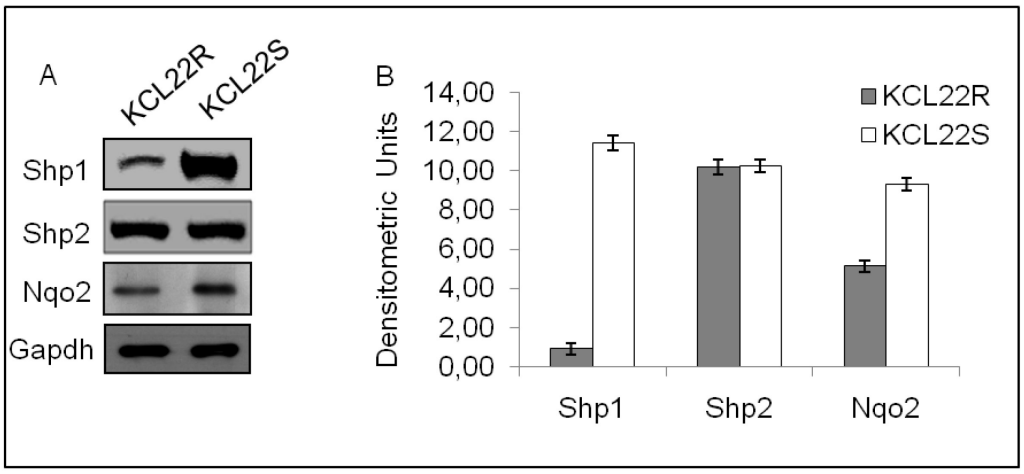

Figure 25. Western blot analysis on total protein lysates of KCL22R cells and KCL22S cells. Proteins were separated on 10% SDS-PAGE and immunoblotted with antibodies against Shp1, Shp2 and Nqo2 (A). Gapdh served as control. The densitometric analysis was performed on three samples; the results are shown as means±SD (B).

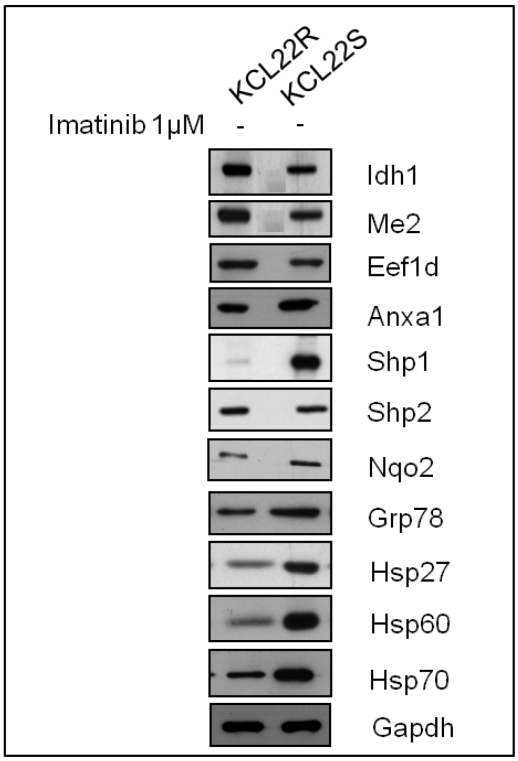

Figure 26. Western blot analysis of total protein lysates of KCL22R and KCL22S cells. Proteins extracts from KCL22S and KCL22R cells, imatinib-deprived for 3 days, were separated on 10% SDS-PAGE and immunoblotted with antibodies against Idh1, Me2, Eef1d, Anxa1, Shp1, Shp2, Nqo2, Grp78, Hsp27, Hsp60 and Hsp70. Gapdh served as control.

In summary, by DIGE and Western blot analysis, 51 differentially expressed proteins were identified: 27 over-expressed and 24 under-expressed in KCL22R *versus* KCL22S cells.

3.5 In *silico* characterization of identified proteins

3.5.1 GeneSpring software analysis

The proteins identified were clustered in functional classes according to Gene Ontology (www.geneontology.org) annotations on molecular function (Figure 27A and B) and cellular localization (Figure 28A and B) using GeneSpring GX software. Over-expressed proteins are shown in Figure 27A and 28A, and under-expressed proteins in Figure 27B and 28B. Statistical analysis by Fisher exact test of the identified proteins (Table 7 and Table 8) indicated that the most relevant molecular functions of the over-expressed proteins are related to oxidoreductase activity, being enclosed in the main area related to catalytic activity and to translation regulator activity (Figure 27A). The two most relevant functions of the under-expressed proteins are related to peptidase activity, which is enclosed in the main area related to catalytic activity and nucleotide binding activity (Figure 27B). Some of the classified proteins are included in more than one functional group. Almost 50% of the up-regulated proteins are localized in the cytoplasm; 35% of down-regulated proteins are localized in the cytoplasm, and 27% are nuclear proteins (Figure 28A and B).

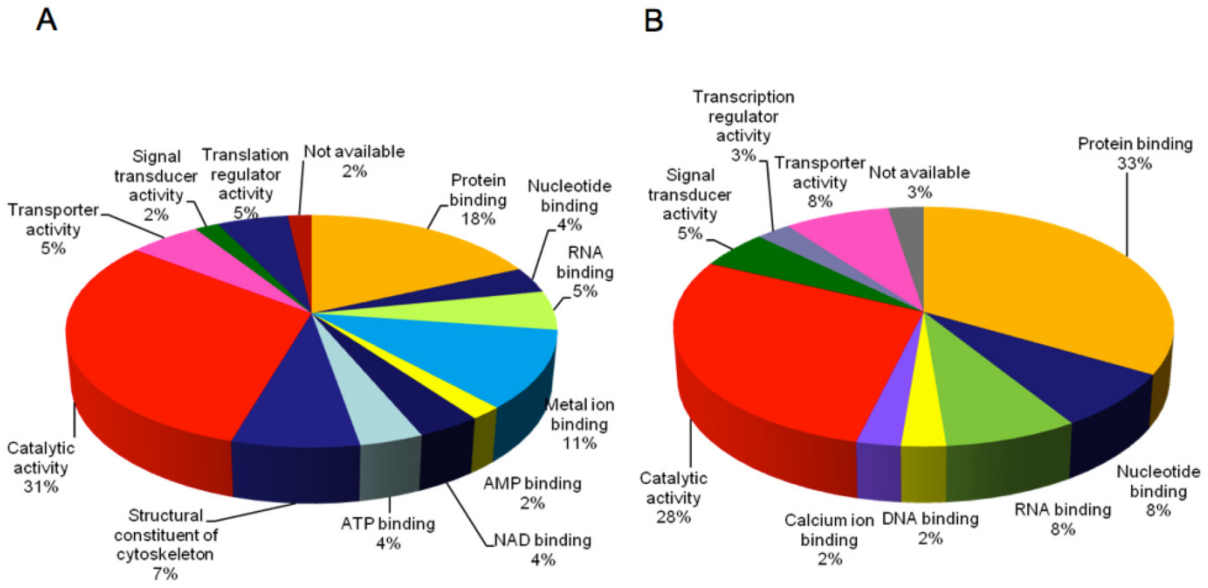

Figure 27. Classification of the over-expressed (A) and under-expressed (B) proteins in KCL22R cells according to Gene Ontology molecular functions.

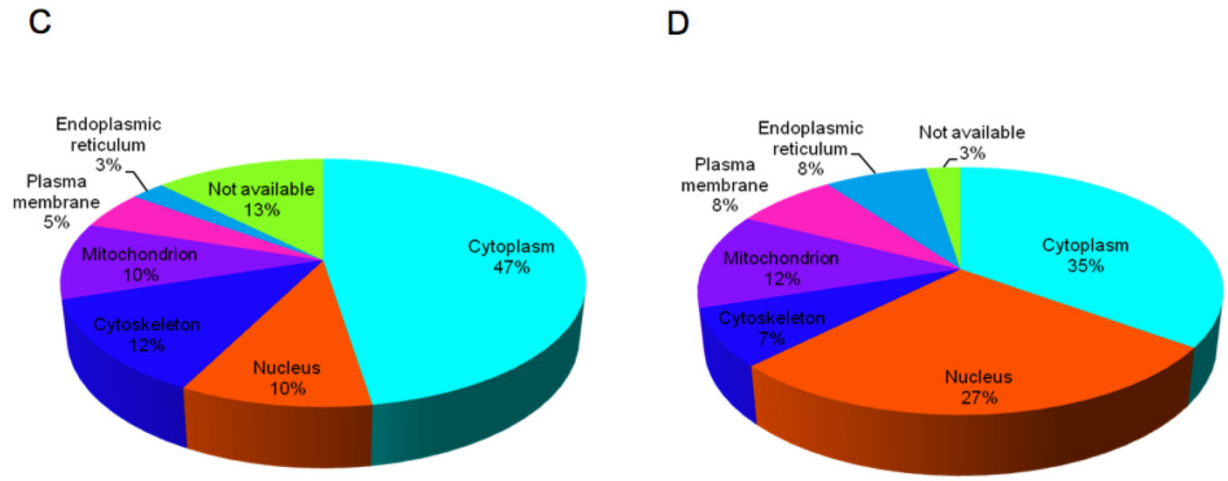

Figure 28. Classification of the over-expressed (A) and under-expressed (B) proteins in KCL22R cells according to Gene Ontology cellular localization.

TABLE 7. Gene Ontology analysis of over-expressed proteins in KCL22R *versus* KCL22S cells

Molecular Functions	**p-value**
Oxidoreductase activity	$1.86\ 10^{-6}$
Translation regulator activity	$2.17\ 10^{-5}$
Phosphoribosyltransferase activity	$1.27\ 10^{-3}$
NAD binding	$1.48\ 10^{-3}$
Ligase activity	$2.61\ 10^{-3}$
Hydrolase activity	$3.79\ 10^{-3}$
Isomerase activity	$3.79\ 10^{-3}$
Transporter activity	$6.31\ 10^{-3}$
GDP-dissociation inhibitor activity	$1.01\ 10^{-2}$
Proteasome activator activity	$1.02\ 10^{-2}$
Ferric ion binding	$2.25\ 10^{-2}$
RNA binding	$2.63\ 10^{-2}$
AMP binding	$3.12\ 10^{-2}$
Peptidase activity	$3.24\ 10^{-2}$
Protein binding	$3.5\ 10^{-2}$
Carbonate dehydratase activity	$3.61\ 10^{-2}$
Actin binding	$3.71\ 10^{-2}$
Signal transducer activity	$3.84\ 10^{-2}$
Structural constituent of cytoskeleton	$3.87\ 10^{-2}$
ATP binding	$3.91\ 10^{-2}$
Calcium ion binding	$4\ 10^{-2}$
Metal ion binding	$4.32\ 10^{-2}$

TABLE 8. Gene Ontology analysis of under-expressed proteins in KCL22R *versus* KCL22S cells

Molecular Functions	**p-value**
Peptidase activity	$8.59\ 10^{-4}$
Nucleotide binding	$3.58\ 10^{-4}$
Phosphoribosyltransferase activity	$4.29\ 10^{-3}$
Oxidoreductase activity	$4.7\ 10^{-3}$
Ligase activity	$6.85\ 10^{-3}$
Phospholipase inhibitor activity	$8.56\ 10^{-3}$
Peptidase inhibitor activity	$8.56\ 10^{-3}$
Isomerase activity	$1.2\ 10^{-2}$
Calcium ion binding	$2.55\ 10^{-2}$
Hydrolase activity	$3.63\ 10^{-2}$
Protein binding	$3.74\ 10^{-2}$
Helicase activity	$3.88\ 10^{-2}$
Transcription regulator activity	$3.91\ 10^{-2}$
Signal transducer activity	$4\ 10^{-2}$
RNA binding	$4.3\ 10^{-2}$
DNA binding	$4.35\ 10^{-2}$
Transporter activity	$4.9\ 10^{-2}$

3.5.2 Ingenuity software analysis

To identify molecular networks involving proteins described above, the obtained data were analyzed using Ingenuity Pathway Analysis (IPA) software (Ingenuity Systems, www.ingenuity.com) [76]. The system created three major protein networks. The three networks and the related proteins are listed in Table 9. The networks are related to cellular function and maintenance, post-translational modification, protein folding (score=38), cell-to-cell signaling and interaction, haematological system development and function (score=29), and cell death (score=27). The identified proteins are shown in red (over-expressed) and green (under-expressed).

Table 9. Functional networks generated by IPA

Networks	Molecules in Network	Score[a]	Top Functions[b]
1	ACTB, ANXA1, ASB9, ATP5A1, CA2, CAP1, ERK, ERP29, F- Actin, HSBP1, HSF1, HSP70, HSPA5, HSPA1A, HSPB1, HSPB6, HSPD1, Jnk, LASP1, Mapk, MAPKAPK3, MAPKAPK5, MAPKAPK2/3, NFkB (complex), P38 MAPK, PACRG, PI3K, Pkc(s), PLS1, PTPN6, PTPN11, SIGLEC11, TCP1, VDAC1, XRCC5	38	Cellular function and maintenance, post-translational modification, protein folding
2	APRT, CDC42EP2, CDC42EP3, CHI3L1, CLIC1, CLTCL1, CTNNB1, F13A1, FAHD1, GAS6, GH1, HNF4A, HSPA4L, HSPB1, IL1B, IMPDH2, KCNJ11, KITLG, LCP1, LDHB, LTA4H, MME, MTHFD1, NQO2, PIP5K1A, PSAT1, RPSA, SEPT2, SEPT6, SEPT7, SNX5, TAGLN2, TXNIP, VDAC2, XRCC4	29	Cell to cell signaling and interaction, hematological system development and function
3	ANXA11, CASP3, CCK, CHI3L1, COTL1, DARS2, ECH1, EEF1D, EEF1G, EIF4G1, GARS, HNRNPH3, HNRNPL, HSPBP1, IL2, IL24, KTN1, LAP3, ME2, PCBP2, PHGDH, PIM2, PRTN3, PSME1, pyruvaldehyde, retinoic acid, RPS4X, SERPINB1, SERPINB8, SSB, TNF, TNFRSF1B, TPI1, VEGFA, WNK1	27	Cell death

The table reports the significant functional networks associated with the identified proteins. Each network is constituted by focus gene products, indicated in red (over-expressed) and green (under-expressed) and non focus gene products, indicated in black, which allow connecting all the gene products in a network.

[a] The fit of the user's set of focus genes/gene products with all the genes/gene products stored in the knowledge base. The score is derived from a p-value (equal to or smaller than 0.05, Fischer's exact test). The p-value indicates the likelihood of the focus genes/gene products in a network being found together due to random chance.

[b] The most statistically significant biological functions assigned to each network.

Because the IPA server's restriction that a single network cannot contain more than 35 genes/gene products, the three networks were merged into a single network (Figure 29). The network is constituted by 42 focus gene products (identified in our analysis) and 61 non focus gene products, indicated by white icons, which allow connecting all the gene products in a network. Interestingly, several identified proteins were correlated, in the IPA network 1, to Ras-mitogen-activated protein kinase signaling (Ras-MAPKs) (Figure 30), which is associated with proliferation and drug resistance of hematopoietic cells [77].

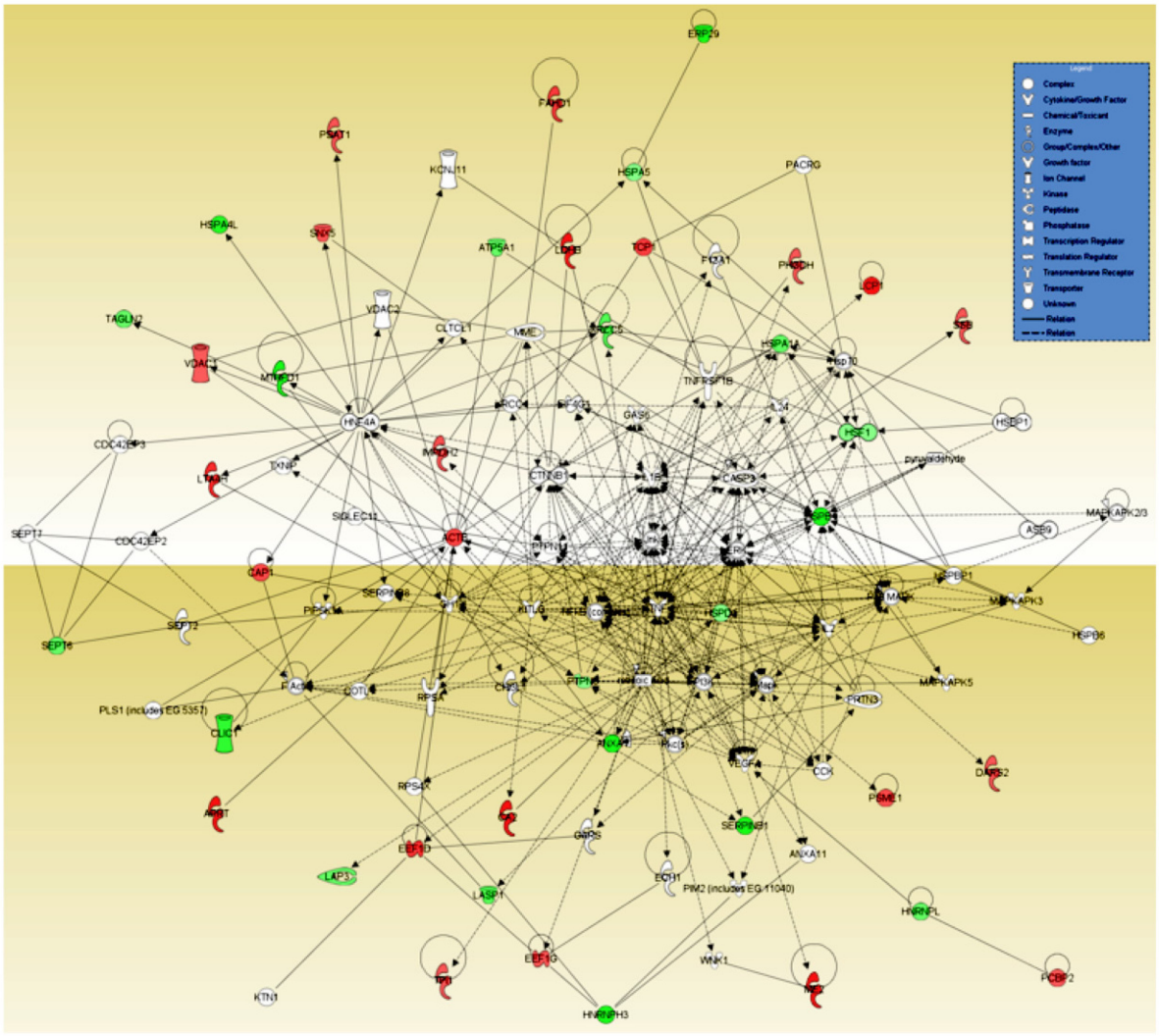

Figure 29. Ingenuity merged network derived from networks 1, 2, 3 as reported in Table 9. Green represents a decrease, red indicates an increase in protein expression and white represent proteins not identified in this study, which allow in connecting all the proteins together in a network. Proteins are identified by gene code. The intensity of shading increases with the magnitude of change. Nodes are indicated by various shapes that represent the functional class of the gene product. Solid lines indicate direct interactions between nodes, and dashed lines indicate indirect interactions. Lines beginning and ending on the same node indicate self-regulation. Arrowheads show directionality of the relationship.

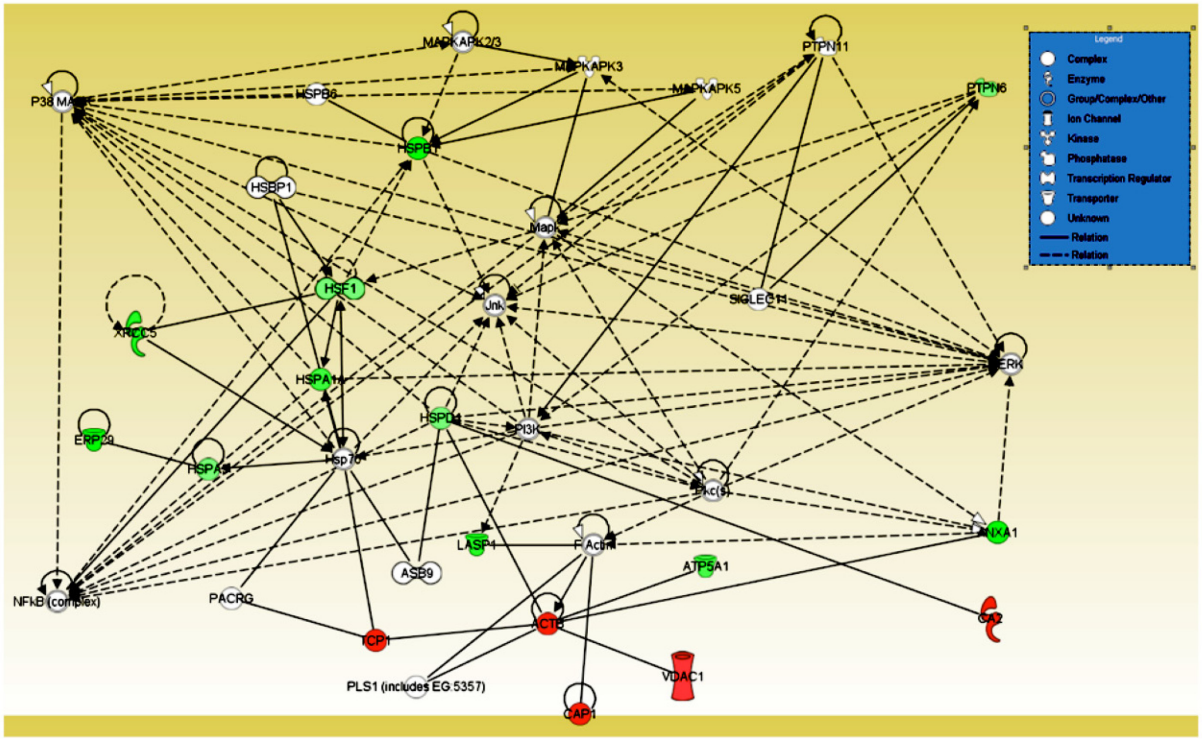

Figure 30. Ingenuity network 1 as reported in Table 9.

3.6 NADP/NADPH and GSH levels in KCL22R and KCL22S cells

NADP-dependent isocitrate dehydrogenase (IDH1) and Malic enzyme (ME2) were found to be over-expressed in KCL22R cells by DIGE analysis described above. Both enzymes are involved in the regulation of intracellular level of glutathione (GSH) by providing the NADPH necessary for the activity of glutathione reductase [78,79]. The level of NADP/NADPH and GSH were then tested in KCL22R and KCL22S cells. The results (Figure 31) showed that the ratio of NADP/NADPH in KCL22R cells is higher than in KCL22S cells; this suggests that there is an increase in NADPH consumption probably required for GSH synthesis. In line with this observation, GSH increased in KCL22R cells (Figure 32). Taken together, these observations suggest that the level of expression of Idh1 and Me2 could affect the balance between NADPH and GSH.

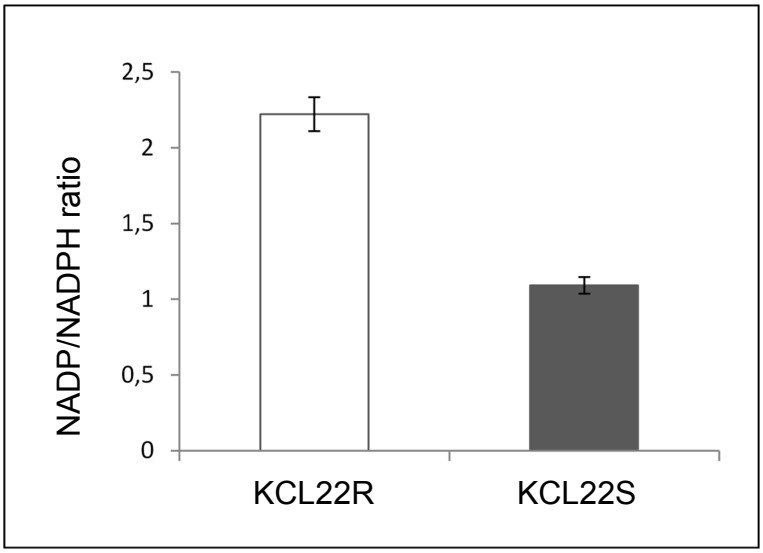

Figure 31. NADP/NADPH ratio measured in KCL22R and KCL22S cells. The NADP/NADPH ratio was calculated as (NADPt-NADPH)/NADPH. Data represent the mean of three independent experiments.

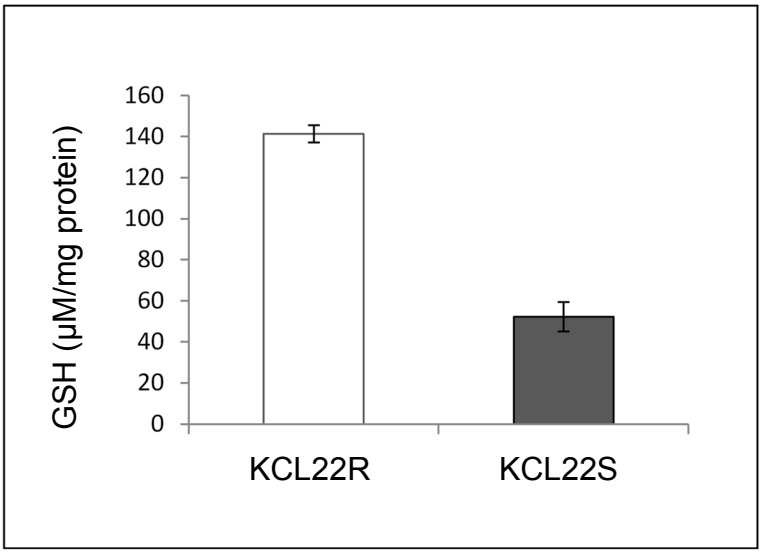

Figure 32. Glutathione (GSH) concentration measured in KCL22R and KCL22S cells as described in the 'Materials and methods' section. GSH content was normalized as the ratio between O.D./mg protein. Data represent the mean of three independent experiments.

3.7 Evaluation of Erk activation in KCL22R and KCL22S cells

Closed examination of the IPA network 1 displays that several differentially expressed proteins between KCL22R and KCL22S cells are directly or indirectly connected with key cell signaling proteins, involved in the modulation of cellular proliferation and apoptosis (Figure 30). The level of activation of Erk 1/2, a mitogen-activated protein kinase family that contributes to the survival of leukemia cells [77], was analysed. The level of Erk and its phosphorylated form was measured by Western blot. The experiment showed that the level of total Erk 1/2 was similar in KCL22R and KCL22S cells (Figure 33). In contrast, the level of phosphorylated Erk 1/2 was increased in KCL22R (Figure 33), suggesting that continuous activation of Erk occurred in KCL22R cells.

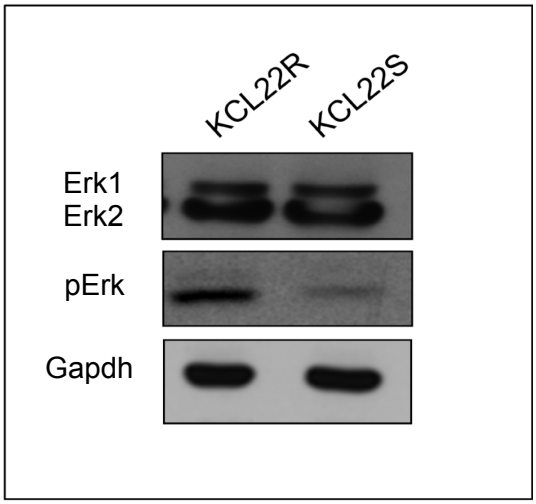

Figure 33. Western blot analysis on total protein lysates of KCL22R cells and KCL22S cells Proteins were separated on 10% SDS-PAGE and immunoblotted with antibodies against Erk 1/2 and pErk. Gapdh served as control.

3.8 IPA network 1 analysis

3.8.1 Analysis of Shp2 phosphorylation in KCL22R and KCL22S cells

Network 1, generated by IPA analysis (Table 9 and Figure 30), showed that several differentially expressed proteins were connected with Erk signaling. The Raf/Mek/Erk pathway influences chemotherapeutic drug resistance which is usually associated with proliferation and drug resistance of hematopoietic cells [77]. Interestingly the network 1 includes two SH2-containing, non-receptor protein tyrosine phosphatases, Shp1 (PTPN6) and Shp2 (PTPN11). Shp2 positively regulates the Ras-Erk pathway [80] and is activated by the phosphorylation at the Tyr542 and Tyr580 residues in its carboxy-terminus, in response to growth factor receptor activation and oncogenic protein-tyrosine kinases such as Bcr-Abl [81]. These phosphorylation events seem to reduce basal inhibition and stimulate the tyrosine phosphatase activity [82]. The activation status of Shp2 was analysed in KCL22S and KCL22R cells, evaluating the phosphorylation on Tyr542 that is one of the Grb2 binding site, upstream of Ras/Raf/Erk activation [83, 84]. Immunoblot analysis using an antibody specific for the pShp2 showed that the level of phosphorylated Tyr542 in KCL22R cells was higher than in KCL22S cells (Figure 34), suggesting that continuous activation of Shp2 occurred in KCL22R cells.

3.8.2 The Effect of SHP2 knock-down on KCL22R viability

The role of Shp2 in KCL22R viability was next investigated, knocking-down the expression of the phosphatase by shRNA technology. Interestingly, SHP2 Knock-down KCL22R ($KCL22R^{SHP2-}$), cultured in the presence of 1μM imatinib for 4 days, showed a reduction in cell viability (Figure 35), as assessed by trypan blue exclusion assay, comparing to KCL22R. This result suggests a synergistic effect between the

Shp2 suppression and imatinib treatment on the inhibition of the KCL22R cell viability.

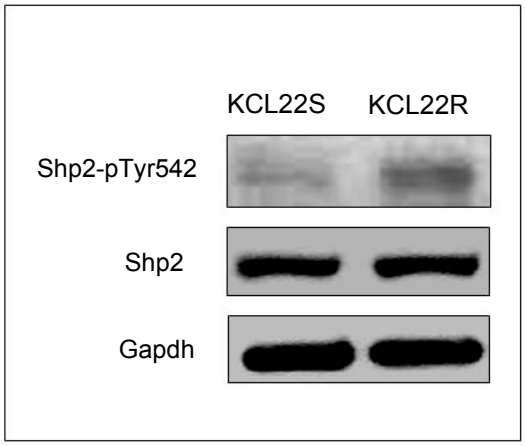

Figure 34. Western blot analysis on total protein lysates of KCL22S cells and KCL22R cells. Proteins were separated on 10% SDS-PAGE and immunoblotted with antibodies against Shp2-pTyr542 and Shp2. Gapdh served as control.

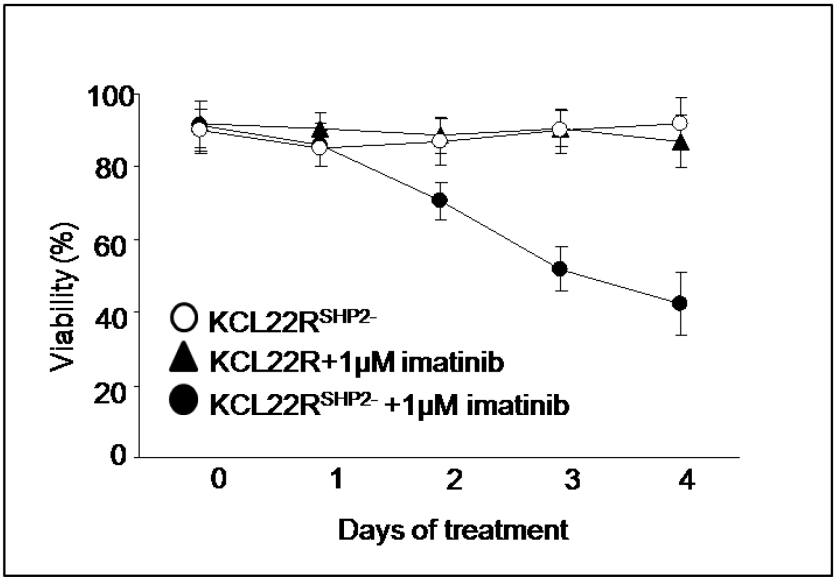

Figure 35. Cell viability, assessed by trypan blue exclusion assay, on SHP2 Knock-down KCL22R ($KCL22R^{SHP2-}$) without imatinib, KCL22R and $KCL22R^{SHP2-}$ with 1 μM imatinib. All experiments were performed in triplicate and results were expressed as means±SD.

3.8.3 The Effect on Erk activation of SHP2 knock-down in KCL22R cells

The level of Erk and its phosphorylated form was measured by Western blot in KCL22R and KCL22R^{SHP2-} cells, in presence of 1μM imatinib. The experiment showed that the level of phosphorylated Erk was significantly suppressed in KCL22R^{SHP2-}, with no change in the level of total Erk 1/2, in comparison to the KCL22R cells (Figure 36). This result showed that the knock-down of Shp2 significantly reduced the activation of Erk 1/2 in KCL22R cells and suggests a positive role of this phosphatase in Erk activation.

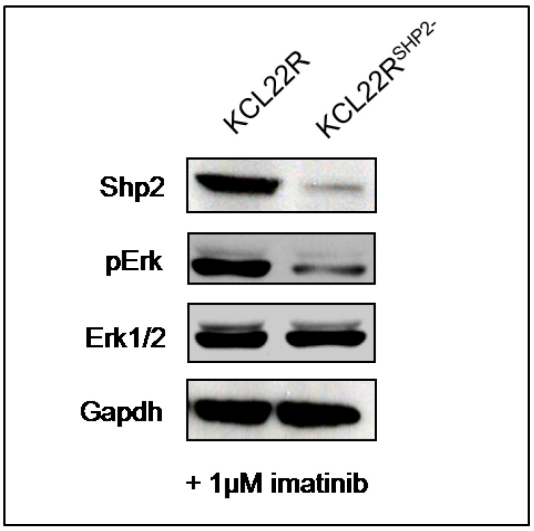

Figure 36. Western blot analysis on total protein lysates of KCL22R and SHP2 Knock-down KCL22R (KCL22R^{SHP2-}), with 1 μM imatinib. Proteins were separated on 10% SDS-PAGE and immunoblotted with antibodies against Shp2, pErk and Erk 1/2. Gapdh served as control.

3.8.4 Shp1 and Shp2 interaction in KCL22R and KCL22S cells

Since a previous work demonstrated that Shp1 plays a role in regulating the function of Shp2, in colorectal adenocarcinoma cells [72], co-immunoprecipitation assays were carried out to investigate if these proteins interact in KCL22 cells. Resistant and sensitive KCL22 total protein extracts were immunoprecipitated with an antibody against the endogenous Shp2 protein. As shown in Figure 37 Western blot analysis with an antibody against Shp1 demonstrated that Shp1 and Shp2 interacted in KCL22S cells (Figure 37A) while in KCL22R cells, where Shp1 is expressed at very low level, this interaction was not detected (Figure 37B). To confirm these data an immunoprecipitation experiment was performed with an antibody against the endogenous Shp1 in KCL22S and in KCL22R cells. Another CML Ph+ cell line, sensitive to imatinib, K562, was used as a control. As shown in Figure 38, Western blot analysis carried out with an antibody against Shp2 confirmed the interaction between Shp2 and Shp1 in KCL22S and K562 sensitive cells (Figure 38A and B), while this interaction was not detected in resistant cells (Figure 38C).

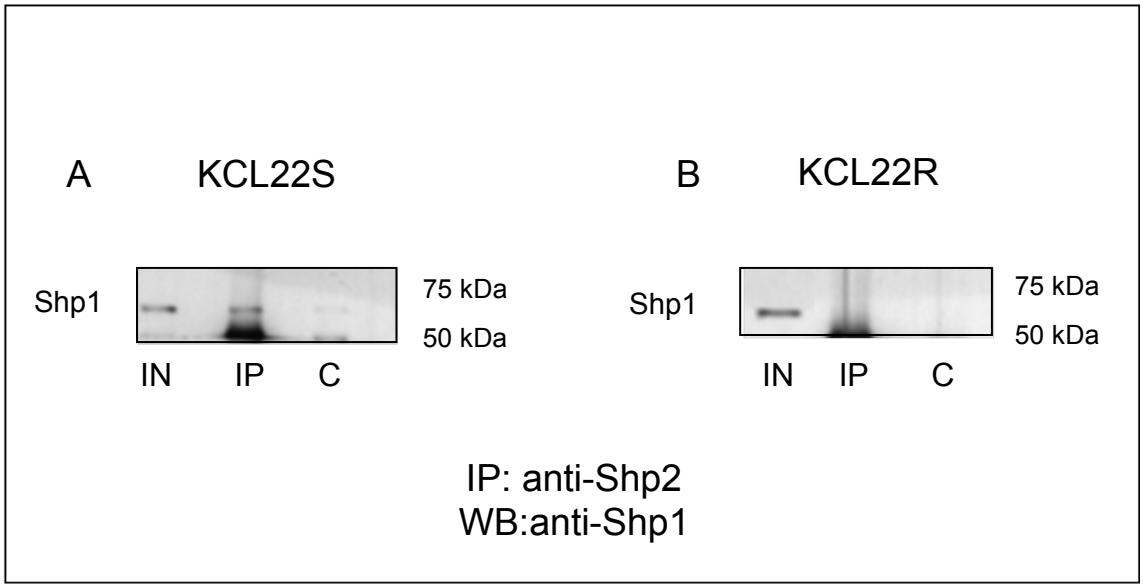

Figure 37. KCL22 sensitive (A) and resistant (B) cellular extracts were immunoprecipitated (IP) with anti-Shp2 antibody and the immunoprecipitates were subjected to Western blot analyses with an anti-Shp1 as indicated. An irrelevant rabbit IgG was used as control. IN = input, IP = immunoprecipitate, C = control.

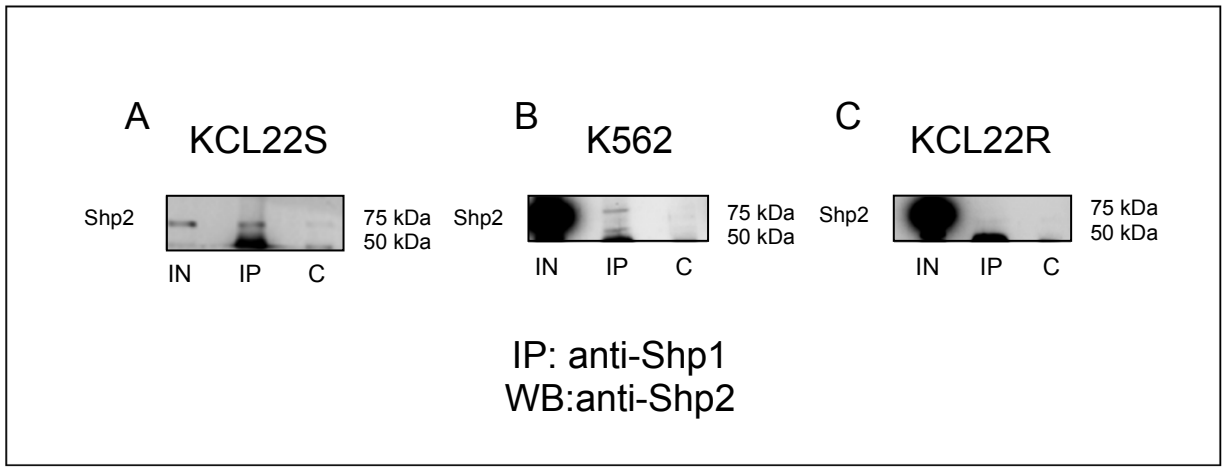

Figure 38. KCL22 sensitive (A), K562 (B) KCL22 resistant (C) cellular extracts were immunoprecipitated (IP) with anti-Shp1 and the immunoprecipitates were subjected to Western blot analyses with an anti-Shp2 as indicated. An irrelevant rabbit IgG was used as control. IN = input, IP = immunoprecipitate, C = control.

Moreover, an immunoprecipitation experiment was performed with an antibody against the endogenous Shp1 in KCL22R cells transfected with a plasmide coding for the human full-length SHP1-sequence ($KCL22R^{SHP1+}$). As shown in Figure 39, the Shp1 over-expression in resistant cell line restored the interaction with the Shp2 phosphatase, suggesting that the lack of co-immunoprecipitation of Shp1 and Shp2 in resistant cells could be related to the low Shp1 expression more than a real inability to interact.

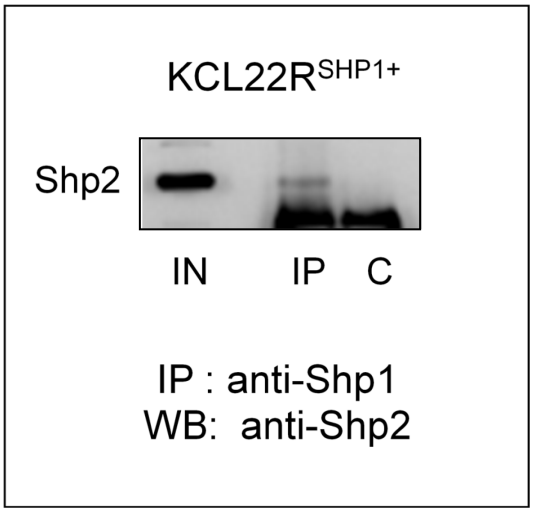

Figure 39. KCL22R Shp1 Knock-in ($KCL22R^{SHP1+}$) cellular extract was immunoprecipitated (IP) with an anti-Shp1 and the immunoprecipitates were subjected to Western blot analyses with an anti-Shp2 as indicated. An irrelevant rabbit IgG was used as control. IN = input, IP = immunoprecipitate, C = control.

3.8.5 Shp1 Knock-in increases the level of Shp2-Tyr542 phosphorylation in KCL22R cells

To evaluate if the induced expression of Shp1 phosphatase in KCL22R cells could affect the level of phosphorylation of Shp2 on Tyr542, a Western blot analysis was performed, using an antibody against the pShp2-Tyr542 on KCL22S, KCL22R and KCL22R^{SHP1+} cells, in presence of 1μM imatinib. As showed in Figure 40 the level of phosphorylated Shp2-Tyr542 was lower in KCL22R^{SHP1+} cells in comparison to the KCL22R cells. Furthermore, the phosphorylation level of pShp2-Tyr542 in KCL22R with an induced expression in Shp1 was similar to that assessed in KCL22S cells (Figure 40). This result suggests that Shp1 could play a role in the modulation of Shp2 phosphorylation and suggests a negative role of Shp1 phosphatase on Shp2 activation, in KCL22S cells.

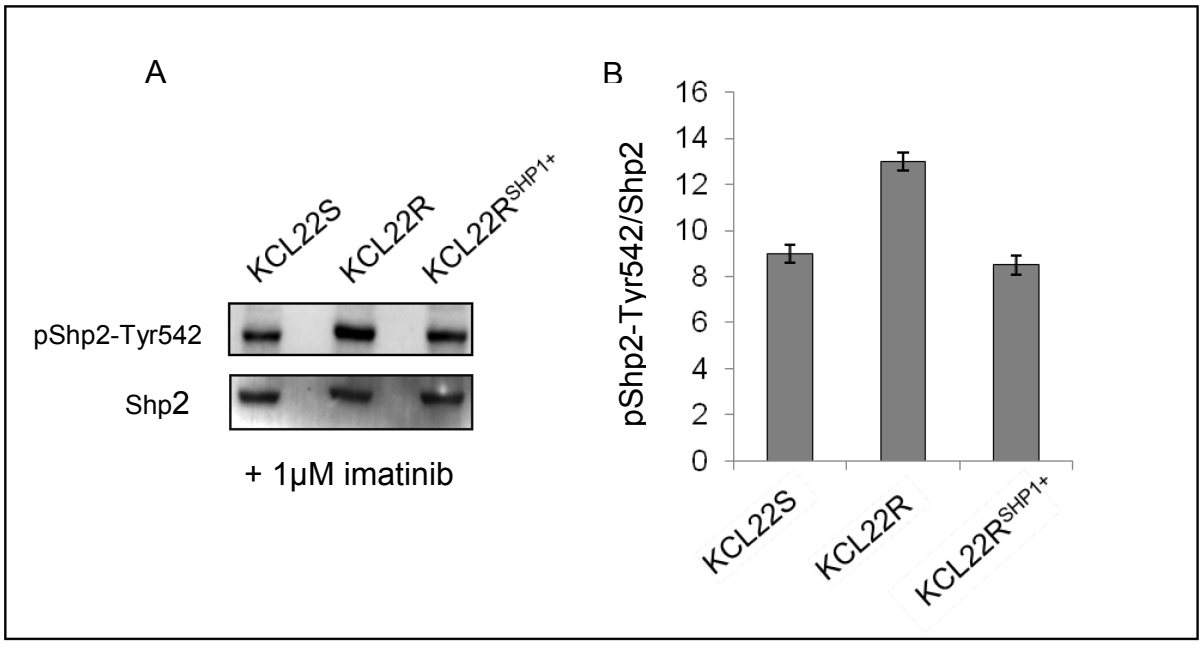

Figure 40. Western blot analysis on total protein lysates of KCL22S, KCL22R and Shp1 Knock-in cell line, KCL22R^{SHP1+}. Proteins were separated on 10% SDS-PAGE and immunoblotted with antibodies against pShp2-Tyr542 and Shp2 (A). The densitometric analysis is shown in B; Shp2 served as control. Results are shown as means±SD of three independent experiments.

3.8.6 Shp2, Annexin A1 and Hsp70 interactions in KCL22S cell line

To try to understand the biological pathway underlying the Shp1 and Shp2 interaction in KCL22 cells, additional Shp2 binding proteins were searched, within the same IPA network 1 (Figure 30). Interestingly a previous work [85] demonstrated, in COS 1 cells derived from monkey kidney, that Annexin A2 binds Shp2 and that this binding is modulated by the Hsp70 level. Since Annexin A1, another annexin family protein, and Hsp70 are connected (IPA network 1) with Erk, which in turn is regulated by Shp2, a co-immunoprecipitation experiment was carried out to investigate if Annexin A1 could associate with Shp2 in our cellular system. The experiment was performed in KCL22S cells in which Annexin A1 was found over-expressed in comparison to KCL22R cells. The KCL22S immunoprecipitate against the endogenous Shp2 was subjected to Western blot analysis with an antibody against Annexin A1. As shown in Figure 41 Annexin A1 and Shp2 interacted in KCL22S cells.

By co-immunoprecipotation assay was also demonstrated, that Hsp70 and Annexin A1 interacted in KCL22S cells (Figure 42).

The direct or indirect interaction of Annexin A1 and Hsp70 with Shp2 suggests that these proteins, down-regulated in KCL22R cells, could play a role in regulating the Shp2 functions.

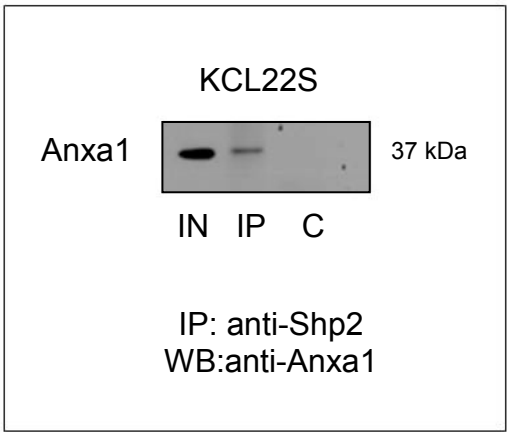

Figure 41. KCL22 sensitive cellular extract was immunoprecipitated (IP) with anti-Shp2 antibody and the immunoprecipitate was subjected to Western blot analyses with an anti-Anxa1 antibody as indicated. An irrelevant rabbit IgG was used as control. IN = input, IP = immunoprecipitate, C = control.

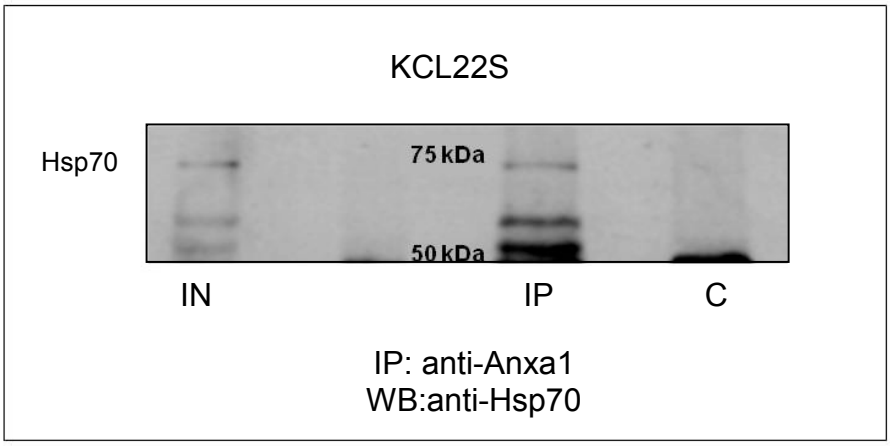

Figure 42. KCL22 sensitive cellular extract was immunoprecipitated (IP) with an Anxa1 antibody and the immunoprecipitate was subjected to Western blot analyses with an Hsp70 antibody as indicated. An irrelevant rabbit IgG was used as control. IN = input, IP = immunoprecipitate, C = control.

3.9 Detection of Hsp70, Hsp60, Hsp27 and Grp78 proteins in CML patients

The expression of four Heat shock proteins (Hsp70, Hsp60, Hsp27 and Grp78) was evaluated on samples from nine untreated patients with CML in chronic phase, at diagnosis, using Western blot. After imatinib treatment at the standard dose, five had an optimal response based on criteria defined by the European Leukemia Net [86], whereas the remaining four were classifiable as failure of treatment based on the same criteria. Hsp70, Hsp60, Hsp27 and Grp78 expression was lower in cells of imatinib-resistant CML patients than in imatinib-responding CML patients (Figure 43). Although the experiments were performed on a very small number of patients, because the very limited sample availability, the results obtained suggest that this class of proteins could play a role of prognostic marker in imatinib resistance.

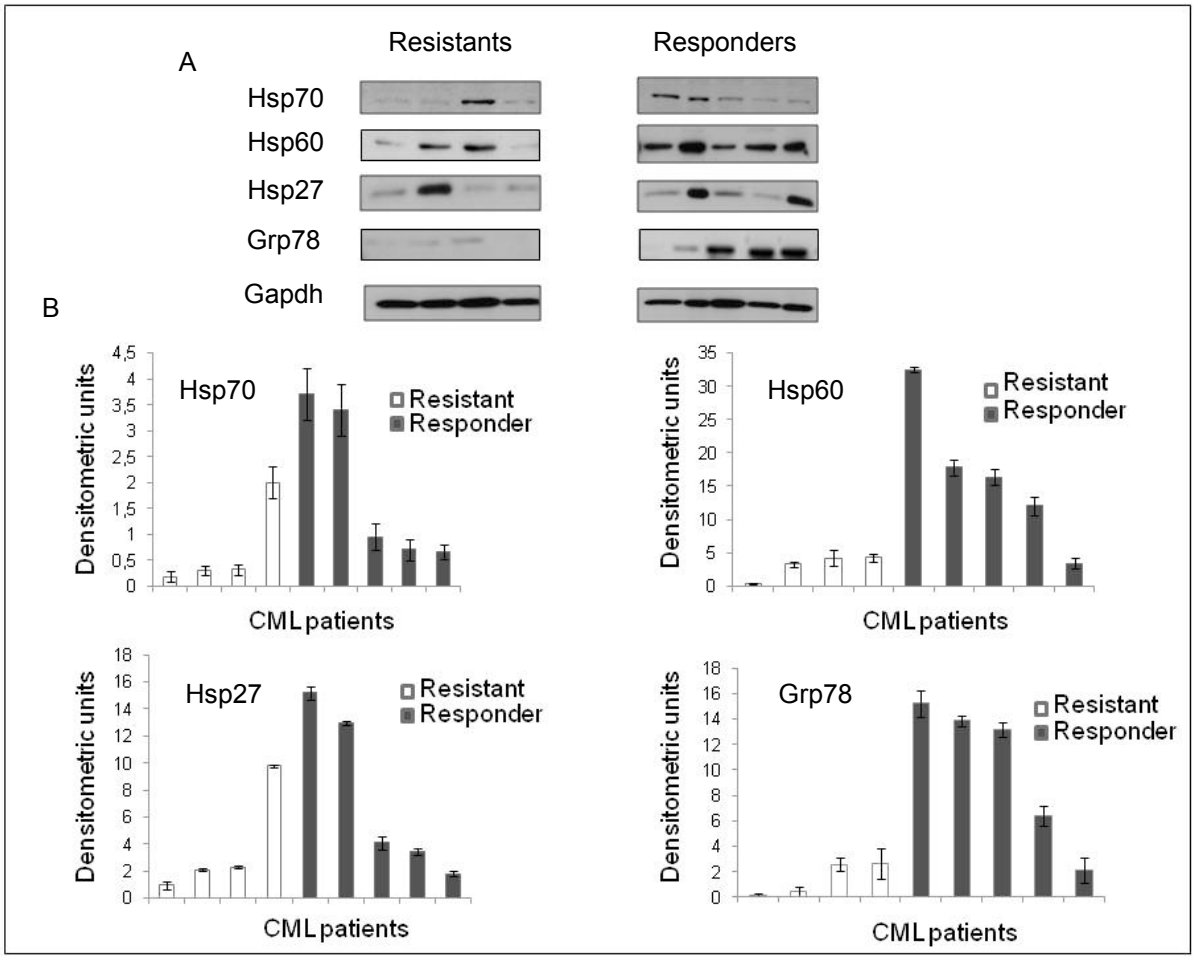

Figure 43. Western blot analysis of total protein lysates of cells from chronic myeloid leukemia patients in chronic phase, before imatinib treatment. Proteins were separated on 10% SDS-PAGE and immunoblotted with antibodies against Hsp70, Hsp60, Hsp27 and Grp78 proteins. Gapdh served as control (A). The densitometric analysis was performed on three experiments. The results are shown as means±SD (B).

Chapter 4

DISCUSSION

Imatinib masylate, a potent inhibitor of the Bcr-Abl tyrosine kinase activity, is used as first-line therapy of CML patients; however a major concern in imatinib treatment is the emergence of resistance to the drug during disease progression [23]. The aim of this study was to obtain insights into the Bcr-Abl activity-independent mechanisms of imatinib resistance. The imatinib-resistant KCL22R and sensitive KCL22S cells were used as experimental model. None of the known resistance mechanisms has been detected in these cell lines [24] and therefore novel mechanisms could be envisaged. Moreover, KCL22S cells exhibited typical features of the Ph+ hematopoietic stem cells [69]. It has been in fact shown that imatinib, in combination with a farnesyltransferase inhibitor, induced KCL22S growth arrest but the apoptosis was less evident in KCL22S than in other CML cells [70]. Therefore, KCL22 cells represent a good cellular system to investigate imatinib resistance, based on Bcr-Abl activity-independent mechanisms. Using a proteomic approach (two-dimensional differential gel electrophoresis, [2D-DIGE] coupled with mass spectrometry) 51 differentially expressed proteins were characterized: 27 over-expressed and 24 under-expressed in KCL22R cells *versus* KCL22S cells.

Gene Ontology analysis of the over-expressed proteins in KCL22R cells showed that the two most statistically relevant molecular functions are oxidoreductase activity and translation regulator activity (Table 7). Two proteins were annotated in the oxidoreductase activity: NADP-dependent isocitrate dehydrogenase (IDH1) and malic enzyme (ME2). Both enzymes are involved in production of NADPH, which is an important cofactor in many biosynthesis pathways and in particular in the regeneration of reduced glutathione (GSH) [78]. GSH functions as a cellular

antioxidant, and is thus critical for maintenance of redox balance [87]. GSH concentration was found significantly higher in KCL22R cells than in KCL22S cells. In addition a previous study showed that the supplementation of GSH to KCL22S cells resulted in an increase in the IC50 value of imatinib [88]. It is well known that imatinib mesylate is metabolized via conjugation with glutathione (GSH) catalyzed by glutathione S-transferase enzymes [89]. Thus, GSH accumulation may affect imatinib catabolism together with other biological functions as intracellular signaling. In fact, GSH affects activation of anti-apoptotic MAP-kinase and NF-kB signaling [90, 91] (Figure 44). Interestingly, within the under-expressed proteins in KCL22R cells, was found a NAD(P)H quinone oxidoreductase, Nqo2. Nqo2 is a cytosolic flavoprotein that carries out the 2-electron reduction of quinones using electron donors such as nicotinamide riboside (NRH) and is known to be involved in metabolic activation and/or detoxification of xenobiotics [92,93], although its precise physiological role remained uncertain [94]. Recently, it has been reported that the oxidoreductase Nqo2 was bound and inhibited by imatinib in K562 and CML patient samples [73], although the role of this process on the efficacy of imatinib remained unknown. The differential expression of Nqo2 across KCL22R and KCL22S cells could play a role in the imatinib metabolism (Figure 44).

Another statistically relevant molecular function was related to translation regulator activity. The human elongation factor-1-delta (EEF1D), being in this class, is involved in the positive regulation of the I-KappaB kinase/NFkappaB cascade [95]. In imatinib-resistant CML patients, the NF-kB cellular pathway is activated in a Bcr-Abl-independent fashion [96]. This pathway could be enhanced by the over-expression of EEF1D (Figure 44).

To identify molecular networks involving proteins identified in this study, the obtained data were analysed using IPA software. Drawing on published literature, IPA constructs networks of direct and indirect interactions between orthologous mammalian genes, proteins and endogenous chemicals. The system created three major protein networks. The three networks and the related proteins are listed in Table 9. Examination of network 1, the most statistically significant interaction network, (Table 9 and Figure 30) showed that several differentially expressed proteins were connected with Erk signaling [97, 98]. The Raf/MEK/ERK pathway influences chemotherapeutic drug resistance [77]. Interestingly, the level of phosphorylated Erk 1/2 in KCL22R was found higher than in KCL22S cells (Figure 33), suggesting that activation of Erk occurred in KCL22R cells, in line with a study showing that the Bcr-Abl-independent activation of Erk 1/2 may contribute to imatinib resistance in K562 CML cells [99].

Protein network 1 (Figure 30) includes two SH2-containing, non-receptor protein tyrosine phosphatases Shp1 (PTPN6) and Shp2 (PTPN11). Although many studies have been focused on the role of tyrosine kinases involved in imatinib resistance [43,100], few data are available on the role of tyrosine phosphatases in Ph+ cells and in patients who lack or loose response to the imatinib treatment [101]. Shp1 and Shp2 have important physiological roles and may be implicated in the neoplastic transformation of hematopoietic cells [102]. Reduction of SHP1 gene expression is observed in natural killer cell lymphomas as well as other types of lymphoma and leukemia [103,104]. Interestingly, decreased expression level of Shp1 is associated with progression of chronic myeloid leukemia [105]. Shp2 positively regulates the Ras-Erk pathway [80] and is activated by the phosphorylation at the Tyr542 and Tyr580 residues in its carboxy-terminus, in response to growth factor receptor and

oncogenic protein-tyrosine kinases, included Bcr-Abl, activation [81]. These phosphorylation events seem to reduce basal inhibition and stimulate the tyrosine phosphatase activity [82]. The role of Shp1 and Shp2 phosphatases in imatinib resistance of KCL22R cells was then investigated. The activation status of Shp2 in KCL22S and KCL22R cells was analysed, evaluating the protein phosphorylation on Tyr542 that is as one of the Grb2 binding site, upstream of Ras/Raf/Erk activation [80]. Western blot analysis showed that the level of phosphorylated Tyr542 in KCL22S cells was lower than in KCL22R cells (Figure 34), suggesting that continuous activation of Shp2 occurred in KCL22R cells. Thus, to elucidate whether the low expression of Shp1 and the higher activation status of Shp2, could be directly associated with imatinib resistance in KCL22R cells, Shp2 was knock-down and Shp1 was over-expressed in resistant cells. Interestingly, by knocking-down the expression of Shp2 in KCL22R cells, it was observed a reversion of the KCL22R phenotype, in the presence of 1μM imatinib (Figure 35). These data suggest a synergistic effect between the Shp2 suppression and imatinib treatment on the reduction of KCL22R cell survival. This study also demonstrated that the knock-down of Shp2 significantly reduced the activation of Erk 1/2 in KCL22R cells and suggests a positive role of this phosphatase in Erk activation.

Shp1 has been generally considered a negative regulator of cell proliferation essentially as antagonist of Shp2 that is an oncogenic protein [72]. Most importantly, this study demonstrated that Shp1 and Shp2 interact in KCL22 cells and that Shp1 plays a role in regulating the Shp2 phosphorylation. The Shp1 induced expression in KCL22R cells, in fact, leads to a decrease in the level of Shp2 phosphorylation (Figure 40), suggesting that Shp1 plays a role of negative regulator of Shp2 activation. Therefore the Shp1 down-regulation in KCL22R cells is in line with the

increased level of Shp2 phosphorylation and thus with the continuous Erk activation (Figure 44 and 45).

Moreover, to try to understand the biological pathway underlying the Shp1 and Shp2 interaction in KCL22 cells, additional Shp2 binding proteins were searched, within the IPA network 1 (Figure 30). By co-immunoprecipitation assay it was demonstrated that Shp2 interacts with Annexin A1. The last protein was down-regulated in KCL22R cells. Annexin A1 is a 37-kDa member of the annexin family that structurally belongs to a family of ubiquitous phospholipids and calcium-binding proteins. It is implicated in apoptosis induction [106], caspase-3 activation [107, 108] and cell growth inhibition [109]. Annexin A1 reduces cell proliferation by the induction of aberrant cytoskeletal organization through modification of Erk activation [110]. In line with these observations, it was found that imatinib significantly reduced cell proliferation in KCL22S cells, while KCL22R cells exhibited an elevated growth-rate in presence of imatinib (Figure 14). In this context, it is interesting to note that actin beta (ACTB), adenyl cyclase-associated protein 1 (CAP1) and chaperonin-containing TCP1 (TCP1), which play a role in the actin remodelling [111] and protection of the cytoskeleton during stress [112] were over-expressed in KCL22R cells (Figure 44).

Network 1 (Figure 30) also includes several stress response and chaperone proteins. In particular, different members of the Heat shock family were found to be modulated in KCL22 cells and in imatinib-resistant CML patients *versus* responders, as Hsp70 (HSPA1A), Hsp60 (HSPD1), Hsp27 (HSPB1) and Grp78 (HSPA5) (Figure 43 and 44). Recent studies showed that the over-expression of Hsp70 could be related to imatinib resistance in K562 CML cells and that Hsp60 and Grp78 were under-expressed in these cells [71,113]. Interestingly, this study showed an opposite trend for Hsp70 suggesting that the mechanisms of imatinib resistance in KCL22R cells

could be unlike these showed by other resistant CML cell lines. Moreover this study demonstrated that Hsp70 interacts with Annexin A1 in KCL22S cells, suggesting that this protein could be involved, in concert with Annexin A1, in the regulation of Shp2 functions (Figure 45). Although the results obtained highlight the complexity and multifactorial nature of the alterations associated with the imatinib resistance, the proteomic approach, based on 2D-DIGE, mass spectrometry and bioinformatic tools, has proved to be an efficient strategy to identify proteins that could play a role in imatinib resistance. Significant differences between KCL22R and KCL22S cells were found, as regards the expression levels of proteins involved in the modulation of mechanisms related to redox balance and activation of anti-apoptotic pathways mediated by NF-kB and Ras-MAPK signaling (Figure 44). In particular this study demonstrated that a reduced Shp1 expression in KCL22R cells could contribute to a continuous Shp2 activation, sustaining a Bcr-Abl activity-independent pathway of proliferation and survival to imatinib treatment, mediated by Erk (Figure 45). These two proteins could be used as putative biomarkers to evaluate the efficacy of imatinib treatment and to develop new combinatorial therapeutic approaches.

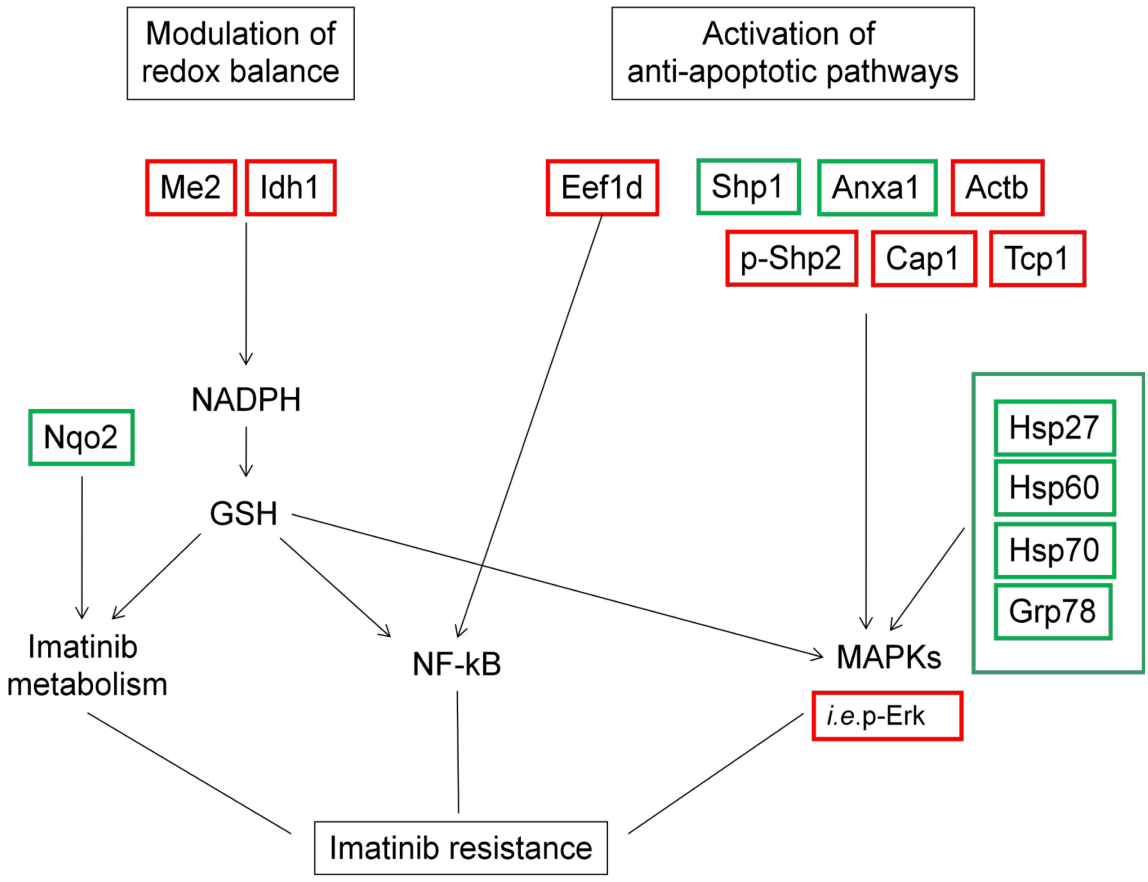

Figure 44. Proposed mechanisms potentially involved in imatinib resistance, as indicated by comparative proteomic analysis between KCL22 resistant and KCL22 sensitive cells. NAD(P)H quinone oxidoreductase (Nqo2), Malic enzyme (Me2), NADP-dependent isocitrate dehydrogenase (Idh1) proteins are involved in the modulation of redox balance. Human elongation factor-1-delta (Eef1d), SH2-containing non-receptor protein tyrosine phosphatases Shp1 and Shp2 (phosphorylated form), annexin A1 (Anxa1), actin beta (Actb), adenyl cyclase-associated protein 1 (Cap1), chaperonin-containing TCP1 (Tcp1) cytoskeletal proteins and Hsp27, Hsp60, Hsp70, Grp78 stress response and chaperone proteins are involved in the activation of anti-apoptotic pathways mediated by NF-kB and Ras-MAPK (*i.e.* p-Erk*)* signaling. Green represents a decrease, red indicates an increase in protein expression in KCL22R *versus* KCL22S cells.

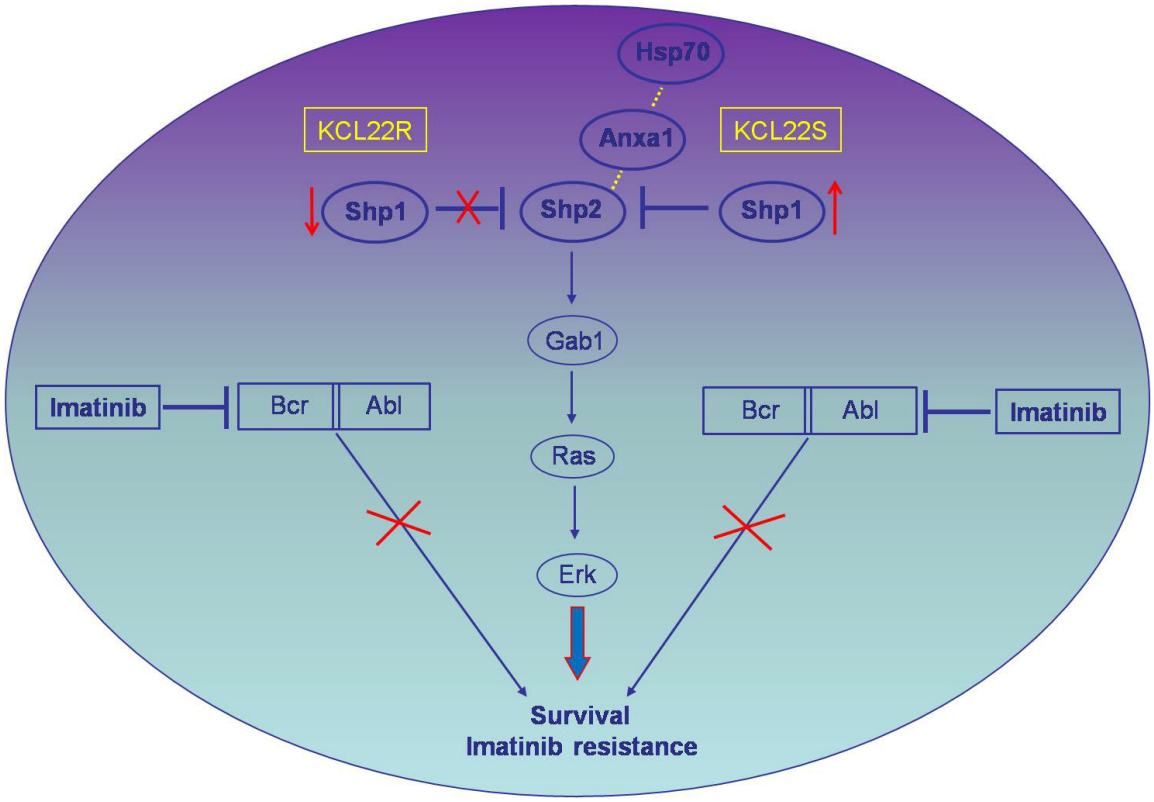

Figure 45. The effect of Shp1 under-expression on Shp2 and Erk activation resulting in imatinib resistance, in KCL22R *versus* KCL22S cells. Shp1 acts as a negative regulator of cell proliferation essentially as antagonist of Shp2 that positively regulates the Ras-Erk pathway. Therefore the Shp1 down-regulation in KCL22R cells results in the increased level of Shp2 activation as compared to the KCL22S cells, sustaining a Bcr-Abl activity-independent pathway of proliferation and survival to imatinib treatment, mediated by Erk. Annexin A1 and Hsp70 could also play a role on the modulation of this pathway, by the direct or indirect interaction with Shp2.

REFERENCES

[1] Sattler M, Griffin JD. Molecular mechanisms of transformation by the BCR–ABL oncogene. *Semin. Hematol.* 2003, **40**: 4-10

[2] Ren R. Mechanisms of BCR-ABL in the pathogenesis of chronic myelogenous leukaemia. *Nat. Rev. Cancer* 2005**, 5**:172-183

[3] Pane F, Mostarda I, Selleri C, Salzano R, Raiola AM, Luciano L, Saglio G, Rotoli B, Salvatore F. BCR/ABL mRNA and the P210(BCR/ABL) protein are down-modulated by interferon-alpha in chronic myeloid leukemia patients. *Blood* 1999, **94**: 2200-2207

[4] Deininger MWN, Goldman JM, Melo JV. The molecular biology of chronic myeloid leukemia. *Blood* 2000, **96**: 3343-3356

[5] Melo JV, Hughes TP, Apperley JF. Chronic Myeloid Leukemia. *Hematology Am. Soc. Hematol. Educ. Program.* 2003, **1**: 132-152

[6] Melo JV, Deininger MWN. Biology of chronic myelogenous leukemia-signaling pathways of initiation and transformation. *Hematol. Oncol. Clin. North. Am.* 2004, **18**: 545-568

[7] Melo JV, Barnes DJ. Chronic myeloid leukaemia as a model of disease evolution in human cancer. *Nat. Rev. Cancer* 2007, **7**: 441-453

[8] Chissoe SL, Bodenteich A, Wang YF, Wang YP, Burian D, Clifton SW, et al. Sequence and analysis of the human ABL gene, the BCR gene, and regions involved in the Philadelphia chromosomal translocation. *Genomics* 1995, **27**: 67-82

[9] Melo JV. The diversity of BCR-ABL fusion proteins and their relationship to leukemia phenotype. *Blood* 1996, **88**: 2375-2384

[10] Ravandi F, Cortes J, AlBitar M, Arlinghaus R, Qiang GJ, Talpaz M, Kantarjian HM. Chronic myelogenous leukaemia with p185(BCR/ABL) expression: characteristics and clinical significance. *Br. J. Haematol.* 1999, **107**: 581-586

[11] Pane F, Frigeri F, Sindona M, Luciano L, Ferrara F, Cimino R, Meloni G, Saglio G, Salvatore F, Rotoli B. Neutrophilic-chronic myeloid leukemia (CML-N): a distinct disease with a specific molecular marker (BCR/ABL with C3/A2 junction). *Blood* 1996, **88**: 2410-2414

[12] Pane F, Intrieri M, Quintarelli C, Izzo B, Muccioli GC, Salvatore F. BCR/ABL genes and leukemic phenotype: from molecular mechanisms to clinical correlations. *Oncogene* 2002, **21**: 8652-8667

[13] Ptasznik A, Nakata Y, Kalota A, Emerson S G, Gewirtz A M. Short interfering RNA (siRNA) targeting the Lyn kinase induces apoptosis in primary, and drug-resistant, BCR–ABL1+ leukemia cells. *Nature Med.* 2004, **10**: 1187–1189

[14] Sattler M, Mohi MG, Pride YB, Quinnan LR, Malouf NA, Podar K, Gesbert F, Iwasaki H, Li S, Van Etten RA, Gu H, Griffin JD, Neel BG. Critical role for Gab2 in transformation by BCR/ABL. *Cancer Cell.* 2002, **1**: 479-492

[15] Goga A, McLaughlin J, Afar D E, Saffran D C, Witte O N. Alternative signals to RAS for hematopoietic transformation by the Bcr–Abl Oncogene. *Cell* 1995, **82**: 981-988

[16] Goldman J M, Druker B J. Chronic myeloid leukemia: current treatment options. *Blood* 2001, **98**: 2039-2042

[17] Druker BJ, Tamura S, Buchdunger E, Ohno S, Segal GM, Fanning S, Zimmermann J, Lydon NB. Effects of a selective inhibitor of the Abl tyrosine kinase on the growth of Bcr–Abl positive cells. *Nature Med.* 1996, **2**: 561-566

[18] Deininger MW, Vieira S, Mendiola R, Schultheis B, Goldman JM, Melo JV. BCR–ABL tyrosine kinase activity regulates the expression of multiple genes implicated in the pathogenesis of chronic myeloid leukemia. *Cancer Res.* 2000, **60**: 2049–2055

[19] Deininger M, Buchdunger, E, Druker BJ. The development of imatinib as a therapeutic agent for chronic myeloid leukemia. *Blood* 2005, **105**: 2640-2653

[20] Stentoft J, Pallisgaard N, Kjeldsen E, Holm MS, Nielsen JL, Hokland P. Kinetics of BCR–ABL fusion transcript levels in chronic myeloid leukemia patients treated with STI571 measured by quantitative real-time polymerase chain reaction. *Eur. J. Haematol.* 2001, **67**: 302-308

[21] Lowenberg, B. Minimal residual disease in chronic myeloid leukemia. *N. Engl. J. Med.* 2003, **349**: 1399-1401

[22] Gorre M E, Sawyers C L. Molecular mechanisms of resistance to STI571 in chronic myeloid leukemia. *Curr. Opin. Hematol.* 2002, **9**: 303-307

[23] Melo JV, Chuah C Resistance to imatinib mesylate in chronic myeloid leukaemia. *Cancer Lett*. 2007, **249**: 121-132

[24] Mahon F X, Deininger MVN, Schultheis B, Chabrol J, Reiffers J, Goldman JM, Melo JV. Selection and characterization of *BCR-ABL* positive cell lines with differential sensitivity to the tyrosine kinase inhibitor STI571: diverse mechanisms of resistance. *Blood* 2000, **96**: 1070-1079

[25] Branford S, Rudzki Z, Walsh S, Parkinson I, Grigg A, Szer J, Taylor K, Herrmann R, Seymour JF, Arthur C, Joske D, Lynch K, Hughes T. Detection of BCR-ABL mutations in patients with CML treated with imatinib is virtually always accompanied by clinical resistance, and mutations in the ATP phosphate-

binding loop (P-loop) are associated with a poor prognosis. *Blood* 2003, **102**: 276-283

[26] Soverini S, Martinelli G, Rosti G, Bassi S, Amabile M, Poerio A, Giannini B, Trabacchi E, Castagnetti F, Testoni N, Luatti S, de Vivo A, Cilloni D, Izzo B, Fava M, Abruzzese E, Alberti D, Pane F, Saglio G, Baccarani M. ABL mutations in late chronic phase chronic myeloid leukemia patients with up-front cytogenetic resistance to imatinib are associated with a greater likelihood of progression to blast crisis and shorter survival: a study by the GIMEMA Working Party on Chronic Myeloid Leukemia. *Journal of Clinical Oncology* 2005, **23**: 4100-4109

[27] Cang, S, and Liu, D. P-loop mutations and novel therapeutic approaches for imatinib failures in chronic myeloid leukemia. *J. Hematol. Oncol.* 2008, **1**: 1-15

[28] Mahon FX, Belloc F, Lagarde V, Chollet C, Moreau-Gaudry F, Reiffers J, Goldman JM Melo J.V., MDR1 gene overexpression confers resistance to imatinib mesylate in leukemia cell line models. *Blood* 2003, **101**: 2368-2373

[29] Burger H, van Tol H, Brok M, Wiemer EA, de Bruijn EA, Guetens G, de Boeck G, Sparreboom A, Verweij J, Nooter K. Chronic imatinib mesylate exposure leads to reduced intracellular drug accumulation by induction of the ABCG2 (BCRP) and ABCB1 (MDR1) drug transport pumps. *Cancer Biotheraphy* 2005, **4**: 747–752

[30] Jordanides NE, Jorgensen HG, Holyoake TL, Mountford JC. Functional ABCG2 is over-expressed on primary CML CD34+ cells and is inhibited by imatinib mesylate. *Blood* 2006, **108**: 1370–1373

[31] Thomas J, Wang L, Clark RE, Pirmohamed M. Active transport of imatinib into and out of cells: implications for drug resistance. *Blood* 2004, **104**: 3739–3745

[32] White DL, Saunders VA, Dang P, Engler J, Zannettino AC, Cambareri AC, Quinn SR, Manley PW, Hughes TP. OCT-1 mediated influx is a key determinant of the intracellular uptake of imatinib but not nilotinib (AMN107); reduced OCT-1 activity is the cause of low in vitro sensitivity to imatinib. *Blood* 2006, **108**: 697–704

[33] Gambacorti-Passerini C, Barni R, Le Coutre P, Zucchetti M, Cabrita G, Cleris L, Rossi F, Gianazza E, Brueggen J, Cozens R, Pioltelli P, Pogliani E, Corneo G, Formelli F, D'Incalci M. Role of α1 acid glycoprotein in the *in vivo* resistance of human BCR- ABL(+) leukemic cells to the Abl inhibitor STI571. *Journal of the National Cancer Institute* 2000, **92**: 1641–1650

[34] Donato NJ, Wu JY, Stapley J, Gallick G, Lin H, Arlinghaus R Talpaz M. BCR-ABL independence and LYN kinase overexpression in chronic myelogenous leukemia cells selected for resistance to STI571. *Blood* 2003, **101**: 690–698

[35] Tipping AJ, Deininger MW, Goldman JM, Melo JV. Comparative gene expression profile of chronic myeloid leukemia cells innately resistant to imatinib mesylate. *Experimental Hematology* 2003, **31**: 1073–1080

[36] Hochhaus A, Kreil S ,Corbin A S, La Rosee P, Muller M C, Lahaye T, Hanfstein B, Schoch C, Cross N C, Berger U, Gschaidmeier H, Druker B J, Hehlmann R, Molecular and chromosomal mechanisms of resistance to imatinib (STI571) therapy. *Leukemia* 2002, **16**: 2190–2196

[37] Cang S, Liu D. P-loop mutations and novel therapeutic approaches for imatinib failures in chronic myeloid leukemia. *J. Hematol. Oncol.* 2008, **1**: 1-15

[38] Luzzatto L., Melo JV, Acquired resistance to imatinib mesylate: selection for pre-existing mutant cells. *Blood* 2002, **100**: 1105-1106

[39] Gorre ME, Mohammed M, Ellwood K, Hsu N, Paquette R, Rao PN, Sawyers CL. Sawyers, Clinical resistance to STI-571 cancer therapy caused by BCR-ABL gene mutation or amplification. *Science* 2001, **293**: 876–880

[40] Barnes DJ, Schultheis B, Adedeji S, Melo JV. Dose-dependent effects of Bcr-Abl in cell line models of different stages of chronic myeloid leukemia. *Oncogene* 2005, **24**: 6432–6440

[41] Gottesman M M, Fojo T, Bates SE. Multidrug resistance in cancer: role of ATP-dependent transporters. *Nature Review of Cancer* 2002, **2**: 48–58

[42] Illmer t, Schaich M, Platzbecker U, Freiberg-Richter J, Oelschlagel U, von Bonin M, Pursche S, Bergemann T, Ehninger G, Schleyer E. P-glycoprotein-mediated drug efflux is a resistance mechanism of chronic myelogenous leukemia cells to treatment with imatinib mesylate. *Leukemia* 2004, **18**: 401–408

[43] Wu J, Meng F, Kong LY, Peng Z, Ying Y, Bornmann WG, Darnay BG, Lamothe B, Sun H, Talpaz M, Donato NJ. Association Between Imatinib-Resistant BCR-ABL Mutation- Negative Leukemia and Persistent activation of lyn kinase. *J. Natl. Cancer Inst.* 2008, **100**: 926-939

[44] Roginskaya,V, Zuo S, Caudell E, Nambudiri G, Kraker AJ, Corey SJ. Therapeutic targeting of Src-kinase Lyn in myeloid leukemic cell growth. *Leukemia* 1999, **13**: 855-861

[45] Csete ME, Doyle JC. Reverse engineering of biological complexity. *Science* 2002, **295**: 1664-1669

[46] Tyres M, Mann M. From genomics to proteomics. *Nature* 2003, 422: 193-197

[47] Krishna RG, Wold F. "Posttranslational modification of proteins". *Adv. Enzymol. Mol. Biol.* 1993, **67***:* 265-298

[48] Cohen AA, Geva-Zatorsky N, Eden E, Frenkel-Morgenstern M, Issaeva I, Sigal A, Milo R, Cohen-Saidon C, Liron Y, Kam Z, Cohen L, Danon T, Perzov N, Alon U. Dynamic proteomics of individual cancer cells in response to a drug. *Science* 2008, **322**:1511-1516

[49] Corthals GL, Wasinger VC, Hochstrasser DF, Sanchez JC. The dynamic range of protein expression: a challenge for proteomic. *Electrophoresis* 2000, **21**:1104-1115

[50] Washburn MP, Wolters D, Yates JR. Large-scale analysis of the yeast proteome by multidimensional protein identification technology. *Nat. Biotechnol.* 2001, **19**: 242-247

[51] Rix U, Superti-Furga G. Target profiling of small molecules by chemical proteomics. *Nat. Chem. Biol.* 2009, **9**: 616-24

[52] O'Farell PH. High resolution two-dimentional electrophoresis of proteins. *J. Biol. Chem.* 1975, **250**: 4007-4021

[53] Bjellqvist B, Ek K, Righetti PG, Gianazza E, Görg A, Westermeier R, Postel W.Isoelectric focusing in immobilized pH gradients: principle, methodology and some applications. *J. Biochem. Biophys. Methods*. 1982, **6** :317-319

[54] Unlu M, Morgan M E, Minden J S. Difference gel electrophoresis: a single gel method for detecting changes in protein extracts. *Electrophoresis* 1997, **18**: 2071-2077

[55] Marouga R, David S, Hawkins E. The development of the DIGE system: 2D fluorescence difference gel analysis technology. *Anal. Bioanal. Chem.* 2005, **382**: 669-678

[56] Mann M, Hendrickson RC, Pandey A. Analysis of proteins and proteomes by mass spectrometry. *Annu. Rev. Biochem.* 2001, **70**: 437-473

[57] Aebersold R. A mass spectrometric journey into protein and proteome research. *J. Am. Soc. Mass. Spectrom.* 2003, **14**: 685-695

[58] Lin D, Tabb DL, Yates JR. Large-scale protein identification using mass spectrometry. *Biochim. Biophys. Acta* 2003, **1646**: 1-10

[59] Fenn JB, Mann M, Meng CK, Wong SF, Whitehouse CM. Electrosprayionization for mass spectrometry of large biomolecules. *Science* 1989, **246**: 64-71

[60] Aebersold R, Goodlett DR. Mass spectrometry in proteomics. *Chem. Rev.* 2001, **101**: 269-295

[61] Henzel WJ, Billeci TM, Stults JT, Wong SC, Grimley C, Watanabe C.Identifying proteins from two-dimensional gels by molecular mass searching of peptide fragments in protein sequence databases. *Proc. Natl. Acad. Sci. USA* 1993, **90**: 5011-5015

[62] Pappin DJ, Hojrup P, Bleasby AJ. Rapid identification of proteins by peptidemass fingerprinting. *Curr. Biol.* 1993, **3**: 327-332

[63] Yates JR, Speicher S, Griffin PR, Hunkapiller T. Peptide mass maps: a highly informative approach to protein identification. *Anal. Biochem.* 1993, **214**: 397-408

[64] Clauser KR, Hall SC, Smith DM, Webb JW, Andrews LE, Tran HM, Epstein LB, Burlingame AL. Rapid mass spectrometric peptide sequencing and massmatching for characterization of human melanoma proteins isolated by twodimensional PAGE. *Proc. Natl. Acad. Sci. U S A.* 1995, **92**: 5072-5076

[65] McLuckey SA, Goeringer DE, Glish GL. Collisional activation with random noise in ion trap mass spectrometry. *Anal. Chem.* 1992, **64**: 1455-1460

[66] Fontana S, Alessandro R, Barranca M, Giordano M, Corrado C, Zanella-Cleon I, Becchi M, Kohn EC, De Leo G. Comparative proteome profiling and functional analysis of chronic myelogenous leukemia cell lines. *J. Proteome Res.* 2007, **6**: 4330-4342

[67] Rosenhahn J, Weise A, Michel S, Hennig K, Hartmann I, Schiefner J, Schubert K, Liehr T, Von Eggeling F, and Loncarevic V. Cytogenetic characterisation and proteomic profiling of the Imatinib-resistant cell line KCL22-R. *Int. J. Oncol.* 2007, **31**: 121-128

[68] Ohmine K, Nagai T, Tarumoto T, Miyoshi T, Muroi K, Mano H, Komatsu H, Takaku F, Ozawa K. Analysis of gene expression profiles in an imatinib-resistant cell line, KCL22/SR. *Stem Cells* 2003, **21**: 315-321

[69] Jørgensen HG, Holyoake TL. Characterization of cancer stem cells in chronic myeloid leukaemia. *Biochem. Soc. Trans.* 2007, **35**: 1347-1351

[70] Miyoshi T , Nagai T , Ohmine K , Nakamura M , Kano Y, Muroi K , Komatsu N, Ozawa K. Relative importance of apoptosis and cell cycle blockage in the synergistic effect of combined R115777 and imatinib treatment in BCR/ABL-positive cell lines. *Biochem. Pharmacol.* 2005, **69**: 1585-1594

[71] Pocaly M, Lagarde V, Etienne G, Dupouy M, Lapaillerie D, Claverol S, Vilain S, Bonneu M, Turcq B, Mahon FX, Pasquet JM. Proteomic analysis of an imatinib-resistant K562 cell line highlights opposing roles of heat shock cognate 70 and heat shock 70 proteins in resistance. *Proteomics* 2008, **8**: 2394-2406

[72] Wang N, Li Z, Ding R, Frank GD, Senbonmatsu T, Landon EJ, Inagami T, Zhao ZJ. Antagonism or synergism. Role of tyrosine phosphatases SHP-1 and SHP-2 in growth factor signaling. *J. Biol. Chem.* 2006, **281**: 21878-21883

[73] Rix U, Hantschel O, Dürnberger G, Remsing Rix LL, Planyavsky M, Fernbach NV, Kaupe I, Bennett KL, Valent P, Colinge J, Köcher T, Superti-Furga G. Chemical proteomic profiles of the BCR-ABL inhibitors imatinib, nilotinib, and dasatinib reveal novel kinase and nonkinase targets. *Blood* 2007, **110**: 4055-4063

[74] Winger JA, Hantschel O, Superti-Furga G, Kuriyan J. The structure of the leukemia drug imatinib bound to human quinone reductase 2 (NQO2). *BMC Struct. Biol.* 2009, **9**: 7

[75] Bantscheff M, Eberhard D, Abraham Y, Bastuck S, Boesche M, Hobson S, Mathieson T, Perrin J, Raida M, Rau C, Reader V, Sweetman G, Bauer A, Bouwmeester T, Hopf C, Kruse U, Neubauer G, Ramsden N, Rick J, Kuster B, Drewes G. Quantitative chemical proteomics reveals mechanisms of action of clinical ABL kinase inhibitors. *Nat. Biotechnol.* 2007, **25**: 1035-1044

[76] Esteso G, Mora MI, Garrido JJ, Corrales F, Moreno AJ. Proteomic analysis of the porcine platelet proteome and alterations induced by thrombin activation. *Proteomics* 2008, **71**: 547-560

[77] McCubrey JA, Steelman LS, Chappell WH, Abrams SL, Wong EW, Chang F, Lehmann B, Terrian DM, Milella M, Tafuri A, Stivala F, Libra M, Basecke J, Evangelisti C, Martelli AM, Franklin RA. Roles of the Raf/MEK/ERK pathway in cell growth, malignant transformation and drug resistance. *Biochim. Biophys. Acta* 2007, **1773**: 1263-1284

[78] Ayala A, F-Lobato M, Machado A. Malic enzyme levels are increases by the activation of NADPH-consming pathways: detoxification processes. *FEBS Lett.* 1986, **202**: 102-106

[79] Winkler BS, Solomon F. High Activities of $NADP^+$-Dependent Isocitrate Dehydrogenase and Malic Enzyme in Rabbit Lens Epithelial Cells. *Invest Ophthalmol. Vis. Sci.* 1988, **29**: 821-823

[80] Chong ZZ, Maiese K. The Src homology 2 domain tyrosine phosphatases SHP-1 and SHP-2: diversified control of cell growth, inflammation, and injury. *Histol. Histopathol.* 2007, **22**:1251-1267

[81] Chan G, Kalaitzidis D, Neel BG. The tyrosine phosphatase Shp2 (PTPN11) in cancer. *Cancer Metastasis Rev*. 2008, **27** :179-192.

[82] Lu W, Gong D, Bar-Sagi D, Cole PA. Site-specific incorporation of a phosphotyrosine mimetic reveals a role for tyrosine phosphorylation of SHP-2 in cell signaling. *Mol. Cell.* 2001, **8**:759-769

[83] Dance M, Montagner A, Salles JP, Yart A, Raynal P. The molecular functions of Shp2 in the Ras/Mitogen-activated protein kinase (ERK1/2) pathway. *Cell.Signal.* 2008, **20**: 453-459

[84] Sampaio C, Dance M, Montagner A, Edouard T, Malet N, Perret B, Yart A, Salles JP, Raynal P. Signal strength dictates phosphoinositide 3-kinase contribution to Ras/extracellular signal-regulated kinase 1 and 2 activation via differential Gab1/Shp2 recruitment: consequences for resistance to epidermal growth factor receptor inhibition. *Mol. Cell. Biol*. 2008, **28**: 587-600

[85] Yoo JC, Hayman MJ. Annexin II binds to SHP2 and this interaction is regulated by HSP70 levels. *Biochem. Biophys. Res. Commun*. 2007, **356** :906-11

[86] Baccarani M, Saglio G, Goldman J, Hochhaus A, Simonsson B, Appelbaum F, Apperley J, Cervantes F, Cortes J, Deininger M, Gratwohl A, Guilhot F, Horowitz M, Hughes T, Kantarjian H, Larson R, Niederwieser D, Silver R,

Hehlmann R. European LeukemiaNet. Evolving concepts in the management of chronic myeloid leukemia: recommendations from an expert panel on behalf of the European Leukemia Net. *Blood* 2006, **8**: 1809-1820

[87] Rodrigues MS, Reddy MM, Sattler M. Cell Cycle Regulation by Oncogenic Tyrosine Kinases in Myeloid Neoplasias: From Molecular Redox Mechanisms to Health Implications. *Antioxi. Red. Sign.* 2008, **10**: 1813-1848

[88] Tarumoto T, Nagai T, Ohmine K, Miyoshi T, Nakamura M, Kondo T, Mitsugic K, Nakano S, Muroi K, Komatsu N, Ozawa K. Ascorbic acid restores sensitivity to imatinib via suppression of Nrf2-dependent gene expression in the imatinib-resistant cell line. *Exp. Hematol.* 2004, **32**: 375–381

[89] Rochat B. Role of cytochrome P450 activity in the fate of anticancer agents and in drug resistance: focus on tamoxifen, paclitaxel and imatinib metabolism. *Clin. Pharmacokinet.* 2005, **44**: 349-366

[90] Haddad JJ. Redox regulation of pro-inflammatory cytokines and IkappaB-alpha/NF-kappaB nuclear translocation and activation. *Biochem. Biophys. Res. Commun.* 2002, **296**: 847-856

[91] Ranawat P, Bansal MP. Decreased glutathione levels potentiate the apoptotic efficacy of selenium: possible involvement of p38 and JNK MAPKs in vitro*. Mol. Cell. Biochem.* 2008, **309**: 21-32

[92] Celli CM, Tran N, Knox R, Jaiswal AK**.** NRH:quinone oxidoreductase 2 (NQO2) catalyzes metabolic activation of quinones and anti-tumor drugs. *Biochem. Pharmacol.* 2006, **72**: 366-376

[93] Gong X, Gutala R, Jaiswal AK. Quinone Oxidoreductases and Vitamin K Metabolism*. In. Vitam. Horm.* 2008, *78:* 85-101

[94] Vella F, Ferry G, Delagrange P, Boutin JA. NRH:quinone reductase 2: an enzyme of surprises and mysteries. *Biochem. Pharmacol.* 2005, **71**: 1-12

[95] Matsuda A, Suzuki Y, Honda G, Muramatsu S, Matsuzaki O, Nagano Y, Doi T, Shimotohno K, Harada T, Nishida E, Hayashi H, Sugano S. Large-scale identification and characterization of human genes that activate NF-kappaB and MAPK signaling pathways. *Oncogene* 2003, **22**: 3307-3318

[96] Donato NJ, Wu JY, Stapley J, Lin H, Arlinghaus R, Aggarwal BB, Shishodia S, Albitar M, Hayes K, Kantarjian H, Talpaz M. Imatinib Mesylate Resistance Through BCR-ABL Independence in Chronic Myelogenous Leukemia*. Cancer Research* 2004, **64**: 672-677

[97] Kyriakis JM, Avruch J. Mammalian Mitogen-Activated Protein Kinase Signal Transduction Pathways Activated by Stress and Inflammation. *Physiological Reviews* 2001, **81**: 807-869

[98] Wang XZ, Grammatikakis N, Siganou A, Stevenson MA, Calderwood SK. Interactions between Extracellular Signal-regulated Protein Kinase 1, 14-3-3 and Heat Shock Factor 1 during Stress. *J. Biol. Chem.* 2004, **279**: 49460-49469

[99] T. Nambu, N. Araki, A. Nakagawa, A. Kuniyasu, T. Kawaguchi, A. Hamada, H. Saito, Contribution of BCR-ABL-independent activation of ERK1/2 to acquired imatinib resistance in K562 chronic myeloid leukemia cells. *Cancer Sci.* 2010, **101**: 137-142

[100] Lee F, Fandi A, Voi M. Overcoming kinase resistance in chronic myeloid leukemia. *Int. J. Biochem. Cell. Biol.* 2008, **40**: 334-343

[101] Samanta AK, Chakraborty SN, Wang Y, Kantarjian H, Sun X, Hood J, Perrotti D, Arlinghaus RB. Jak2 inhibition deactivates Lyn kinase through the SET-

PP2A-SHP1 pathway, causing apoptosis in drug-resistant cells from chronic myelogenous leukemia patients. *Oncogene* 2009, **28**: 1669-1681

[102] Tidow N, Kasper B, Welte K. SH2-containing protein tyrosine phosphatases SHP-1 and SHP-2 are dramatically increased at the protein level in neutrophils from patients with severe congenital neutropenia (Kostmann's syndrome). *Exp. Hematol*. 1999, **27**: 1038-1045

[103] Oka T, Yoshino T, Hayashi K, Ohara N, Nakanishi T, Yamaai Y, Hiraki A, Sogawa CA, Kondo E, Teramoto N, Takahashi K, Tsuchiyama J, Akagi T. Reduction of hematopoietic cell-specific tyrosine phosphatase SHP-1 gene expression in natural killer cell lymphoma and various types of lymphomas/leukemias : combination analysis with cDNA expression array and tissue microarray. *Am. J. Pathol.* 2001, **159**: 1495-1505

[104] Wu C, Sun M, Liu L, Zhou GW. The function of the protein tyrosine phosphatase SHP-1 in cancer. *Gene* 2003, **306**: 1-12

[105] Amin HM, Hoshino K, Yang H, Lin Q, Lai R, Garcia-Manero G. Decreased expression level of SH2 domain-containing protein tyrosine phosphatase-1 (Shp1) is associated with progression of chronic myeloid leukaemia. *Journal of Pathology* 2007, **212**: 402-410

[106] Garcia Pedrero JM, Fernandez MP, Morgan RO, Herrero Zapatero A, Gonzalez MV, Suarez Nieto C, Rodrigo JP. Annexin A1 down-regulation in head and neck cancer is associated with epithelial differentiation status. *Am. J. Pathol.* 2004, **164**: 73-79

[107] Debret R, El Btaouri H, Duca L, Rahman I, Radke S, Haye B, Sallenave JM, Antonicelli F. Annexin A1 processing is associated with caspase-dependent apoptosis in BZR cells. *FEBS Lett*. 2003, **546**: 195-202

[108] Solito E, De Coupade C, Canaider S, Goulding NJ, Perretti M. Transfection of annexin 1 in monocytic cells produces a high degree of spontaneous and stimulated apoptosis associated with caspase-3 activation. *Br. J. Pharmacol.* 2001, **133**: 217-228

[109] Solito E, Kamal A, Russo-Marie F, Buckingham JC, Marullo S, Perretti M. A novel calciumdependent proapoptotic effect of annexin 1 on human neutrophils. *FASEB J.* 2003, **17**: 1544-1546

[110] Alldridge LC, Bryant CE. Annexin 1 regulates cell proliferation by disruption of cell morphology and inhibition of cyclin D1 expression through sustained activation of the ERK1/2 MAPK signal. *Exp. Cell. Res.* 2003, **290**: 93-107

[111] Moriyama K, Yahara I. Human CAP1 is a key factor in the recycling of cofilin and actin for rapid actin turnover. *J. Cell. Sci.* 2002, **115**: 1591-1601

[112] Hynes GM, Willison KR. Individual subunits of the eukaryotic cytosolic chaperonin mediate interactions with binding sites located on subdomains of b-actin. *J. Biol. Chem.* 2000, **275**: 18985-18994

[113] Pocaly M, Lagarde V, Etienne G, Ribeil JA, Claverol S, Bonneu M, Moreau-Gaudry F, Guyonnet-Duperat V, Hermine O, Melo JV, Dupouy M, Turcq B, Mahon FX, Pasquet JM. Overexpression of the heat-shock protein 70 is associated to imatinib resistance in chronic myeloid leukemia. *Leukemia* 2007, **21**: 93-101

ACKNOWLEDGMENTS

Special thanks to the European School of Molecular Medicine (SEMM) for Ph.D. fellowship and to the Centro Regionale di Competenza GEAR, Regione Campania for 2D-DIGE facility. The experimental work described in this thesis was supported by Ministero della Salute (Roma), Convenzione CEINGE- MIUR (2000) art 5.2 (to F.S.), Convenzione CEINGE-Regione Campania (to F.S.), Progetto S.co.Pe, Centro di eccellenza riconosciuto dal MIUR ex dm 11/2000, Prin 2006 (to M.R.).